AZD2171: A Highly Potent, Orally Bioavailable, Vascular Endothelial Growth Factor Receptor-2 Tyrosine Kinase Inhibitor for the Treatment of Cancer

Stephen R. Wedge,[1] Jane Kendrew,[1] Laurent F. Hennequin,[4] Paula J. Valentine,[1] Simon T. Barry,[1] Sandra R. Brave,[1] Neil R. Smith,[1] Neil H. James,[1] Michael Dukes,[1] Jon O. Curwen,[1] Rosemary Chester,[1] Janet A. Jackson,[1] Sarah J. Boffey,[1] Lyndsey L. Kilburn,[1] Sharon Barnett,[1] Graham H.P. Richmond,[2] Peter F. Wadsworth,[2] Mike Walker,[3] Alison L. Bigley,[2] Sian T. Taylor,[1] Lee Cooper,[1] Sarah Beck,[1] Juliane M. Jürgensmeier,[1] and Donald J. Ogilvie[1]

[1]Cancer Bioscience, [2]Safety Assessment, and [3]Discovery DMPK, AstraZeneca, Alderley Park, Macclesfield, Cheshire, United Kingdom; and [4]AstraZeneca Pharma, Centre de Recherches, Z.I. La Pompelle, Chemin de Vrilly, Reims, France

Abstract

Inhibition of vascular endothelial growth factor-A (VEGF) signaling is a promising therapeutic approach that aims to stabilize the progression of solid malignancies by abrogating tumor-induced angiogenesis. This may be accomplished by inhibiting the kinase activity of VEGF receptor-2 (KDR), which has a key role in mediating VEGF-induced responses. The novel indole-ether quinazoline AZD2171 is a highly potent (IC_{50} < 1 nmol/L) ATP-competitive inhibitor of recombinant KDR tyrosine kinase *in vitro*. Concordant with this activity, in human umbilical vein endothelial cells, AZD2171 inhibited VEGF-stimulated proliferation and KDR phosphorylation with IC_{50} values of 0.4 and 0.5 nmol/L, respectively. In a fibroblast/endothelial cell coculture model of vessel sprouting, AZD2171 also reduced vessel area, length, and branching at subnanomolar concentrations. Once-daily oral administration of AZD2171 ablated experimental (VEGF-induced) angiogenesis *in vivo* and inhibited endochondral ossification in bone or corpora luteal development in ovary; physiologic processes that are highly dependent upon neovascularization. The growth of established human tumor xenografts (colon, lung, prostate, breast, and ovary) in athymic mice was inhibited dose-dependently by AZD2171, with chronic administration of 1.5 mg per kg per day producing statistically significant inhibition in all models. A histologic analysis of Calu-6 lung tumors treated with AZD2171 revealed a reduction in microvessel density within 52 hours that became progressively greater with the duration of treatment. These changes are indicative of vascular regression within tumors. Collectively, the data obtained with AZD2171 are consistent with potent inhibition of VEGF signaling, angiogenesis, neovascular survival, and tumor growth. AZD2171 is being developed clinically as a once-daily oral therapy for the treatment of cancer. (Cancer Res 2005; 65(10): 4389-400)

Introduction

Vascular endothelial growth factor-A (VEGF) is a pivotal stimulus of physiologic and pathologic angiogenesis, including the sustained neovascularization required to support solid tumor growth (1). Tumor blood vessels furnish solid malignancies with oxygen and nutrients, facilitating further dysregulated growth, and provide a route for metastatic dissemination. New vascular capillaries are derived via a complex, orchestrated series of events, involving activation of endothelial and perivascular cells and modifications to the surrounding basement membrane and extracellular matrix. Although many diverse stimuli are implicated in this process, signaling induced by VEGF is considered rate limiting. A dependency on VEGF is attributed to its ability to regulate key processes throughout the angiogenic cascade, including endothelial cell migration, proliferation and protease expression (2–4), microvascular integrin expression (5), recruitment of endothelial cell precursors (6), capillary tube formation (7), neovascular survival (8), interactions with mural cells (9), and enhanced vascular permeability (10). The production of VEGF can be disproportionately up-regulated in tumors via oncogene activation (11), loss of tumor suppressor function (12, 13), or changes in oxygen or glucose status (14). Tumor capillaries induced by overexpression of VEGF are tortuous and dilated (15); an architecture that is reminiscent of immature vessels during early vascular remodeling.

VEGF binds to the second and third immunoglobulin-like domains of its specific transmembrane receptors Flt-1 (VEGFR-1) and KDR (VEGFR-2) on endothelial cells, initiating receptor homodimerization or heterodimerization (16, 17). The conformational change induced in the receptor complex stimulates intrinsic kinase activity which transphosphorylates tyrosine residues within the cytoplasmic domains. These phosphorylated peptide sequences serve as recognition sites for Src homology 2 domain-binding proteins that subsequently propagate intracellular signaling. Activated KDR has been shown the major stimulator of angiogenesis and vascular permeability (18, 19). KDR signaling responses include (i) mitogenic signaling via activation of a phospholipase C-γ/protein kinase C/Raf/mitogen-activated protein kinase (MAPK) pathway (20), (ii) motogenic signaling through phosphorylation of FAK and paxillin (21), and (iii) survival signaling, in a complex with VE-cadherin, β-catenin, and phosphoinositide 3′-kinase (22).

With the exceptions of longitudinal bone extension during growth and cyclical changes in the female reproductive tissues, angiogenesis does not occur in healthy adults. Chronic inhibition of this process may therefore be tolerated and provide a means by which to prevent tumor progression (23). Given that KDR transduces the angiogenic effects of VEGF, and tissue expression

Requests for reprints: Stephen R. Wedge, Cancer and Infection Research, AstraZeneca, Mereside, Alderley Park, Macclesfield, Cheshire, SK10 4TG, United Kingdom. Phone: 44-1625-513236; Fax: 44-1625-513624; E-mail: steve.wedge@astrazeneca.com.

EXHIBIT A

of this receptor is largely confined to the endothelium, inhibition of KDR signaling should provide a means for achieving selective therapeutic intervention.

A number of small molecule approaches to inhibit the intrinsic tyrosine kinase activity of KDR have been described previously, with a range of nanomolar potencies, selectivities, and pharmacokinetic properties (24–27). Here we describe AZD2171, a highly potent (subnanomolar IC_{50}) inhibitor of KDR tyrosine kinase and VEGF-induced signaling in endothelial cells. This compound has pharmacokinetic properties that make it suitable for chronic once-daily oral dosing. AZD2171 prevents VEGF-induced angiogenesis *in vivo* and shows dose-dependent activity in a range of human tumor xenografts in mice; statistically significant inhibition of tumor growth being evident with doses as low as 0.75 to 1.5 mg per kg per day. Furthermore, we show that inhibition of tumor growth is not merely a consequence of preventing new vessel formation; vascular regression can be observed in tumors following AZD2171 treatment.

Materials and Methods

AZD2171. 4-[(4-Fluoro-2-methyl-1*H*-indol-5-yl)oxy]-6-methoxy-7-[3-(pyrrolidin-1-yl)propoxy]quinazoline (AZD2171; Fig. 1) was synthesized according to the processes described in the International Patent Application Publication Number WO 00/47212, in particular those described in Example 240 of WO/47212. The free base of AZD2171 was used in all preclinical studies, with a molecular weight of 450.51. For all *in vitro* assays, AZD2171 was prepared initially as a 10 mmol/L stock solution in DMSO and diluted in the relevant assay media. All *in vivo* studies were conducted by once-daily oral gavage. For studies in mice, AZD2171 was suspended in 1% (w/v) aqueous polysorbate 80 (polyoxyethylene; ref. 20; sorbitan mono-oleate in deionized water) and dosed at 0.1 mL/10 g of body weight. For studies in rats, AZD2171 was suspended in a 0.5% (w/v) hydroxypropyl methylcellulose solution containing 0.1% (w/v) aqueous polysorbate 80 and given at 5 mL/kg body weight.

Kinase inhibition. Flt-4 tyrosine kinase was obtained from ProQinase GmbH (Freiburg, Germany) and c-Kit tyrosine kinase from Upstate Biotechnology, Inc. (Lake Placid, NY). Each additional kinase used was generated as a cell lysate, following infection of insect cells with recombinant baculoviruses containing kinase domains. All enzyme assays were run at, or just below, the respective K_m for ATP (0.2-30 μmol/L). The inhibitory activity of AZD2171 was determined against a range of recombinant tyrosine kinases [KDR, Flt-1, Flt-4, c-Kit, PDGFR-α, PDGFR-β, CSF-1R, Flt-3, FGFR1, Src, Abl, epidermal growth factor receptor (EGFR), ErbB2, Aur-A, and Aur-B] using ELISA methodology described previously (28). Selectivity versus CDK2 and CDK4 serine/threonine kinases was examined using scintillation proximity assays with a retinoblastoma substrate and [γ-^{33}P]ATP (29). Activity versus the dual specificity kinase MAPK kinase (MEK), was determined with a MAPK substrate, [γ-^{33}P]ATP, and paper capture/scintillation counting (29). Microcal Origin software (vs. 3.78, Microcal Software, Inc., Northhampton, MA) was used to interpolate IC_{50} values by nonlinear regression.

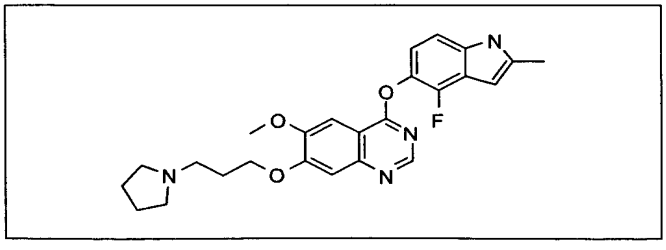

Figure 1. Chemical structure of AZD2171.

Inhibition of growth factor–stimulated receptor phosphorylation. Inhibition of receptor phosphorylation within cells was determined using ELISA (KDR and EGFR) or Western blotting (c-Kit, PDGFR-α and PDGFR-β, or Flt-3) methods, or methods incorporating a fluorescent immunocytochemical end point (CSF1-R or ErbB2). Parental cell lines were purchased from the American Type Tissue Collection (ATCC, Manassas, VA), except for MonoMac6 cells, which were obtained from the German Collection of Microorganisms and Cell Cultures (Braunschweig, Germany). With the exception of experiments examining erbB2, cells were serum starved overnight, incubated with AZD2171 for 60 to 120 minutes, and stimulated, where required, with the relevant ligand: $VEGF_{165}$ (100 ng/mL) for 7 minutes, SCF (50 ng/mL) for 10 minutes, PDGF-AA or PDGF-BB (50 ng/mL) for 5 minutes, EGF (1 μg/mL) for 3 minutes, or CSF-1 (40 ng/mL) for 10 minutes. VEGF, SCF, EGF, and CSF-1 were obtained from R&D Systems, Inc. (Abingdon, United Kingdom) and PDGF-AA and PDGF-BB from Sigma-Aldrich (Poole, United Kingdom). Inhibition of KDR phosphorylation was determined in human umbilical vein endothelial cells (HUVEC) by ELISA at ProQinase. EGFR phosphorylation was examined using a sandwich ELISA in KB human oral squamous tumor cells, with an sc-120 capture antibody (Santa Cruz Biotechnology, Inc., Santa Cruz, CA) and detection via horseradish peroxidase immunoconjugated to a 4G10 phosphotyrosine antibody (Upstate Biotechnology).

Western blotting was done using standard SDS-PAGE methods, loading 50 to 75 μg of protein per lane, with detection by enhanced chemiluminescence. Total and phosphorylated c-Kit was measured in NCI-H526 human small cell lung tumor cells, using antibodies to c-Kit (Santa Cruz Biotechnology) and phospho-c-Kit (Cell Signaling Technology, Inc., Beverly, MA). PDGFR-α and PDGFR-β phosphorylation was examined in MG63 human osteosarcoma cells, using antibodies to total (R&D Systems) and phosphorylated (Santa Cruz Biotechnology and Cell Signaling Technology) receptors. Inhibition of Flt-3 phosphorylation was investigated in MonoMac6 human acute myeloid leukemia cells, which contain an activating mutation in the juxtamembrane sequence of the receptor, using Flt-3 (Cell Signaling Technology) and phospho-Flt-3 (Cell Signaling Technology) antibodies.

ErbB2 phosphorylation was examined in MCF-7 breast carcinoma cells stably expressing constitutively activated wild-type erbB2 receptor. Cells were incubated with AZD2171 for 4 hours at 37°C, fixed in 3.3% formaldehyde/PBS, and immunostained with a phospho-erbB2 primary antibody (Santa Cruz Biotechnology) followed by an Alexa-Fluor 488 secondary antibody (Molecular Probes, Paisley, United Kingdom). ErbB2 phosphorylation was quantitated using an Acumen Explorer fluorescence laser-scanning plate reader (TTP Labtech Ltd., Royston, United Kingdom). CSF-1R phosphorylation was detected in 3T3 murine fibroblasts stably transfected with human CSF-1R. Cells were fixed in 4% formaldehyde and immunostained using a primary antibody to phosphorylated CSF-1R (Cell Signaling Technology). CSF-1R phosphorylation was quantitated using a Cellomics ArrayScan HCS Reader (Cellomics, Inc., Pittsburgh, PA).

Inhibition of KDR phosphorylation was also examined in HUVEC by Western blotting. HUVEC were serum starved overnight, incubated with AZD2171 for 90 minutes and stimulated with VEGF (50 ng/mL) for 8 minutes. Human $VEGF_{165}$ was generated as described previously (29). Antibodies against pKDR (rabbit polyclonal generated to phosphorylated Y1214), KDR (Santa Cruz Biotechnology), pMAPK (Cell Signaling Technology), or MAPK (Cell Signaling Technology) were used.

Inhibition of growth factor–mediated cellular proliferation. HUVEC proliferation in the presence and absence of growth factors was evaluated following a 4-day incubation by ^{3}H-thymidine incorporation, as described previously (28). Proliferation of MG63 osteosarcoma cells was induced by PDGF-AA, which selectively activates PDGFR-α homodimer signaling. Cells were cultured in DMEM without phenol red (Sigma-Aldrich) containing 1% charcoal stripped FCS, 2 mmol/L glutamine, and 1% nonessential amino acids (Invitrogen, Paisley, United Kingdom) for 24 hours. AZD2171 or vehicle was added with PDGF-AA ligand (50 ng/mL; Sigma-Aldrich) and plates reincubated for 72 hours. Cellular proliferation was determined using a bromodeoxyuridine ELISA (Roche Diagnostics Ltd., Lewes, United Kingdom).

Inhibition of tumor cell proliferation *in vitro*. The human tumor cell lines, Calu-6 (lung carcinoma), SW620 (colorectal carcinoma), MDA-MB-231 (mammary gland adenocarcinoma), PC-3 (prostate adenocarcinoma), and SKOV-3 (ovarian adenocarcinoma) were obtained from ATCC. Cell proliferation was determined over a 3-day period as described previously (30).

Human *in vitro* angiogenesis assay. HUVECs and human diploid fibroblasts were obtained (day 0) as cocultures in 24-well plates (AngioKit, TCS CellWorks Ltd., Buckinghamshire, United Kingdom) and the medium immediately replaced with MCDB 131 medium (Life Technologies, Paisley, United Kingdom) containing 2% FCS, 1% glutamine, and 1% penicillin/streptomycin (Sigma, Poole, United Kingdom). AZD2171 or vehicle (0.01% DMSO in MCDB 131) was added to the cocultures. Medium, with AZD2171 or vehicle, was replenished on days 3, 6, and 8. Tubule formation was examined at day 10 following fixing and staining of tubules for CD31 (platelet/endothelial cell adhesion molecule 1) according to the manufacturer's instructions. Comparative treatment with either an antihuman VEGF neutralizing antibody or a control immunoglobulin G antibody (30 μg/mL, R&D Systems) was also examined.

To quantify tubule growth, a novel whole-well image analysis method was developed using a Zeiss KS400 3.0 Image Analyser (Imaging Associates Ltd., Bicester, United Kingdom) and a bespoke computer program. Tubule formations within each well were measured excluding a rim of 100-μm depth to avoid edge retraction artifact. The computer program segmented the images using a gray level threshold tool to select the stained cells of interest. The resultant binary images were skeletonized and nodal junctions (branch points) removed to determine the total length of an individual tubule. The branch points were counted and the total area of CD31 staining determined from the original binary image but with a correction for cells that had not migrated (labeled cells with an area of <20 μm).

Inhibition of vascular endothelial growth factor–induced angiogenesis *in vivo*. A Matrigel plug assay done by Vasculogen (Minneapolis, MN) was used to examine VEGF-induced angiogenesis directly. Briefly, Matrigel (0.5 mL) containing heparin (20 units/mL; Sigma Chemicals, St. Louis, MO) was diluted 3:1 in HBSS or recombinant human $VEGF_{165}$ (150 ng/mL; R&D systems) and injected s.c. into female, BALB/c athymic (*nu/nu* genotype) mice of 6 to 8 weeks of age (five per group). AZD2171 (1.5 or 6 mg per kg per day) or vehicle was given orally, from the day of Matrigel implantation, for 7 days. Matrigel plugs were recovered on day 8, one half being snap-frozen in liquid nitrogen using Tissue-Tek, ornithine carbamyl transferase compound (Fisher Scientific, Pittsburgh, PA) and the other fixed in neutral formalin and embedded in paraffin for H&E staining. Frozen sections were stained with a rat monoclonal antibody reactive to mouse CD31 conjugated to phycoerythrin (BD Biosciences PharMingen, San Diego, CA). Two sections were cut from the Matrigel samples at different levels and analyzed for vessel density. Nuclei were counterstained with 4′,6-diamidino-2-phenylindole (DAPI) and immunofluorescent images (n = 7-10) of CD31 staining obtained from each sample at random. Each area was photographed under both red and UV filters. Morphometric analysis of vessel density and architecture was carried out after converting the images into a binary image using Adobe Software. Images were skeletonized using a program that converts binary data into single pixel density tracings (31). This enabled the number of vessel ends, vessel branch points (nodes), and total vessel length to be quantified with an Image Processing Toolkit (RGI, Inc., Raleigh, NC).

Effect of AZD2171 on bone growth and luteal development. Young female Alderley Park rats (6 weeks of age, Wistar derived, n = 5) were dosed orally, once daily for 28 days with AZD2171 (1.25-5 mg per kg per day) or vehicle. Additional rats (five per group) were treated with AZD2171 (5 mg per kg per day) or vehicle for 28 days and maintained for a further 28 days without treatment, to examine the effect of compound withdrawal. Histologic paraffin wax sections of the femorotibial joints and ovaries were stained with H&E. Morphometric image analysis of femorotibial sections was done (29), with growth plate areas from both the femur and tibia in each joint being combined for an analysis of the effect of compound treatment. The area of corpora lutea in H&E-stained ovary sections was similarly determined by morphometric analysis (Joyce-Loebl Magiscan Image Analyser, Applied Imaging Ltd., Newcastle upon Tyne, United Kingdom).

***In vivo* tumor models.** Protocols for establishing s.c. PC-3, Calu-6, SKOV-3, MDA-MB-231, and SW620 tumors in female nude (*nu/nu* genotype) mice were as described previously (29, 30). When tumors reached a volume of 0.1 to 0.5 cm^3, mice were randomized (6-12 per group) and AZD2171 (0.75-6 mg per kg per day) or vehicle given once daily by oral gavage. Tumor volumes were assessed by bilateral Vernier caliper measurement at least twice weekly and calculated using the formula (length × width) × $\sqrt{}$ (length × width) × (π/6), where length was taken to be the longest diameter across the tumor and width the corresponding perpendicular. Growth inhibition was calculated from the start of treatment by comparison of the mean change in tumor volume for control and treated groups. To remove any size dependency before statistical evaluation (the variance in mean tumor volume data increases proportionally with volume and is therefore disproportionate between groups), data was log-transformed before statistical evaluation using a one-tailed two-sample t test.

Histologic assessment of tumor vasculature in response to AZD2171 therapy. Mice bearing established Calu-6 human lung tumor xenografts (0.2 ± 0.01 cm^3, mean volume ± SE) were selected (day 0) and treated chronically with AZD2171 (6 mg per kg per day, p.o.) or vehicle. Tumors were collected (6-15 per group) 4 hours after the last dose of AZD2171 or vehicle, on days 1, 2, 7, 14, and 21. CD31 was then detected in sections using a chromagen end point or fluorescent immunostaining. CD31 staining with a chromagen end point was done on tumor specimens fixed in zinc fixative (PharMingen) using methodology described previously (29). These were analyzed blind to treatment assignment using a KS400 instrument (Imaging Associates). CD31-positive vessel number and total CD31 staining area/5,000 μm^2 viable tumor area were calculated for each section. For CD31 fluorescent immunostaining, formalin-fixed sections were incubated with a CD31 antibody (Santa Cruz Biotechnology) in serum block followed by an immunoglobulin G conjugated to Alexa Fluor 488 (Molecular Probes) and counterstained using ProLong Gold anti-fade reagent with DAPI (Molecular Probes). Fluorescent CD31 staining was visualized using an Axiovert S100 fluorescent microscope (Carl Zeiss SMT, Inc., Thornwood, NY) and images analyzed using MetaMorph version 6.1 software (Universal Imaging Co., Downingtown, PA).

Results

AZD2171 is a highly potent inhibitor of KDR tyrosine kinase and shows selectivity versus a range of additional kinases. AZD2171 is a highly potent inhibitor of recombinant KDR tyrosine kinase activity *in vitro* (IC_{50} < 1 nmol/L; Table 1). Additional activity is observed against the kinase associated with Flt-1 (IC_{50} = 5 nmol/L) and the VEGF-C and VEGF-D receptor Flt-4 ($IC_{50} \leq 3$ nmol/L). The inhibitory activity of AZD2171 was also examined against each recombinant PDGFR-related kinase *in vitro* because of their structural similarity to the VEGF family of receptors. The IC_{50} values for inhibition of c-Kit and PDGFRβ tyrosine kinase (2 and 5 nmol/L, respectively) were in a range similar to that measured versus Flt-1 and Flt-4. However, when compared with KDR kinase inhibition, AZD2171 selectivity versus the remaining PDGFR-related members ranged from >36-fold (PDGFR-α) to >1,000-fold (Flt-3). Excellent selectivity for KDR was evident versus a range of unrelated tyrosine and serine/threonine kinases, including EGFR (>1,600-fold selectivity) and MEK (>10,000-fold selectivity; Table 1). Furthermore, in addition to the data presented, no inhibition of enzyme activity was detected when 10 μmol/L of AZD2171 was examined with 100 μmol/L ATP against AMPK, ChK1, c-*jun* NH_2-terminal kinase, MAPK2, MSK-1, PKA, Akt/PKB, PKCα, Rock II, SAPK2b, SAPK2c, SGK, CSK, and PI 3-kinase (data not shown).

AZD2171 inhibits vascular endothelial growth factor–induced KDR phosphorylation in human endothelial cells. In

Table 1. AZD2171 inhibition of VEGF receptor tyrosine kinase activity and selectivity profile

Kinase	IC_{50} (μmol/L)*, mean ± SE
VEGFR family	
KDR (VEGFR-2)	<0.001
Flt-1 (VEGFR-1)	0.005 ± 0.002
Flt-4 (VEGFR-3)	≤0.003
PDGFR family	
c-Kit	0.002 ± 0.0001
PDGFR-β	0.005 ± 0.001
PDGFR-α	0.036 ± 0.008
CSF-1R	0.11 ± 0.03
Flt-3	>1
Representatives from other kinase families	
FGFR1	0.026 ± 0.009
Src	0.13 ± 0.02
Abl	0.26 ± 0.05
EGFR	1.6 ± 0.3
ErbB2 (HER-2/*neu*)	>1
CDK2	>1
CDK4	>1
Aur-A	>10
Aur-B	>10
MEK	>10

*The ability of AZD2171 to inhibit human recombinant tyrosine kinase activity was examined with ATP concentrations at, or just below, the respective K_m. Data represent the mean ± SE of at least three separate determinations. IC_{50} values quoted as "greater than" denote the inability to reach an IC_{50} value with the highest concentration tested.

HUVEC, AZD2171 inhibited VEGF-stimulated phosphorylation of KDR in a dose-dependent manner with an IC_{50} value of 0.0005 μmol/L (Table 2). The phosphorylation of MAPK, a downstream marker of VEGF signaling, was inhibited concomitantly (Fig. 2). To assess AZD2171 selectivity more critically, particularly between the PDGFR family of receptors, a range of cell lines were used to examine inhibition of receptor phosphorylation at a cellular level (Table 2). In comparison with inhibition of KDR phosphorylation, the AZD2171 IC_{50} for inhibition of c-Kit phosphorylation in NCI-H562 cells was found only 2-fold higher, whereas 10- and 16-fold higher concentrations, respectively, were required for comparable inhibition of PDGFR-α and PDGFR-β phosphorylation in MG63 osteosarcoma cells. In accordance with the kinase selectivity profile, AZD2171 showed a high degree of selectivity (420- to >20,000-fold) for inhibition of KDR phosphorylation versus the remaining PDGFR family members, CSF-1R and Flt-3, and versus the erb family members, EGFR and erbB2 (Table 2).

AZD2171 inhibits vascular endothelial growth factor–induced proliferation potently and shows selectivity versus mitogenesis induced by other growth factors. Consistent with the activity shown against VEGF-stimulated KDR autophosphorylation in HUVEC, AZD2171 inhibited VEGF-stimulated HUVEC proliferation potently with an IC_{50} value of 0.0004 ± 0.0002 μmol/L (Table 3). AZD2171 was found more potent against VEGF-induced HUVEC proliferation (IC_{50} = 0.4 nmol/L) than other VEGFR tyrosine kinase inhibitors that have entered clinical development, including the pthalazine PTK787 (IC_{50} = 0.008 ± 0.001 μmol/L, mean ± SE; n = 4), the indolinone SU11248 (IC_{50} = 0.04 ± 0.02 μmol/L, mean ± SD; n = 2) and the isothiazole CP-547,632 (IC_{50} = 0.06 ± 0.001 μmol/L, mean ± SD; n = 2; data not shown). To address the functional relevance of inhibiting receptor phosphorylation in human cells, AZD2171 selectivity was examined further against proliferation induced by different growth factors. In HUVEC, AZD2171 showed selectivity of 275-fold for inhibition of VEGF-induced proliferation versus basic fibroblast growth factor (bFGF)–induced proliferation, and 1,250-fold selectivity versus an effect on EGF-induced proliferation (Table 3). The effect of AZD2171 on PDGFR-α–dependent cellular proliferation (stimulated by PDGF-AA) was examined in MG63 cells, and an IC_{50} value of 0.04 μmol/L determined. This concentration is 100-fold greater than that required for comparable inhibition of VEGF-induced proliferation in HUVEC. The data indicate that AZD2171 can selectively inhibit VEGFR-dependent proliferation, in contrast to proliferation mediated by FGFR1 or EGFR, and that appreciable functional selectivity is also evident versus PDGFRα.

Micromolar concentrations of AZD2171 are required to inhibit tumor cell proliferation directly *in vitro*. The ability of AZD2171 to inhibit tumor cell growth directly was examined *in vitro* to ascertain whether subsequent antitumor activity *in vivo* could be ascribed to a direct antiproliferative effect or an indirect effect from inhibiting VEGF signaling. AZD2171 only inhibited tumor cell proliferation *in vitro* at comparatively high concentrations. The IC_{50} values (mean ± SE) determined from three to five independent experiments against tumor cells were 3.0 ± 0.4 μmol/L (SKOV-3), 3.8 ± 0.5 μmol/L (MDA-MB-231), 5.8 ± 0.2 μmol/L (PC-3), 6.4 ± 0.6 μmol/L (Calu-6), and 7.4 ± 0.7 μmol/L (SW620). These concentrations are between 7,500- and 18,500-fold greater than required for comparable inhibition of VEGF-stimulated HUVEC proliferation and were not attained within *in vivo* tumor xenograft experiments (data not shown). The ability of AZD2171 to inhibit tumor growth *in vivo* can therefore be attributed to inhibition of VEGF signaling.

AZD2171 inhibits tubule sprouting *in vitro* at subnanomolar concentrations and prevents VEGF-induced angiogenesis *in vivo*. Although the complex angiogenic phenotype cannot be

Table 2. AZD2171 inhibition of growth factor–stimulated receptor phosphorylation

Activated receptor	Cell line	IC_{50} (μmol/L), mean ± SE	Fold selectivity versus KDR
KDR	HUVEC	0.0005 ± 0.0003	—
c-Kit	NCI-H526	0.001 ± 0.0003	2
PDGFR-α	MG63	0.005 ± 0.0002	10
PDGFR-β	MG63	0.008 ± 0.0009	16
CSF-1R	NIH3T3/CSF1R	0.21 ± 0.05	420
Flt-3	MonoMac6	>10	20,000
EGFR	KB	1.1 ± 0.1	2,200
ErbB2	MCF-7/neu	>3	6,000

NOTE: The ability of AZD2171 to inhibit receptor phosphorylation was determined in cells following compound incubation and stimulation with the relevant ligand where required. Values represent the mean ± SE from three to four independent experiments.

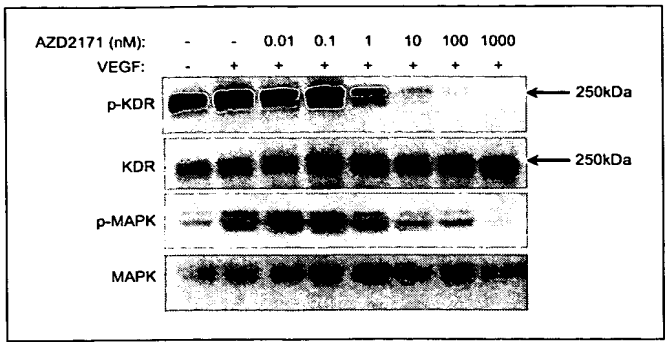

Figure 2. AZD2171 inhibits VEGF-stimulated KDR phosphorylation in human endothelial cells. Detection and quantitation by enhanced chemiluminescence revealed an AZD2171 IC_{50} value of 0.5 nmol/L for inhibition of KDR phosphorylation that is in agreement with the value determined by ELISA (Table 2).

completely replicated *in vitro*, assays can be used to model vascular sprouting. We modified a commercially available fibroblast/endothelial cell coculture system (AngioKit, TCS CellWorks) so that exogenous bFGF was omitted from the incubation medium. Under these conditions, tubule growth is regulated more directly by VEGF, production of which increases during the course of the assay.[5] When compared with treatment with an isotype control antibody (Fig. 3*B*, *iv*) that did not affect tubule growth, a VEGF-neutralizing antibody inhibited vessel development significantly (Fig. 3*B*, *v*). Consistent with potent activity against VEGF signaling, AZD2171 inhibited vessel branching, length, and area (Fig. 3) with IC_{50} values (mean ± SE; five independent experiments) of 0.0001 ± 0.00004, 0.0001 ± 0.00003, and 0.0002 ± 0.00007 μmol/L, respectively. To examine inhibition of angiogenesis *in vivo* that was selectively driven by VEGF, Matrigel plugs containing VEGF were implanted s.c. in mice and vessel development examined over the course of 8 days. AZD2171 completely abolished VEGF-induced vessel formation. The data obtained with 6 mg per kg per day AZD2171 versus number of vessel ends, branch points and total vessel length was not significantly different to that observed with 1.5 mg per kg per day (Fig. 4; $P > 0.05$ by one-tailed t test). Collectively, these data show that AZD2171 is a potent inhibitor of VEGF-induced angiogenesis.

AZD2171 induces hypertrophy in bone growth plate and inhibits luteal development in ovary: physiologic processes that are dependent upon angiogenesis. Angiogenesis and VEGF signaling are essential events in endochondral ossification. An inhibitor of VEGF receptor tyrosine kinase activity should therefore prevent further ossification in the epiphyseal growth plates of growing animals (growth plates are closed in adults) and increase the zone of hypertrophy. AZD2171 produced a dose-dependent increase in the hypertrophic chondrocyte zone of the tibial and femoral growth plates in female rats (Fig. 5*A* and *B*). Administration of 1.25, 2.5, or 5.0 mg per kg per day AZD2171 (p.o.) increased the combined epiphyseal growth plate area by 36%, 283%, and 481%, respectively. A further 28-day period without treatment (subsequent to administration of 5 mg per kg per day AZD2171 for 28 days) resulted in complete reversal of this phenotype (Fig. 5*C*).

[5] Unpublished data.

The rapid development and growth of the ovarian corpus luteum is also critically dependent upon vascular growth. This angiogenic process is predominantly regulated by VEGF. An ovarian cycle time of only 4 days in rat means that histologic sections of an ovary reveal a dynamic picture of preovulatory and regressing follicles. Chronic administration of AZD2171 (5 mg per kg per day p.o. for 28 days) afforded a marked reduction in luteal area when compared with the ovaries of control (vehicle treated) animals (67% inhibition: Fig. 5*D* and *E*).

The effect of AZD2171 treatment on bone growth plate and ovary is supportive of inhibition of VEGF-induced angiogenesis within complex physiologic settings.

AZD2171 shows broad-spectrum activity in human tumor models at doses that are well tolerated. Once-daily oral administration of AZD2171 (1.5 mg per kg per day) inhibited growth of all human tumor xenografts examined in *nude* mice, irrespective of the histologic type (Table 4; Fig. 6). Statistically significant growth inhibition was obtained with 0.75 mg per kg per day AZD2171 in three of five tumor models examined, and the growth of each tumor model inhibited by >90% following administration of 6 mg per kg per day. AZD2171 treatment was well tolerated; following continuous administration of 6 mg per kg per day for 3 weeks (data accumulated from all experiments over 21 days), body weights were comparable with pretreatment values and only 1.5 % different to those of control animals (Fig. 6*B*). This is particularly notable when the weight of the additional tumor burden in control animals is considered. The broad-spectrum antitumor activity observed with AZD2171 may be attributed to a common effect on tumor vasculature, and its good tolerability to a comparatively selective profile *in vivo*.

AZD2171 induces vascular regression in human lung tumor xenografts. To determine whether AZD2171 affects the survival and morphology of tumor vasculature, mice bearing established Calu-6 tumors were randomized and treated chronically with AZD2171 (6 mg per kg per day) or vehicle. Mice were removed from each group at intervals to compare changes in tumor vascular area and vessel number (Fig. 7*A*). The mean control Calu-6 tumor volume was found to increase by ~6-fold over the 21-day period examined, and AZD2171 treatment was found to inhibit this tumor growth by 68% (Fig. 7*A*).

Immunohistochemical analysis of control tumors indicated that when the CD31-positive area or number of microvessels were normalized to tumor area, the values remained relatively constant throughout the duration of the experiment, irrespective

Table 3. AZD2171 inhibition of growth factor–stimulated cellular proliferation

Cell type	Growth factor	IC_{50} (μmol/L)*, mean ± SE	No. independent tests
HUVEC	VEGF	0.0004 ± 0.0002	6
	bFGF	0.11 ± 0.01	9
	EGF	0.50 ± 0.09	9
MG63	PDGF-AA	0.04 ± 0.007	3

*The effect of AZD2171 on growth factor–stimulated proliferation was examined using human endothelial cells (HUVEC) or MG63 human osteosarcoma tumor cells.

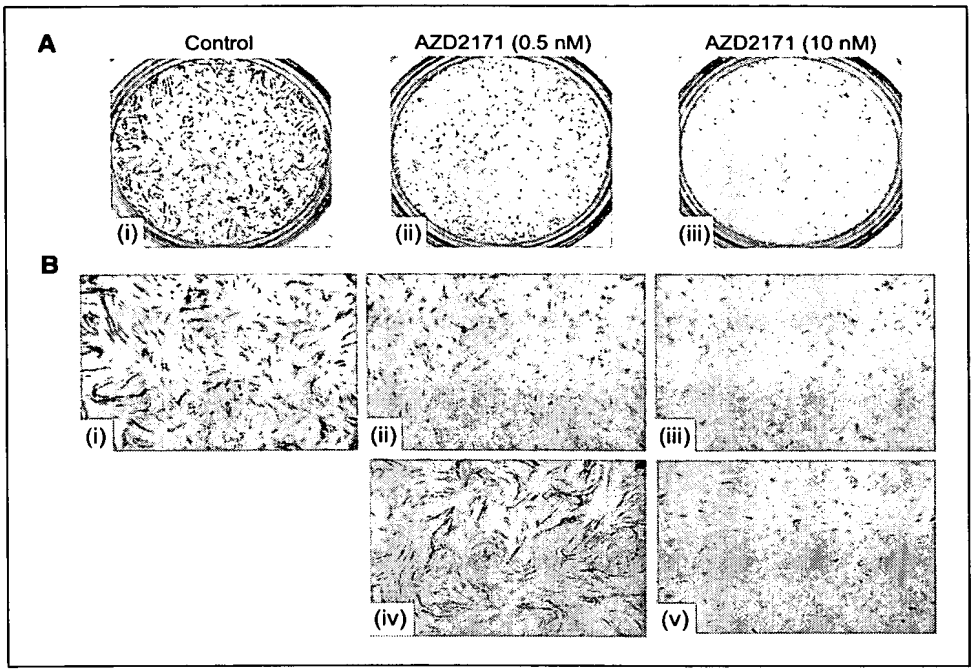

Figure 3. AZD2171 inhibits tubule growth *in vitro*. HUVECs and human fibroblasts were obtained as commercial cocultures (AngioKit, TCS Cellworks). Cells were maintained in MCDB 131 medium with 2% FCS in the presence or absence of AZD2171 for 10 days, after which they were fixed and immunostained for CD31. *A*, whole well (24-well plate) image of (*i*) control or AZD2171-treated cocultures [(*ii*) 0.5 nmol/L and (*iii*) 10 nmol/L]. *B*, magnification (×4) of (*i*) control, (*ii*) 0.5 nmol/L AZD2171 treated, (*iii*) 10 nmol/L AZD2171 treated, (*iv*) 30 μg/mL control immunoglobulin G antibody treated, and (*v*) following treatment with 30 μg/mL of an antihuman VEGF antibody. While the VEGF-neutralizing antibody suppressed tubule growth significantly, it remained unaffected by treatment with the isotype control. Morphometric image analysis of whole wells indicated that AZD2171 inhibited tubule branching, length, and area with an IC_{50} value of ≤0.2 nmol/L.

of the accompanying volume change (Fig. 7*B* and *C*). Whereas an apparent difference (P = 0.02, one-tailed t test) was found between CD31 area (per 5,000 μm^2) on day 1 versus day 21, the CD31 area measured on day 1 was higher than in all subsequent groups, including day 2 where tumor volumes were directly comparable. The CD31 area on day 21 was not significantly different (P = 0.3) from that measured on day 2 (Fig. 7*B*), and the vessel density (number of vessels per 5,000 μm^2) on day 21 was not significantly different from that on day 1 (P = 0.3; Fig. 7*C*).

With acute AZD2171 treatment (day 1: two doses of AZD2171 given 28 and 4 hours before sampling) neither vascular variable was affected significantly. However, following an additional dose of AZD2171 (i.e., day 2: AZD2171 given at 52, 28, and 4 hours before sampling), a 47% reduction in vessel number was observed (P = 0.02), accompanied by a 40% reduction in CD31 area that was just outside statistical significance (P = 0.06). By day 21, vessel number and CD31 area were reduced by ≥70% (P < 0.005). These data indicate that AZD2171 can cause significant vascular regression in tumors. The rapid onset of vessel regression is most probably due to a direct effect of AZD2171 on tumor endothelium, which is likely to be derived from potent inhibition of VEGF signaling.

Discussion

Inhibition of VEGF signaling is being pursued avidly as a therapeutic strategy in oncology, to inhibit angiogenesis, neovascular survival, and vascular permeability in tumors. These VEGF-induced responses are thought dependent upon the KDR signal transduction in endothelial cells (18, 19, 32). AZD2171 may therefore have potential as an antitumor therapy, by virtue of its potent inhibitory activity against KDR tyrosine kinase. Subnanomolar IC_{50} values were obtained when AZD2171 was examined against recombinant KDR kinase activity and VEGF-induced KDR phosphorylation in human endothelial cells, with concomitant inhibition of VEGF-induced phenotypes.

AZD2171 also showed activity at low nanomolar concentrations in enzyme assays, versus the kinases associated with the two other VEGF receptor family members, Flt-1 and Flt-4. The exact role of Flt-1 signaling in physiologic and pathologic angiogenesis remains unclear. Flt-1 has a relatively weak signaling capacity *in vitro* and, in contrast to KDR, a number of reports suggest that its stimulation has minimal effects on mitogenic, motogenic, or permeability responses in endothelial cells (33–35). Flt-1 with a deleted kinase domain has also been shown to support normal vascular development in mice, suggesting that Flt-1–stimulated angiogenic sprouting may be mediated by ligand sequestration, to regulate the spatial availability of VEGF, rather than via an intrinsic signaling response (36). Despite these observations, Flt-1 has been shown to co-operate directly with KDR via heterodimerization, and Flt-1 homodimers may transactivate KDR through cross-talk (37). Furthermore, Flt-1 alone can bind two additional VEGF homologues, PlGF and VEGF-B, and the former has been shown, under experimental *in vitro* conditions, to induce differential signaling through Flt-1 when compared with VEGF itself (37). These findings support the possibility that direct inhibition of Flt-1 tyrosine kinase may be beneficial. In contrast to Flt-1, Flt-4 does not bind VEGF, PlGF, or VEGF-B but only binds the homologues VEGF-C and VEGF-D. This receptor has a critical role in lymphangiogenesis (38) and a prognostic link with expression of VEGF-C and/or VEGF-D and nodal metastasis has been identified for different tumor types (39, 40). Experimentally, lymph node metastasis can be promoted by expression of VEGF-C (41) and inhibited with an antibody to Flt-4 (42). Direct inhibition of Flt-4 signaling may therefore also have therapeutic benefit in limiting subsequent tumor dissemination. However, it has recently been suggested that KDR heterodimerization (induced by VEGF-C or VEGF-D) is required for ligand-stimulated phosphorylation of Flt-4 and its

associated cellular signaling (43); a dependency that would be perturbed directly by a KDR tyrosine kinase inhibitor. Determining the full relevance of AZD2171 activity against Flt-1 and Flt-4 kinase will necessitate additional investigation of receptor signaling in cells.

The selectivity of an ATP-competitive kinase inhibitor *in vivo* is dependent upon the comparative potency of the compound against a target, the degree of inhibition required to prevent a given phenotypic effect and the level of plasma/tissue exposure attained at the evaluated dose. Collectively, the enzyme, receptor phosphorylation, and cellular proliferation data obtained with AZD2171 indicate that it has selectivity for inhibition of VEGF signaling but also suggest that it may have relevant activity versus c-Kit tyrosine kinase which could provide added therapeutic benefit in the treatment of c-Kit–dependent tumors (44, 45). That large concentrations of AZD2171 were required to inhibit the growth of tumor cells directly *in vitro*, and that AZD2171 was particularly well tolerated in tumor xenograft models at doses that proved highly efficacious, is in further support of a selective inhibitory profile.

AZD2171 combines potent activity versus KDR tyrosine kinase and selectivity with pharmacokinetic properties that are appropriate for oral once-daily administration. In female rat, studies examining i.v. (5 mg/kg) and oral (30 mg/kg) dosing of AZD2171 revealed a terminal plasma half-life of 9 hours, a relatively low clearance of 0.8 L per hour per kg, an oral bioavailability of 60%, and an unbound plasma fraction of 6% (data not shown). For this reason, all preclinical *in vivo* work was conducted by daily oral gavage.

AZD2171 treatment inhibited physiologic processes that are critically dependent upon VEGF signaling and angiogenesis. During endochondral bone formation, VEGF expression by hypertrophic chondrocytes regulates metaphyseal angiogenesis (46), with capillaries that invade the cartilage expressing both Flt-1 and KDR (47). This vascular invasion is critical to enable the terminal differentiation and apoptosis of growth plate chondrocytes, matrix resorption by osteoclasts, and mineralization by osteoblasts. The survival of osteoclasts (48) and migration and differentiation of osteoblastic cells (49, 50), both of which express Flt-1 and KDR, can also be influenced directly by VEGF signaling. Furthermore, chondrocyte survival has recently been suggested to have a VEGF dependency (51). Consistent with a fundamental regulatory role for VEGF signaling in bone morphogenesis, AZD2171 perturbed endochondral ossification in growing rats significantly and produced a marked growth plate hypertrophy; a phenotype also

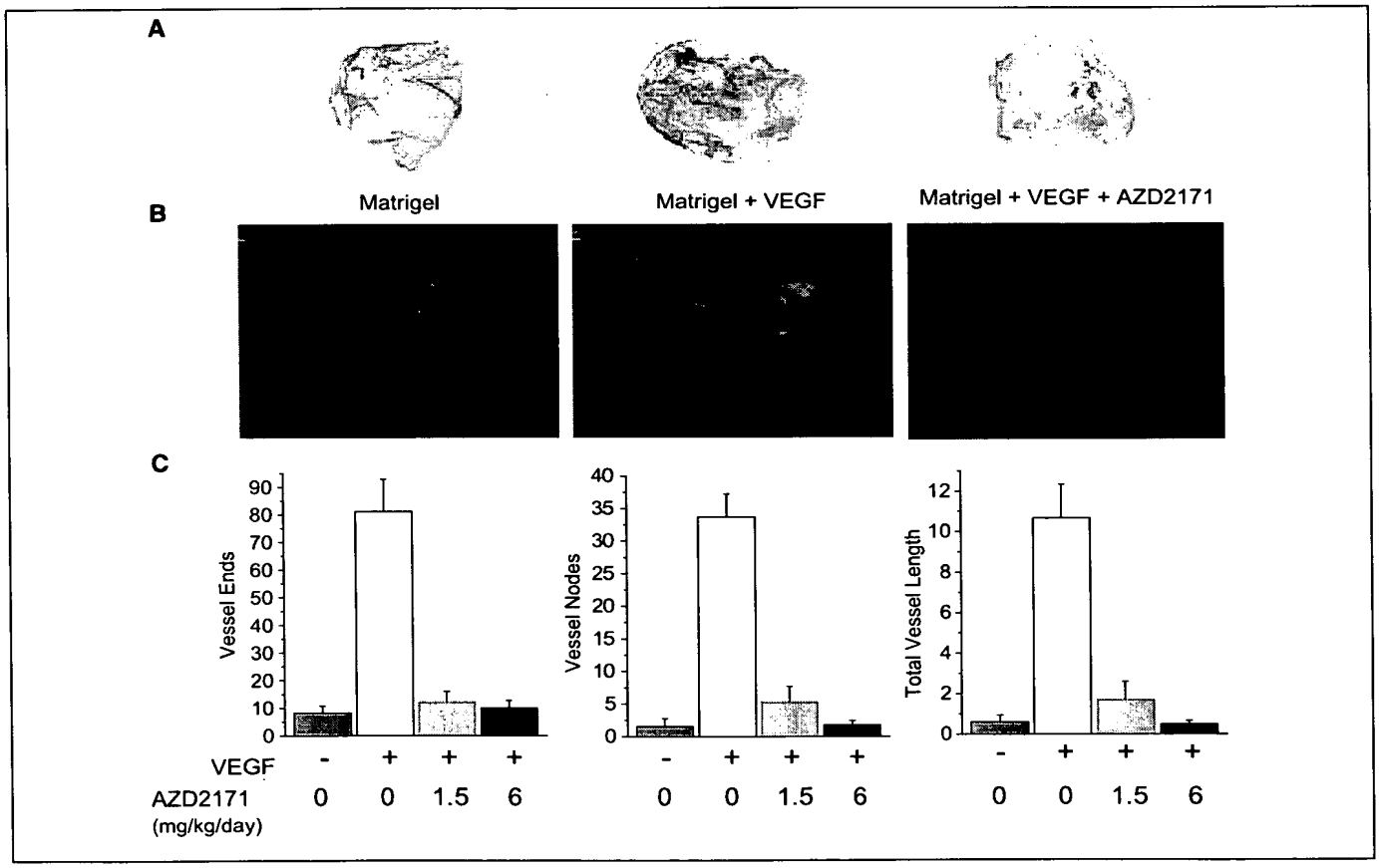

Figure 4. AZD2171 inhibits VEGF-induced angiogenesis *in vivo*. Matrigel plugs containing VEGF were implanted s.c. in nude mice. AZD2171 (1.5 or 6 mg per kg per day) or vehicle was administered orally, from the day of implantation, and vessel development quantitated after 8 days. *A*, representative plugs retrieved at day 8. *B*, corresponding immunofluorescent images of CD31 staining (red is anti-CD31 staining and blue is a DAPI counterstain). *C*, CD31 images from Matrigel plugs were analyzed using a skeletonization program, which enabled the number of vessel ends, branch points and total vessel length to be quantitated. Values (mean ± SE) were derived from seven to 10 independent images per sample, with five samples per group. *P*s (one-tailed *t* test) were ≤0.001 for AZD2171-treated versus control (Matrigel containing VEGF) for all variables examined.

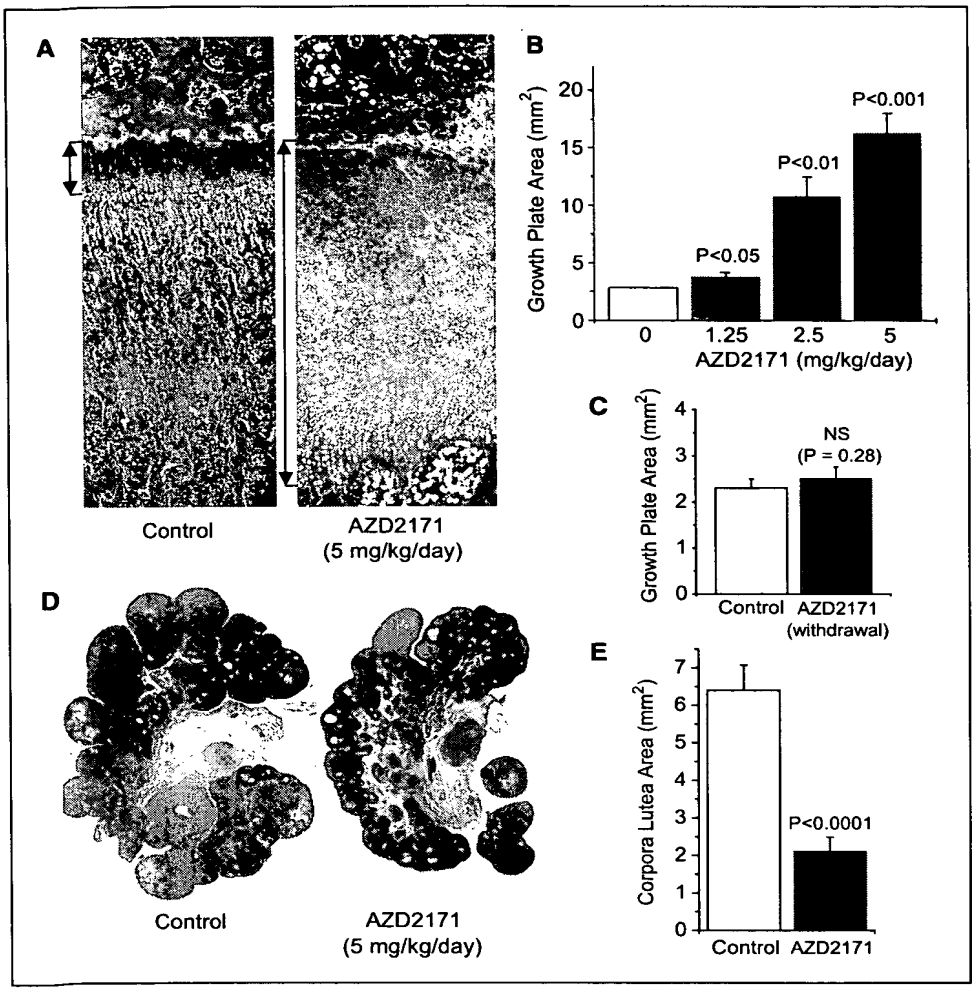

Figure 5. Consequences of inhibiting VEGF signaling and physiologic angiogenesis *in vivo*: effect of AZD2171 on bone morphogenesis and ovarian cycling in young female rats. *A*, H&E-stained tibial epiphyseal growth plate (×5) showing severe epiphyseal growth plate dysplasia following AZD2171 treatment (5 mg per kg per day, p.o. for 28 days). *B*, morphometric image analysis of the combined tibial and femoral growth plates following 28 days of AZD2171 treatment reveals a dose-dependent epiphyseal hypertrophy (five per group). *C*, epiphyseal hypertrophy is reversed completely 28 days after AZD2171 withdrawal (five per group). *D*, AZD2171 treatment (5 mg per kg per day, p.o. for 28 days) also induces a marked reduction in the number of corpora lutea in ovary, when compared to vehicle-treated rats. H&E-stained section, ×2.5. *E*, morphometric image analysis of total corpora lutea area (7-10 ovaries per group) following treatment with vehicle or AZD2171 (5 mg per kg per day, p.o. for 28 days). *P*s were derived using a one-tailed *t* test.

induced by VEGF sequestration (52) or conditional knockout of VEGF in cartilage (53). Whereas this phenotype has also been reported with other VEGF receptor tyrosine kinase inhibitors (26, 30), the doses of AZD2171 that produce significant effects are comparatively much lower. The magnitude of hypertrophy induced by AZD2171 has also not been shown previously. This phenotype was reversed completely following an additional 28-day period of AZD2171 withdrawal, indicating that chronic inhibition of VEGF signaling is required to maintain an effect *in vivo*. In addition to inhibiting ossification in bone growth plate, AZD2171 also markedly reduced corpora luteal area in rat ovary. The cyclic corpus luteum of the ovary is considered the site of strongest physiologic angiogenesis, with rapid luteal development involving distinct phases of VEGF-dependent blood vessel growth and maturation, followed by vessel regression during luteolysis that involves endothelial cell detachment (54). This is the first study to report the effects of a VEGF receptor kinase inhibitor on follicular development, although a soluble VEGF receptor construct has been previously found to have inhibitory effects on corpora luteal angiogenesis and development in mice (55) and a KDR blocking antibody shown to significantly delay follicular development in rhesus monkey (56). Analogous changes in bone growth plate and ovary have also been observed in primate following treatment with the VEGF-neutralizing antibody, bevacizumab (57).

AZD2171 (1.5 and 6 mg per kg per day) completely abolished VEGF-dependent angiogenesis *in vivo*, in a s.c. Matrigel plug assay, suggesting that it might also inhibit tumor growth at comparatively small doses. Doses of 6 mg per kg per day AZD2171 and lower were examined for activity in a panel of established, histologically distinct (colon, lung, prostate, breast, and ovary), human tumor xenograft models in athymic mice. Statistically significant inhibition was obtained with 1.5 mg per kg per day AZD2171 in all models and with 0.75 mg per kg per day in a number of models. The broad-spectrum antitumor profile observed with AZD2171 is consistent with an effect on tumor vasculature, a common growth-limiting target in all models, as opposed to tumor cell targets that are subject to variable expression and dependency. AZD2171 was efficacious at doses that are significantly lower than reported with other VEGFR tyrosine kinase inhibitors, which require administration within the 20 to 100 mg per kg per day range to achieve significant inhibition of tumor growth in mice (24–26).

To investigate temporal changes in tumor vessel growth and survival following AZD2171 treatment, a Calu-6 lung tumor

Table 4. Chronic oral once-daily administration of AZD2171 inhibits established human tumor xenograft growth

Tumor xenograft	Tumor origin	Dose (mg/kg/d)	Tumor age at treatment onset (d)	No. doses	% Inhibition of tumor volume	Significance (*t* test, one-tailed)
SW620	Colon	6.0	5	28	94	<0.001
		3.0	5	28	73	<0.001
		1.5	5	28	43	<0.001
		0.75	5	28	37	<0.01
Calu-6	Lung	6.0	10	28	91	<0.001
		3.0	10	28	69	<0.001
		1.5	10	28	49	<0.01
		0.75	10	28	26	NS
PC-3	Prostate	6.0	14	28	98	<0.001
		3.0	14	28	84	<0.001
		1.5	14	28	39	<0.01
		0.75	14	28	18	NS
MDA-MB-231	Breast	6.0	14	24	>100	<0.001
		3.0	14	24	99	<0.001
		1.5	14	24	75	<0.001
		0.75	14	24	65	<0.001
SKOV-3	Ovary	6.0	18	28	>100	<0.001
		3.0	18	28	>100	<0.001
		1.5	18	28	81	<0.01
		0.75	18	28	52	<0.05

NOTE: Nude mice bearing established human tumor xenografts (0.1-0.5 cm^3 volume) were treated orally, once daily with AZD2171 (0.75-6 mg/kg/d) or vehicle [a 1% (w/v) solution of polyoxyethylene (20) sorbitan mono-oleate in deionized water]. Percentage tumor growth inhibition was calculated as the difference between the mean change in control and AZD2171-treated tumor volumes over the period of treatment. Statistical significance was examined on log-transformed data using a one-tailed *t* test (NS, $P > 0.05$). Mean control tumor volumes at the start of treatment were 0.2 cm^3, with the exception of SKOV-3 tumors that were 0.3 cm^3. Control tumor volumes at the end of vehicle treatment were 1.5 ± 0.1 cm^3 (SW620), 1.1 ± 0.1 cm^3 (Calu-6) 0.7 ± 0.1 cm^3 (PC-3), 1.8 ± 0.2 cm^3 (MDA-MB-231), and 0.9 ± 0.1 cm^3 (SKOV-3).
Abbreviation: NS, not significant.

xenograft model was examined, which is known to be growth inhibited by VEGF inhibition but does not regress in response to treatment (29). Vascular density in control Calu-6 tumors did not change significantly during 21 days of growth. In contrast, a comparison of vascular density in AZD2171-treated tumors with corresponding time-matched controls revealed a 47% reduction after 52 hours of treatment and a 73% reduction following 3 weeks of treatment. These data indicate that progressive vascular

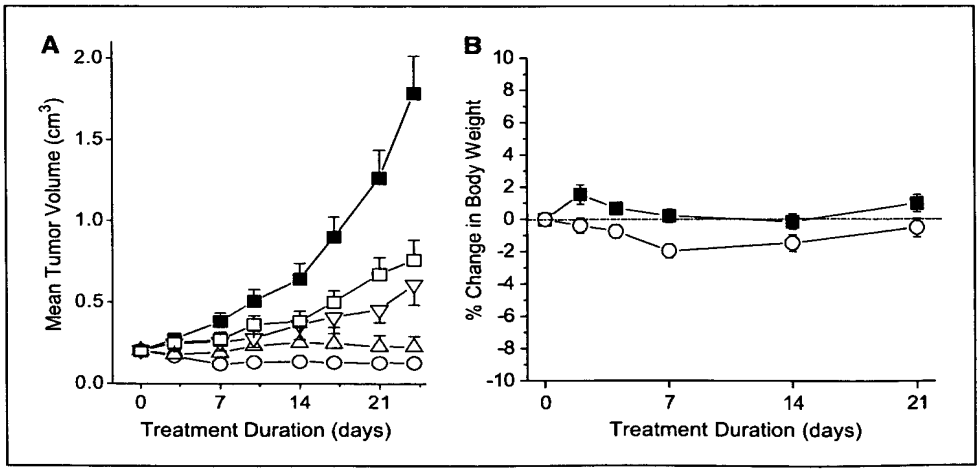

Figure 6. AZD2171 inhibits human tumor xenograft growth at doses that are well tolerated. *A*, effect of AZD2171 (□, 0.75 mg per kg per day; ▽, 1.5 mg per kg per day; △, 3 mg per kg per day; ○, 6 mg per kg per day) or vehicle (■) on growth of MDA-MB-231 human breast tumor xenografts. Xenografts were established s.c. in athymic mice and allowed to reach a volume of 0.2 ± 0.01 cm^3 (mean ± SE) before treatment. Once-daily oral administration of AZD2171 or vehicle then commenced and was continued for the duration of the experiment. *Points*, mean from 10 to 11 mice; *bars*, SE in one direction. *B*, percentage change in mouse body weight over a 21-day period, when treated chronically with vehicle (■) or 6 mg per kg per day AZD2171 (○). The analysis combines body weight data from all mice, bearing colon, lung, prostate, breast, or ovarian tumor xenografts, described in Table 4.

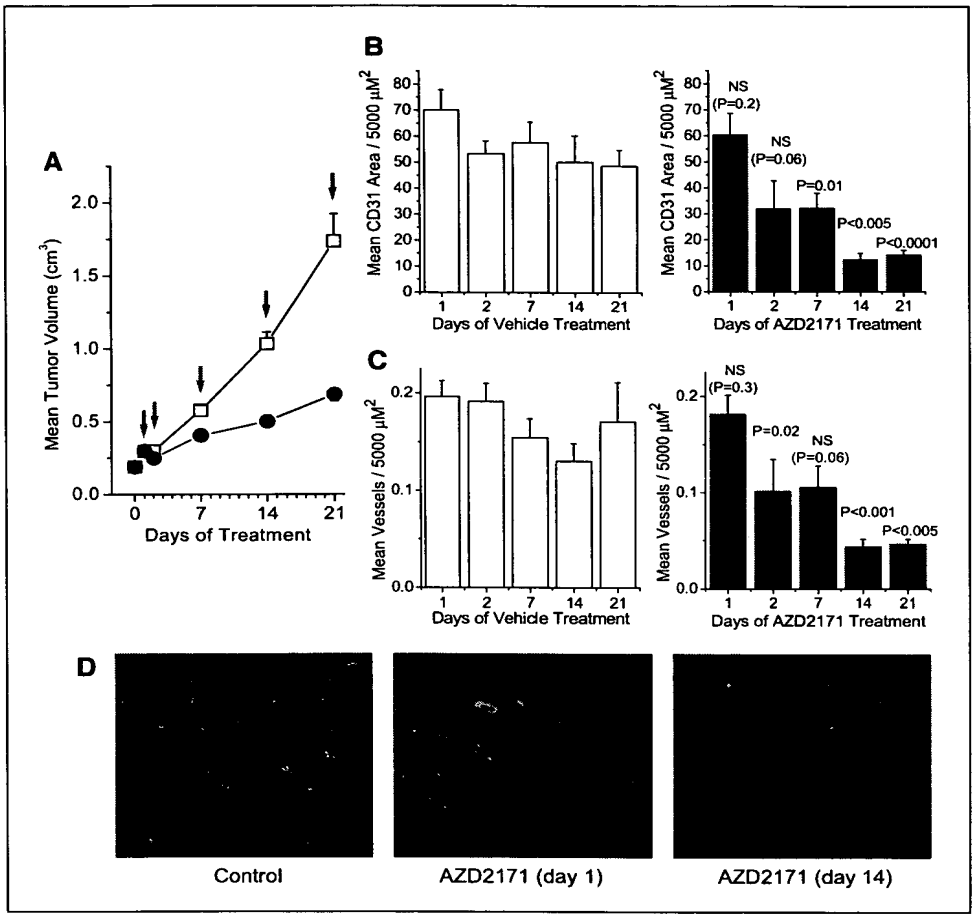

Figure 7. AZD2171 causes vascular regression in Calu-6 lung tumor xenografts. *A*, Calu-6 tumors were established s.c. in nude mice and treated daily (from day 0) with vehicle (□) or 6 mg per kg per day AZD2171 (●). At intervals (*arrows*) tumors (n = 6-15) were collected from each group, 4 hours after dosing with vehicle or AZD2171, to enable CD31 to be determined by immunohistochemistry. *B*, mean CD31 area per 5,000 μm^2 of tumor and (*C*) mean vessel number per 5,000 μm^2 of tumor, for vehicle-treated (*open columns*) and AZD2171-treated (*blue columns*) tumors. The statistical significance of AZD2171 treatment was examined versus the respective time-matched control using a one-tailed t test. While CD31 area and vessel number (both normalized to area) remain relatively constant in control tumors, a ≥70% reduction in both variables was evident following AZD2171 treatment for 21 days. *D*, immunofluorescent images of representative sections from control tumors or those treated with AZD2171 (6 mg per kg per day) and sampled on day 1 or 14. *Green*, CD31 staining; *blue*, DAPI counterstain.

regression occurs in human tumor xenografts treated chronically with AZD2171, demonstrating that inhibition of VEGF signaling can have a potent antivascular effect. A number of preclinical studies with VEGF sequestering agents have also shown evidence of reduced vascular density in tumors following treatment. These include regression of existing tumor vessels with a VEGFR-Fc fusion construct in tumor bearing RIP-Tag2 transgenic mice (58), a KDR blocking antibody in squamous cell tumor xenografts (59), and a VEGF-neutralizing antibody in LS174T colon tumor xenografts (60). Primitive vessels are believed to be susceptible to VEGF blockade, because their survival is highly dependent upon KDR mediated Akt/PKB signaling (8). These data serve to emphasize that the consequences of inhibiting VEGF signaling in pathologic conditions may extend beyond simply preventing new vessel growth.

That inhibition of VEGF signaling can provide clinical benefit to patients with solid tumors, has been confirmed recently by bevacizumab (Avastin, Genentech, South San Francisco, CA), a monoclonal antibody to VEGF-A. In combination with irinotecan, 5-fluorouracil and leucovorin, bevacizumab imparts a significant prolongation of survival and response variables in patients with first-line metastatic colorectal cancer (61). An additional small preoperative biomarker study has also suggested antivascular effects in rectal carcinoma patients, following bevacizumab treatment (62). Direct inhibition of KDR tyrosine kinase activity with a small molecule, such as AZD2171, is an alternative therapeutic approach that may afford advantages to sequestration of VEGF. Inhibiting the kinase domain of KDR is mechanistically different, in that it should prevent receptor signaling irrespective of the activating ligand. In addition to VEGF-A, the fully proteolytically cleaved forms of the related VEGF gene family members VEGF-C and VEGF-D can also bind to and activate KDR (63, 64). In particular, VEGF-C can induce proliferative, migratory, tubulogenic, and permeability responses through KDR (63, 65). Chronic administration of a small molecule to generate steady state plasma levels may also provide a pharmacokinetic advantage, because the distribution and clearance of a large biopharmaceutical may possibly be influenced more highly by heterogeneous tumor anatomy and variable tumor blood flow (66).

In summary, AZD2171 is a highly potent inhibitor of KDR tyrosine kinase that has pharmacokinetic properties suitable for once-daily oral administration. VEGF-induced angiogenesis, neovascular survival, and growth of human tumor xenografts, are inhibited significantly by AZD2171, at comparatively low doses. AZD2171 is currently being evaluated in clinical trials as a once-daily oral therapy for the treatment of a variety of malignancies. Encouragingly, these clinical studies indicate that AZD2171 retains a good pharmacokinetic profile in man, with dose-proportional increases in plasma exposure and a mean terminal plasma half-life of 20 hours (67).

Acknowledgments

Received 12/9/2004; revised 2/16/2005; accepted 3/2/2005.

The costs of publication of this article were defrayed in part by the payment of page charges. This article must therefore be hereby marked *advertisement* in accordance with 18 U.S.C. Section 1734 solely to indicate this fact.

We thank Karen Malbon, Claire Barnes, Minwei Ye, Stephen Brightwell, John Stawpert, and Sandra Oakes for the technical assistance in selectivity testing; Kevin Randal for morphometric image analysis; David Blowers, Ian Taylor, Hazel Weir, and Rick Davies for protein production and purification; Mick Shaw for the isolation and supply of HUVECs; and Michel Vautier for doing the initial synthesis of AZD2171.

References

1. Ferrara N. VEGF and the quest for tumour angiogenesis factors. Nat Rev Cancer 2002;2:795–803.
2. Rousseau S, Houle F, Huot J. Integrating the VEGF signals leading to actin-based motility in vascular endothelial cells. Trends Cardiovasc Med 2000;10:321–7.
3. Keck PJ, Hauser SD, Krivi G, et al. Vascular permeability factor, an endothelial cell mitogen related to PDGF. Science (Washington DC) 1989;246: 1309–12.
4. Lamoreaux WJ, Fitzgerald ME, Reiner A, Hasty KA, Charles ST. Vascular endothelial growth factor increases release of gelatinase A and decreases release of tissue inhibitor of metalloproteinases by microvascular endothelial cells *in vitro*. Microvasc Res 1998;55: 29–42.
5. Senger DR, Ledbetter SR, Claffey KP, Papadopoulos-Sergio A, Perruzzi CA, Detmar M. Stimulation of endothelial cell migration by vascular endothelial growth factor through cooperative mechanisms involving the $\alpha v\beta 3$ integrin, osteopontin, and thrombin. Am J Pathol 1996;149:293–305.
6. Asahara T, Takahashi T, Masuda H, et al. VEGF contributes to postnatal neovascularisation by mobilizing bone marrow-derived endothelial progenitor cells. EMBO J 1999;18:3964–72.
7. Koolwijk P, Peters E, van der Vecht B, et al. Involvement of VEGFR-2 (kdr/flk-1) but not VEGFR-1 (flt-1) in VEGF-A and VEGF-C induced tube formation by human microvascular endothelial cells in fibrin matrices *in vitro*. Angiogenesis 2001;4:53–60.
8. Gerber H-P, McMurtrey A, Kowalski J, et al. Vascular endothelial growth factor regulates endothelial survival through the phosphatidylinositol 3′-kinase/Akt signal transduction pathway. Requirement for Flk-1/KDR activation. J Biol Chem 1998;273:30336–43.
9. Benjamin LE, Hemo I, Keshet E. A plasticity window for blood vessel remodelling is defined by pericyte coverage of the preformed endothelial network and is regulated by PDGF-B and VEGF. Development 1998;125: 1591–8.
10. Bates DO, Heald RI, Curry FE, Williams B. Vascular endothelial growth factor increases Rana vascular permeability and compliance by different signalling pathways. J Physiol (Lond) 2001;533:263–72.
11. Rak J, Mitsuhashi L, Bayo L, et al. Mutant *ras* oncogenes upregulate VEGF/VPF expression: implications for induction and inhibition of tumour angiogenesis. Cancer Res 1995;55:4575–80.
12. Mukhopadhyay D, Knebelmann B, Cohen HT, Anath S, Sukhatme VP. The von Hippel-Lindau tumor suppressor gene product interacts with Sp1 to repress vascular endothelial growth factor promoter activity. Mol Cell Biol 1997;17:5629–39.
13. Zhou YZ, Xiong YX, Wu XT, et al. Inactivation of PTEN is associated with increased angiogenesis and VEGF overexpression in gastric cancer. World J Gastroenterol 2004;10:3225–9.
14. Shweiki D, Neeman M, Itin A, Keshet E. Induction of vascular endothelial growth factor expression by hypoxia and by glucose deficiency in multicell spheroids: implications for tumor angiogenesis. Proc Natl Acad Sci U S A 1995;92:768–72.
15. Tse V, Xu L, Yung YC, et al. The temporal-spatial expression of VEGF, angiopoietins-1 and -2, and Tie-2 during tumor angiogenesis and their functional correlation with tumor neovascular architecture. Neurol Res 2003;25:729–38.
16. Wiesmann C, Fuh G, Christinger HW, Eigenbrot C, Wells JA, de Vos AM. Crystal structure at 1.7 Å resolution of VEGF in complex with domain 2 of the Flt-1 receptor. Cell 1997;91:695–704.
17. Lu D, Kussie P, Pytowski B, et al. Identification of the residues in the extracellular region of KDR important for interaction with vascular endothelial growth factor and neutralizing KDR-antibodies. J Biol Chem 2000;275: 14321–30.
18. Meyer M, Clauss M, Lepple-Wienhues A, et al. A novel vascular endothelial growth factor encoded by Orf virus, VEGF-E, mediates angiogenesis via signalling through VEGFR-2 (KDR) but not VEGFR-1 (Flt-1) receptor tyrosine kinase. EMBO J 1999;18:363–74.
19. Gille H, Kowalski J, Li B, et al. Analysis of biological effects and signalling properties of Flt-1 and KDR: a reassessment using novel highly receptor-specific VEGF mutants. J Biol Chem 2001;244:3222–30.
20. Takahashi T, Ueno H, Shibuya M. VEGF activates protein kinase-C dependent, but Ras-independent Raf-MEK-MAP kinase pathway for DNA synthesis in primary endothelial cells. Oncogene 1999;18:2221–30.
21. Rousseau S, Houle F, Kotanides H, et al. Vascular endothelial growth factor (VEGF)-driven actin-based motilityis mediated by VEGFR2 and requires concerted activation of stress-activated protein kinase 2 (SAPK2/p38) and geldanamycin-sensitive phosphorylation of focal adhesion kinase. J Biol Chem 2000;275:10661–72.
22. Carmeliet P, Lampugnani MG, Moons L, et al. Targeted deficiency or cytosolic truncation of the VE-cadherin gene in mice impairs VEGF-mediated endothelial survival and angiogenesis. Cell 1999;98:147–57.
23. Folkman J. Tumor angiogenesis: therapeutic implications. N Engl J Med 1971;285:1182–6.
24. Wood JM, Bold G, Buchdunger E, et al. PTK787/ZK 222584, a novel and potent inhibitor of vascular endothelial growth factor receptor tyrosine kinases, impairs vascular endothelial growth factor-induced responses and tumor growth after oral administration. Cancer Res 2000;60:2178–89.
25. Mendel DB, Laird AD, Xin X, et al. *In vivo* antitumor activity of SU11248, a novel tyrosine kinase inhibitor targeting vascular endothelial growth factor and platelet-derived growth factor receptors: determination of a pharmacokinetic/pharmacodynamic relationship. Clin Cancer Res 2003;9:327–37.
26. Beebe JS, Jani JP, Knauth E, et al. Pharmacological characterization of CP-547,632, a novel vascular endothelial growth factor receptor-2 tyrosine kinase inhibitor for cancer therapy. Cancer Res 2003;63:7301–9.
27. Sepp-Lorenzino L, Rands E, Mao X, et al. A novel orally bioavailable inhibitor of kinase insert domain-containing receptor induces antiangiogenic effects and prevents tumor growth *in vivo*. Cancer Res 2004;64: 751–6.
28. Hennequin LF, Thomas AP, Johnstone C, et al. Design and structure-activity relationship of a new class of potent VEGF receptor tyrosine kinase inhibitors. J Med Chem 1999;42:5369–89.
29. Wedge SR, Ogilvie DJ, Dukes M, et al. ZD6474 inhibits vascular endothelial growth factor signaling, angiogenesis, and tumor growth following oral administration. Cancer Res 2002;62:4645–55.
30. Wedge SR, Ogilvie DJ, Dukes M, et al. ZD4190: an orally active inhibitor of vascular endothelial growth factor signaling with broad-spectrum antitumor efficacy. Cancer Res 2000;62:970–5.
31. Wild R, Ramakrishnan S, Sedgewick J, Griffioen AW. Quantitative assessment of angiogenesis and tumor vessel architecture by computer-assisted digital image analysis: effects of VEGF-toxin conjugate on tumor microvessel density. Microvasc Res 2000;59: 368–76.
32. Zeng H, Sanyal S, Mukhopadhyay D. Tyrosine residues 951 and 1059 of vascular endothelial growth factor receptor-2 (KDR) are essential for vascular permeability factor/vascular endothelial growth factor-induced endothelium migration and proliferation, respectively. J Biol Chem 2001;276:32714–9.
33. Waltenberger J, Claesson-Welsh L, Siegbahn A, Shibuya M, Heldin CH. Different signal transduction properties of KDR and Flt-1, two receptors for vascular endothelial growth factor. J Biol Chem 1994; 269:26988–95.
34. Rahimi N, Dayanir V, Lashkari K. Receptor chimeras indicate that the vascular endothelial growth factor receptor-1 (VEGFR-1) modulates mitogenic activity of VEGFR-2 in endothelial cells. J Biol Chem 2000;275: 16986–92.
35. Hillman NJ, Whittles CE, Pocock TM, Williams B, Bates DO. Differential effects of vascular endothelial growth factor-C and placental growth factor-1 on the hydraulic conductivity of frog mesenteric capillaries. J Vasc Res 2001;38:176–86.
36. Hiratsuka S, Minowa O, Kuno J, Noda T, Shibuya M. Flt-1 lacking the tyrosine kinase domain is sufficient for normal development and angiogenesis in mice. Proc Natl Acad Sci U S A 1998;95:9349–54.
37. Autiero M, Waltenberger J, Communi D, et al. Role of PlGF in the intra- and intermolecular cross talk between the VEGF receptors Flt1 and Flk1. Nat Med 2003;9:936–43.
38. Karkkainen MJ, Haiko P, Sainio K, et al. Vascular endothelial growth factor C is required for sprouting of the first lymphatic vessels from embryonic veins. Nat Immunol 2004;5:74–80.
39. Onogawa S, Kitadai Y, Tanaka S, Kuwai T, Kimura S, Chayama K. Expression of VEGF-C and VEGF-D at the invasive edge correlates with lymph node metastasis and prognosis of patients with colorectal carcinoma. Cancer Sci 2004;95:32–9.
40. Arinaga M, Noguchi T, Takeno S, Chujo M, Miura T, Uchida Y. Clinical significance of vascular endothelial growth factor C and vascular endothelial growth factor receptor 3 in patients with nonsmall cell lung carcinoma. Cancer 2003;97:457–64.
41. Padera TP, Kadambi A, di Tomaso E, et al. Lymphatic metastasis in the absence of functional intratumor lymphatics. Science 2002;296:1883–6.
42. Shimizu K, Kubo H, Yamaguchi K, et al. Suppression of VEGFR-3 signaling inhibits lymph node metastasis in gastric cancer. Cancer Sci 2004;95:328–33.
43. Alam A, Herault J-P, Barron P, et al. Heterodimerization with vascular endothelial growth factor receptor-2 (VEGFR-2) is necessary for VEGFR-3 activity. Biochem Biophys Res Commun 2004;324:909–15.
44. Rubin BP, Singer S, Tsao C, et al. KIT activation is a ubiquitous feature of gastrointestinal stromal tumors. Cancer Res 2001;61:8118–21.
45. Beghini A, Ripamonti CB, Cairoli R, et al. KIT activating mutations: incidence in adult and pediatric acute myeloid leukaemia, and identification of an internal tandem duplication. Haematologica 2004;89: 920–5.
46. Horner A, Bishop NJ, Bord S, et al. Immunolocalisation of vascular endothelial growth factor (VEGF) in human neonatal growth plate cartilage. J Anat 1999;194: 519–24.
47. Petersen W, Tsokos M, Pufe T. Expression of VEGF121 and VEGF165 in hypertrophic chondrocytes of the human growth plate and epiphyseal cartilage. J Anat 2002;201:153–7.
48. Nakagawa M, Kaneda T, Arakawa T, et al. Vascular endothelial growth factor (VEGF) directly enhances osteoclastic bone resorption and survival of mature osteoclasts. FEBS Lett 2000;473:161–4.
49. Mayr-Wohlfart U, Waltenberger J, Hausser H, et al. Vascular endothelial growth factor stimulates chemotactic migration of primary human osteoblasts. Bone 2002;30:472–747.

50. Midy V, Plouet J. Vasculotropin/vascular endothelial growth factor induced differentiation in cultured osteoblasts. Biochem Biophys Res Commun 1994;199:380–6.
51. Zelzer E, Mamluk R, Ferrara N, Johnson RS, Schipani E, Olsen BR. VEGFA is necessary for chondrocyte survival during bone development. Development 2004; 131:2161–71.
52. Gerber H-P, Vu TH, Ryan AM, Kowalski J, Werb Z, Ferrara N. VEGF couples hypertrophic cartilage remodeling, ossification and angiogenesis during endochondral bone formation. Nature Med 1999;5:623–8.
53. Haigh JJ, Gerber H-P, Ferrara N, Wagner EF. Conditional inactivation of VEGF-A in areas of collagen2a1 expression results in embryonic lethality in the heterozygous state. Development 2000;127:1445–53.
54. Modlich U, Kaup FJ, Augustin HG. Cyclic angiogenesis and blood vessel regression in the ovary: blood vessel regression during luteolysis involves endothelial cell detachment and vessel occlusion. Lab Invest 1996; 74:771–80.
55. Ferrara N, Chen H, Davis-Smyth T, et al. Vascular endothelial growth factor is essential for corpus luteum angiogenesis. Nat Med 1998;4:336–40.
56. Zimmermann RC, Xiao E, Bohlen P, Ferin M. Administration of antivascular endothelial growth factor receptor-2 antibody in the early follicular phase delays follicular selection and development in the rhesus monkey. Endocrinology 2002;143:2496–502.
57. Ryan AM, Eppler DB, Hagler KE, et al. Preclinical safety evaluation of rhuMAbVEGF, an antiangiogenic humanized monoclonal antibody. Toxicol Pathol 1999; 27:78–86.
58. Inai T, Mancuso M, Hashizume H, et al. Inhibition of vascular endothelial growth factor (VEGF) signaling in cancer causes loss of endothelial fenestrations, regression of tumor vessels, and appearance of basement membrane ghosts. Am J Pathol 2004;165:35–52.
59. Kiessling F, Farhan N, Lichy MP, et al. Dynamic contrast-enhanced magnetic resonance imaging rapidly indicates vessel regression in human squamous cell carcinomas grown in nude mice caused by VEGF receptor 2 blockade with DC101. Neoplasia 2004;6:213–23.
60. Yuan F, Chen Y, Dellian M, Safabakhsh N, Ferrara N, Jain RK. Time-dependent vascular regression and permeability changes in established human tumor xenografts induced by an anti-vascular endothelial growth factor/vascular permeability factor antibody. Proc Natl Acad Sci U S A 1996;93:14765–70.
61. Hurwitz H, Fehrenbacher L, Novotny W, et al. Bevacizumab plus irinotecan, fluorouracil, and leucovorin for metastatic colorectal cancer. N Engl J Med 2004;350:2335–42.
62. Willett CG, Boucher Y, di Tomaso E, et al. Direct evidence that the VEGF-specific antibody bevacizumab has antivascular effects in human rectal cancer. Nat Med 2004;10:145–7.
63. Joukov V, Sorsa T, Kumar V, et al. Proteolytic processing regulates receptor specificity and activity on VEGF-C. EMBO J 1997;16:3898–911.
64. Jia H, Bagherzadeh A, Bicknell R, Duchen MR, Liu D, Zachary I. Vascular endothelial growth factor (VEGF)-D and VEGF-A differentially regulate KDR-mediated signaling and biological function in vascular endothelial cells. J Biol Chem 2004;279:36148–57.
65. Koolwijk P, Peters E, van der Vecht B, et al. Involvement of VEGFR-2 (kdr/flk-1) but not VEGFR-1 (flt-1) in VEGF-A and VEGF-C induced tube formation by human microvascular endothelial cells in fibrin matrices *in vitro*. Angiogenesis 2001;4:53–60.
66. Jayson GC, Zweit J, Jackson A, et al. Molecular imaging and biological evaluation of HuMV833 anti-VEGF antibody: implications for trial design of antiangiogenic antibodies. J Natl Cancer Inst 2002;94:1484–93.
67. Medinger M, Mross K, Zirrgiebel U, et al. Phase I dose escalation study of the highly potent VEGF receptor tyrosine kinase inhibitor, AZD2171, in patients with advanced cancers with liver metastases. Proc Am Soc Clin Oncol 2004;23:208.

Available online at www.sciencedirect.com
ScienceDirect
Experimental Eye Research 83 (2006) 1005–1016
EXPERIMENTAL EYE RESEARCH
www.elsevier.com/locate/yexer

Review

Vascular endothelial growth factor receptors: Molecular mechanisms of activation and therapeutic potentials

Nader Rahimi*

Departments of Ophthalmology and Biochemistry, School of Medicine, Boston University, Boston, MA 02118, USA

Received 10 February 2006; accepted in revised form 24 March 2006
Available online 19 May 2006

Abstract

Angiogenesis-associated eye diseases are among the most common cause of blindness in the United States and worldwide. Recent advances in the development of angiogenesis-based therapies for treatment of angiogenesis-associated diseases have provided new hope in a wide variety of human diseases ranging from eye diseases to cancer. One group of growth factor receptors critically implicated in angiogenesis is vascular endothelial growth factor receptors (VEGFR), a subfamily of receptor tyrosine kinases (RTKs). VEGFR-1 and VEGFR-2 are closely related receptor tyrosine kinases and have both common and specific ligands. VEGFR-1 is a kinase-impaired RTK and its kinase activity is suppressed by a single amino acid substitution in its kinase domain and by its carboxyl terminus. VEGFR-2 is highly active kinase, stimulates a variety of signaling pathways and broad biological responses in endothelial cells. The mechanisms that govern VEGFR-2 activation, its ability to recruit signaling proteins and to undergo downregulation are highly regulated by phosphorylation activation loop tyrosines and its carboxyl terminus. Despite their differential potentials to undergo tyrosine phosphorylation and kinase activation, both VEGFR-1 and VEGFR-2 are required for normal embryonic development and pathological angiogenesis. VEGFR-1 regulates angiogenesis by mechanisms that involve ligand trapping, receptor homodimerization and heterodimerization. This review highlights recent insights into the mechanism of activation of VEGFR-1 and VEGFR-2, and focuses on the signaling pathways employed by VEGFR-1 and VEGFR-2 that regulate angiogenesis and their therapeutic potentials in angiogenesis-associated diseases.

Keywords: vascular endothelial growth factor receptor-1 (VEGFR-1); vascular endothelial growth factor receptor-2 (VEGFR-2); FLT-1; FLK-1; angiogenesis; vasculogenesis; receptor tyrosine kinases; Src kinases; phosphoinositide 3-kinase; PLC-gamma1; c-Cbl; ubiquitination; downregulation; signal transduction; tyrosine phosphorylation

1. Introduction

VEGFR-1/FLT-1 (fms-like tyrosine kinase) and VEGFR-2/KDR/FLK-1 (fetal liver kinase) are the prototypes of a gene family encoding structurally related receptors, FLT-3/FLK-2 and FLT-4/VEGFR-3 and belong to the receptor tyrosine kinase (RTK) subfamily (Hanks and Quinn, 1991; Blume-Jensen and Hunter, 2001). VEGFR-1 and VEGFR-2 are primarily involved in angiogenesis (Yancopoulos et al., 2000) where FLT-3 and FLT-4 are involved in hematopoiesis and lymphogenesis (Jussila and Alitalo, 2000). The diversification of the VEGFR family proteins during evolution, through the advent of multiple ligands and receptors has created a decisive signaling network capable of controlling angiogenesis. Through utilization of receptor homo- and heterodimers, activated by specific and common ligands, diverse angiogenic signals are propagated. An additional level of angiogenic signaling diversity is obtained through differential activation of distinct signaling molecules downstream of each receptor.

VEGFR-1 is a kinase-impaired RTK, and may signal in the context of receptor heterodimer (Rahimi et al., 2000; Autiero et al., 2003; Neagoe et al., 2005). In contrast, VEGFR-2 is highly kinase active receptor and activates broad signaling cascades leading to diverse biological responses (Waltenberger et al.,

* Tel.: +1 617 638 5011; fax: +1 617 638 5337.
E-mail address: nrahimi@bu.edu

0014-4835/$ - see front matter © 2006 Elsevier Ltd. All rights reserved.
doi:10.1016/j.exer.2006.03.019

EXHIBIT B

1994; Meyer and Rahimi, 2003; Rahimi, 2006). Three different gene products including, PLGF, VEGF-A, VEGF-B are known to bind VEGFR-1. VEGF-A, VEGF-D and VEGF-C are known to bind VEGFR-2 (Neufeld et al., 1999; Tammela et al., 2005). VEGF-C and VEGF-D also bind to VEGFR-3, an RTK that is expressed by lymphatic endothelial cells and hematopoietic progenitor cells (Jussila and Alitalo, 2000; Tammela et al., 2005). VEGFR-1 and VEGFR-2 are structurally similar, consisting of an extracellular ligand-binding domain with a seven immunoglobulin (Ig)-like motif, a single transmembrane domain, a juxtamembrane domain, a kinase domain split by a kinase insert, and a carboxyl terminus. Overall, there is 43.2% sequence homology between VEGFR-1 and VEGFR-2. The extracellular domain of VEGFR-1 and VEGFR-2 displays 33.3% homology and the cytoplasmic region 54.6%. The kinase domains of VEGFR-1 and VEGFR-2 represent the most conserved region with 70.1% homology. In contrast, the carboxyl terminus represents the most divergent region with only 28.1% sequence homology (Fig. 1).

2. VEGFR-1 and angiogenesis

Initial evidence linking VEGFR-1 to endothelial cell function and angiogenesis was provided by targeted deletion of VEGFR-1, which resulted in early embryonic lethality due to abnormal blood vessel growth (Fong et al., 1995). Although the precise role of VEGFR-1 in endothelial cell functions is still emerging, in recent years several lines of evidence have developed that suggest VEGFR-1 may play both negative and positive roles in angiogenesis. The negative role of VEGFR-1 in angiogenesis was suggested based on the observation that loss of *VEGFR-1/flt-1* in mice caused an increase in the number of endothelial progenitors, resulting in the vascular disorganization (Fong et al., 1995, 1999). How VEGFR-1 contributes to angiogenesis in a negative manner is not fully clear. Some studies have suggested that the negative role of VEGFR-1 in angiogenesis is associated with its ability to alter endothelial cell division (Kearney et al., 2002, 2004). However, work from several laboratories indicates that selective activation of VEGFR-1, either by creating VEGFR-1 chimeras (Rahimi et al., 2000; Zeng et al., 2001) or VEGF mutants is not associated with proliferation of endothelial cells in vitro (Keyt, 1996). In these studies ligand stimulation of VEGFR-1 induced neither cell proliferation nor apoptosis. Selective activation of VEGFR-1 also did not promote cell migration or intracellular calcium release (Meyer et al., 2004a, 2004b). It could be argued that in a defined condition when VEGFR-1 is activated by a ligand that only allows receptor homodimerization and with no cross-talk with other RTKs such as VEGFR-2 and VEGFR-3, VEGFR-1 is not capable of promoting biological responses such as endothelial cell migration, cell proliferation and intercellular calcium release. In line with this notion, in a recent gene targeting study where the entire cytoplasmic region of *VEGFR-1* including its kinase domain was deleted, the knockin truncated *VEGFR-1* mice developed with no aberrant vasculogenesis (Hiratsuka et al., 1998). This was in startling contrast to the *VEGFR-1* knockout mice, which mice died in early development due to overgrowth of endothelial cells (Fong et al., 1995, 1999).

In sum, these observations reinforce the idea that VEGFR-1 may act as a decoy receptor and its function in angiogenesis may involve its ligand biding extracellular region, acting as a VEGF-trap to modulate VEGFR-2 function (Fig. 2).

It should be noted that role of VEGFR-1 in angiogenesis is far more complex than initially thought. Clearly, the ability of VEGFR-1 to modulate angiogenesis is not limited to a mechanism in which it acts as a VEGF-trapping receptor. For example, stimulation of VEGFR-1 with PLGF, (a VEGFR-1 specific ligand) promotes heterodimerization of VEGFR-1 with VEGFR-2 leading to transactivation of VEGFR-2 and angiogenesis (Autiero et al., 2003). Overexpression of PLGF, in transgenic mice is also reported to promote angiogenesis (Odorisio et al., 2002). These findings suggest that VEGFR-1 when paired with VEGFR-2 via a mechanism of heterodimerization its activity positively regulates angiogenesis. Also, it is increasingly apparent that activation of VEGFR-1 in endothelial cells and its final biological function is subject to the microenvironment of endothelial cells, in particular, the presence or absence of the other VEGFR family proteins and neuropilins (Klagsbrun et al., 2002). Likewise, VEGFR-1 homodimerization and heterodimerization may define the inhibitory or stimulatory nature of its signaling relays (Rahimi et al., 2000; Zeng et al., 2001; Autiero et al., 2003).

Another factor that may determine the nature of VEGFR-1 signaling in the endothelium microenvironment is the type of ligand being utilized to activate VEGFR-1. The nature of the signal induced by PLGF, which selectively binds VEGFR-1, might be different than that induced by VEGF-A and VEGF-B. In agreement with this idea, the impaired angiogenesis associated with *plgf* null mice was not rescued by VEGF-B (Carmelite, 2003). Also, a naturally occurring VEGF-PLGF heterodimer may favor the formation of certain heterodimerization complexes among the VEGFR family involving VEGFR-1, VEGFR-2 and neuropilins, which may activate a unique signaling pathway that might not be possible by stimulation with either VEGF or PLGF alone. It should also be noted that endothelial cells are morphologically and genetically different from each other (Cleaver and Melton, 2003) raising the possibility that variation in endothelial cells may ultimately determine or modify the nature of VEGFR-1 signaling. Finally, there are also some evidences that suggest VEGFR-1 signaling in non-endothelial cells might be different that of the endothelial cells. For example, stimulation of VEGFR-1 with PLGF in non-endothelial cells such as monocytes and trophoblasts induce cell migration and proliferation (Clauss et al., 1996; Athanassiades and Lala, 1998; Dikov et al., 2005). VEGFR-1 activity also is linked to pathological angiogenesis such as cancer and retinopathy of prematurity. It has been reported that activation of VEGFR-2 prevents pathological regression of blood vessels from oxygen-induced retinal vascular degeneration in retinopathy of prematurity (Shih et al., 2003) and VEGFR-1 is also expressed by some carcinomas and is involved in cell migration and cell invasion (Wey et al., 2005).

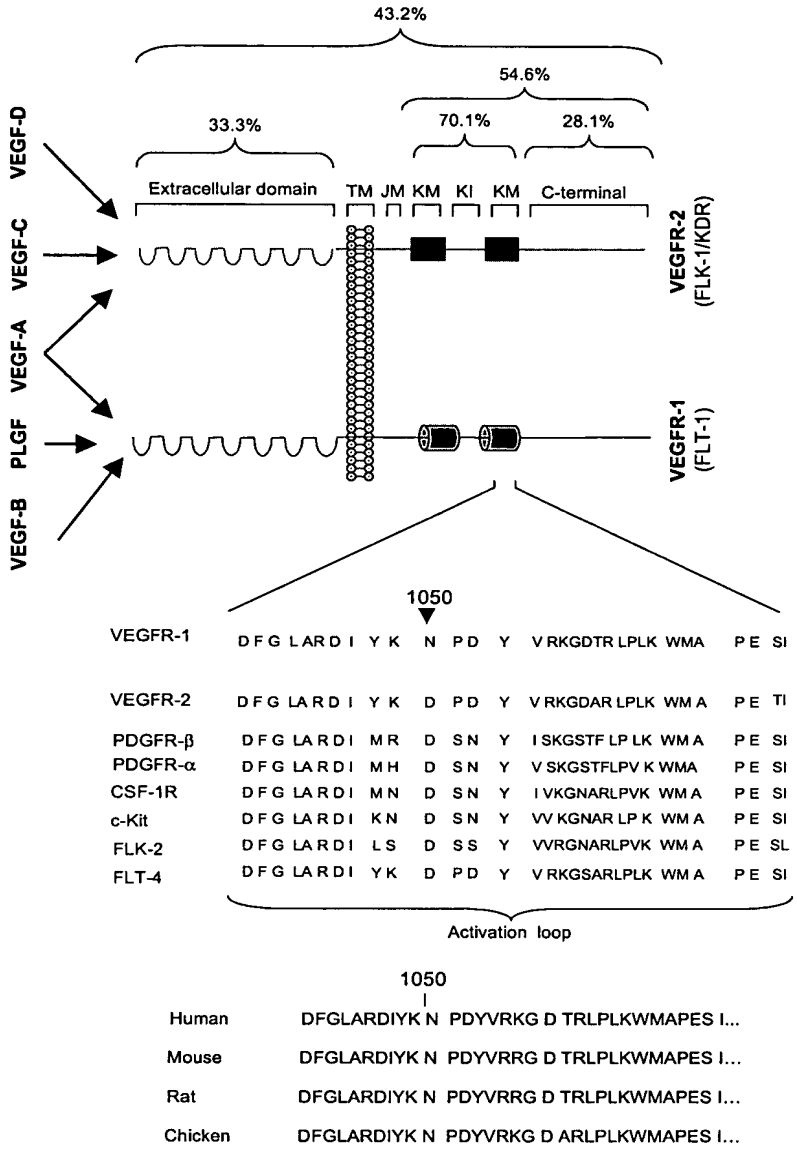

Fig. 1. Schematic representation of VEGFR-1, VEGFR-2 and their corresponding ligands: multiple VEGF ligands bind to VEGFR-1 and VEGFR-2. Placenta growth factor (PLGF) and VEGF-B bind to VEGFR-1 but not to VEGFR-2. VEGF-C and VEGF-D bind VEGFR-2 but not to VEGFR-1. VEGF-A binds to both VEGFR-1 and VEGFR-2. VEGFR-1 and VEGFR-2 are structurally similar, consisting of an extracellular ligand-binding domain with seven immunoglobulin (Ig)-like motifs, a single transmembrane domain (TM) and juxtamembrane (JM) domain, a kinase domain (KD) split by a kinase insert (KI), and a carboxyl terminus. The sequence homology between VEGFR-1 and VEGFR-2 also is shown. The kinase domain of VEGFR-1 and VEGFR-2 represent the most conserved region with 70.1% homology. The carboxyl terminus represents the most divergent region with only 28.1% sequence homology. Sequence alignment of the catalytic and activation loop regions of human VEGFR-1 and various receptor tyrosine kinases of type III family are shown. The residue corresponding to asparagine (N) 1050 of VEGFR-1 is aspartic acid (D) in type III kinases. The location asparagine (N) 1050 in the activation loop of human VEGFR-1 is indicated by arrow. This residue is highly conserved and is invariable among the type III family kinases except VEGFR-1. Asparagine 1050 of VEGFR-1 is conserved among human (GenBank accession number: NM002019), mouse (GenBank accession number: BAA24498) rat (GenBank accession number: P53767) and chicken (GenBank accession number: BAB84690).

3. VEGFR-1 is a kinase-impaired RTK

The mechanisms by which most RTKs are activated are well characterized. Transphosphorylation of RTK and their ability to phosphorylate target proteins are the hallmark of RTK activation. In this context, VEGFR-1 is considered to be a kinase-impaired RTK (e.g., VEGFR-1 is poorly tyrosine phosphorylated and its ability to phosphorylate a polypeptide substrate is negligible). All RTKs, including VEGFR-1 contain an evolutionary conserved kinase domain containing GXGXXG, an ATP binding site, HRDLA, a motif essential for catalysis and one or two tyrosine autophosphorylation sites

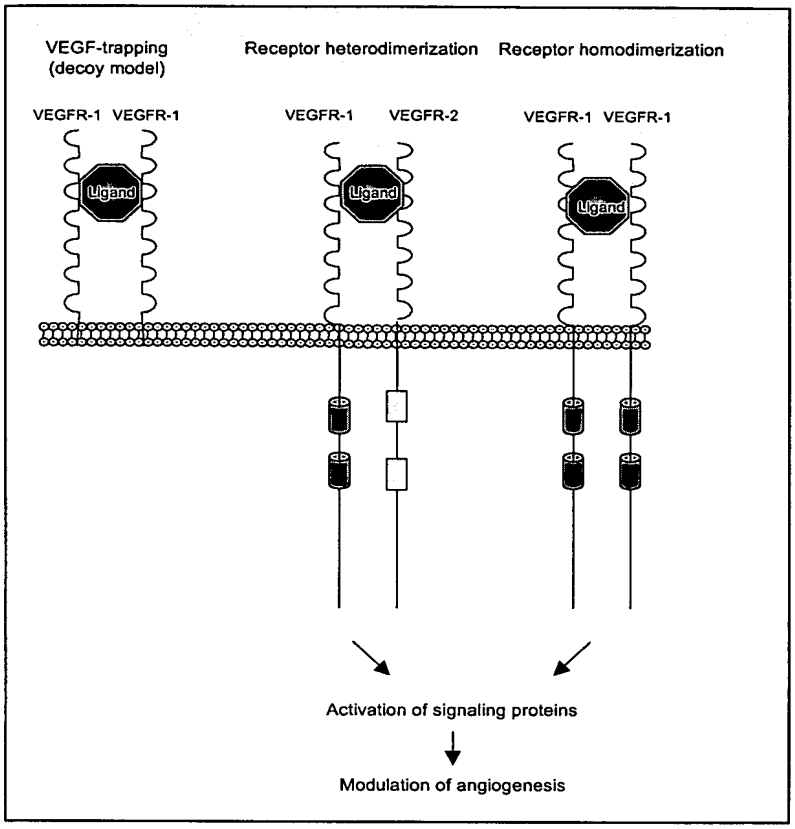

Fig. 2. Schematic representation of the mechanisms of involvement of VEGFR-1 in angiogenesis: VEGF-trapping: the mechanism by which VEGFR-1 binds to VEGF and prevents it from binding to VEGFR-2. The cytoplasmic domain of VEGFR-1 is not required for its VEGF-trapping function (Hiratsuka et al., 1998). VEGFR-1 may elicit its role in angiogenesis by heterodimerization with VEGFR-2 and VEGFR-3 (Rahimi et al., 2000; Autiero et al., 2003; Dixelius et al., 2003). The third mechanism by which VEGFR-1 regulates angiogenesis is through receptor homodimerization. This type of activation of VEGFR-1 leads to activation of signaling proteins that might regulate angiogenesis in either positive or negative manner (Rahimi et al., 2000; Meyer et al., 2004a, 2004b).

(Hanks and Quinn, 1991). Despite having these motifs, the ligand stimulation of VEGFR-1 results only in minor tyrosine phosphorylation of VEGFR-1 in vivo and in vitro (de Vries et al., 1992; Waltenberger et al., 1994; Rahimi et al., 2000). In some RTKs such as colon carcinoma kinase-4 (CCK4), ErbB3/HER3, KLG, Ror1 and DRL abnormalities in the kinase domain have been suggested to contribute to the kinase-defective phenotype of these RTKs (Chou and Hayman, 1991; Guy et al., 1994; Mossie et al., 1995; Yoshikawa et al., 2001). VEGFR-1 has no aberrant amino acid replacement in the GXGXXG and HRDLA motifs.

A recent study suggests that the kinase-impaired activity of VEGFR-1 can be rescued, in part, by swapping the carboxyl terminus of VEGFR-1 with that of VEGFR-2. The carboxyl-terminus swapped VEGFR-1 promoted ligand-dependent autophosphorylation of VEGFR-1 and induction of endothelial cell proliferation (Meyer et al., 2004a, 2004b). It appears that this effect is selectively associated with its carboxyl terminus because replacement of the juxtamembrane (JM) region of VEGFR-1 with that of VEGFR-2 does not rescue its kinase-impaired characteristic (Gille et al., 2000). A detailed understanding of the molecular mechanism underlying the carboxyl terminus of VEGFR-1 in its poor tyrosine phosphorylation should wait until the crystal structure of VEGFR-1 is resolved. To date, the crystal structure of VEGFR-1 is not available, only its ligand-binding region is resolved (Wiesmann et al., 1997). How the carboxyl terminus of VEGFR-2 is able to rescue the kinase-impaired activity of VEGFR-1 is not fully understood. However, it is feasible that the carboxyl terminus of VEGFR-1 somewhat obstructs ligand-mediated autophosphorylation of VEGFR-1. In some RTKs, such as Tie-2, deletion of carboxyl terminus has been shown to enhance its autophosphorylation and kinase activation, suggesting that the carboxyl terminus negatively regulates tyrosine autophosphorylation possibly by interacting with activation loop and keeping it in an inhibitory conformation (Niu et al., 2002).

The molecular explanation for the kinase-impaired characteristic of VEGFR-1 is provided by a recent finding that the decoy characteristic of VEGFR-1 is linked to the replacement of a highly conserved amino acid residue, located in its activation loop (Meyer et al., 2006). This amino acid is highly conserved among all the type III RTKs and corresponds to aspartic acid (D) but in VEGFR-1 is substituted to asparagine (N) (Fig. 1). Mutation of asparagine (N1050) within the

activation loop to aspartic acid promoted enhanced ligand-dependent tyrosine autophosphorylation and kinase activation in vivo and in vitro. This mutation promotes endothelial cell proliferation, but not tubulogenesis. It also displayed an oncogenic phenotype as its expression in fibroblast cells elicited transformation and colony growth. It has been suggested that the conserved aspartic acid in the activation loop favors the transphosphorylation of the activation loop tyrosines and its absence renders VEGFR-1 to a less potent enzyme perhaps by disfavoring transphosphorylation of activation loop tyrosines. It should be emphasized that although these observations may explain the decoy characteristic of VEGFR-1 (e.g., impaired kinase activation and tyrosine phosphorylation), nevertheless these findings still do not explain mechanisms by which VEGFR-1 contributes to angiogenesis as a kinase-impaired RTK.

Several RTK including, DRL, CCK4, KLG, Ror1 and ErbB3 all display impaired kinase activity, yet they transduce signals and regulate variety of biological functions (Chou and Hayman, 1991; Guy et al., 1994; Mossie et al., 1995; Yoshikawa et al., 2001). The best-studied kinase-impaired RTK is ErbB3, one of the four members of EGFR family (Citri et al., 2003). Data from several laboratories using various systems revealed that signaling of ErbB3 requires kinase activity of another EGFR family including ErbB1, ErbB2 and ErbB4 (Pinkas-Kramarski et al., 1996; Citri et al., 2003). DRL, another kinase-impaired RTK, although it shows no kinase activity in vivo and in vitro, nevertheless its activity is required for axon guidance in Drosophila (Yoshikawa et al., 2001). The molecular mechanism of DRL signaling and whether DRL transduces signal like ErbB3 is not known. There is some circumstantial evidence suggesting that VEGFR-1 may signal through other VEGFR family kinases, in particular, through VEGFR-2. Both VEGFR-1 and VEGFR-2 are expressed by endothelial cells, suggesting that under a favorable condition such as availability of appropriate ligand, VEGFR-1 may form heterodimer complexes with the other receptors. Indeed, VEGFR-1 has been shown to heterodimerize with VEGFR-2 and that heterodimerization leads to autophosphorylation, activation of VEGFR-2, and angiogenesis (Autiero et al., 2003). Thus, the mechanism by which VEGFR-1 supports angiogenesis is complex and likely involves several different mechanisms including VEGF-trapping, activation by heterodimerization and homodimerization (Fig. 2). VEGFR-1 also has a residual kinase activity and its selective activation that results only in homodimerization leads to activation of a limited number of signaling proteins such as p42/44 MAPK (Meyer et al., 2004a, 2004b). Thus, the unique signaling nature of VEGFR-1 and mechanisms by which it stimulates biological responses indicates that we have more to learn about RTK signaling than the current widely accepted and generalized RTK paradigm would suggest.

4. VEGFR-2 activation is essential for angiogenesis

The role of VEGFR-2 in angiogenesis is well established and more comprehensive reviews on the role of VEGFR-2 in angiogenesis have been recently published (Yancopoulos et al., 2000; Carmeliet, 2003; Jain, 2003). In this review we focus on the recent advancement on VEGFR-2 activation and its signal transduction relays.

4.1. Carboxyl terminus is critical for VEGFR-2 activation and its signaling

The mechanisms by which most RTKs transduce signal have been studied extensively at the molecular level. The basic principles of RTKs activation can be summarized as following: ligand-mediated dimerization of receptor monomers, transphosphorylation by dimerized receptors and docking of signaling proteins to receptor phosphotyrosines (Hubbard et al., 1998; Blume-Jensen and Hunter, 2001). The autophosphorylation sites are either involved in the regulation of kinase activity of the receptor or serve as a binding site for SH2- and PTB-containing proteins (Blume-Jensen and Hunter, 2001; Pawson, 2004). Central to ligand-induced RTK activation is the phosphorylation of one or two tyrosine residues within the activation loop (Hubbard et al., 1998). In the unstimulated form, the activation loop orients these tyrosine sites toward the activation sites of the enzyme and thereby sterically prevents binding to ATP-Mg^{2+}. It is suggested that phosphorylation of these tyrosines in the catalytic loop orients the inhibitory loop away from the active site enabling the RTK to bind ATP-Mg^{2+} and efficiently phosphorylate substrates (Hubbard et al., 1998; Schlessinger, 2000). The recent crystal structure of VEGFR-2 by McTigue et al. (1999) showed that tyrosines 1054 and 1059, two highly conserved tyrosine residues located in the activation loop of VEGFR-2 are phosphorylated. An unexpected feature of the VEGFR-2 structure is the conformation of the activation loop. Although phosphorylated, the activation loop is disordered in the region that includes phosphotyrosine 1059. This is in contrast to the structures of other tyrosine kinases such as FGFR-1 and the insulin receptor, which are well ordered and participate in specific interactions (McTigue et al., 1999).

In last few years some of the paradigms learned from studying other RTKs revealed that catalytic activity is regulated by other segments of RTKs. For instance, substitution of two tyrosine residues with phenylalanine in the juxtamembrane region of the PDGFR-β drastically reduces autophosphorylation and activation of this receptor (Mori et al., 1993). Similar observations were reported for the MuSK tyrosine kinase, a receptor tyrosine kinase for agrin, which is involved in the functioning of the neuromuscular synapse (Till et al., 2002) and EphB2, a receptor tyrosine kinase for ephrins (Wybenga-Groot et al., 2001; Schlessinger, 2003). Recent crystal structures of MuSK and EphB2 revealed that the juxtamembrane domains of these receptors are directly involved in the regulation of kinase activation. The data obtained from the crystal structures suggest that the juxtamembrane domain interacts with the kinase domain and represses catalytic activity (Schlessinger, 2003). Additional biochemical studies demonstrated that these tyrosines also bind to SH2-containing proteins (Wybenga-Groot et al., 2001). There are two tyrosine residues within the juxtamembrane of

VEGFR-2 (tyrosines 799 and 820 in mouse VEGFR-2). Replacement of these tyrosines to phenylalanine in VEGFR-2 does not impair the ligand-dependent activation of VEGFR-2 (Dayanir et al., 2001; Meyer et al., 2002). This suggests that phosphorylation of these tyrosines are not involved in the kinase activation of VEGFR-2.

Unlike juxtamembrane tyrosine phosphorylation sites, however, phosphorylation of tyrosine 1212 (tyrosine 1214 in human VEGFR-2) in the carboxyl terminus plays an important role in autophosphorylation and kinase activation of VEGFR-2. Mutation of tyrosine 1212 to phenylalanine impairs full activation of VEGFR-2 and its ability to efficiently activate signaling proteins. Mutation of the same tyrosine residue to glutamic acid, however, preserved its ability to undergo ligand-dependent autophosphorylation (Meyer et al., 2002). This suggests that tyrosine 1212 regulates VEGFR-2 autophosphorylation in a manner that is similar to that of tyrosine sites in the JM region of MuSK and EphB2. Surprisingly, this mutant receptor as recently reported preserved normal development and angiogenesis in knockin mice (Sakurai et al., 2005). This indicates that either the low level kinase activity of tyrosine 1212 mutant VEGFR-2 is sufficient to promote angiogenesis or that phosphorylation of tyrosine 1212 is not stringently required for function of VEGFR-2 in vivo. It is also conceivable that phosphorylation of other tyrosine sites in VEGFR-2 may compensate the lack of phosphorylation of tyrosine 1212. In agreement with this possibility, the mutant PDGFR-β lacking the binding sites for PLC-γ1, PI 3 kinase, SHP2 and Ras-GAP has been shown to stimulate gene expression in fibroblast cells almost as efficiently as the wild-type PDGFR-β (Fambrough et al., 1999). Similarly, activation of Src kinases by many laboratories has been shown to be important for PDGFR-β autophosphorylation and its biological function (Mori et al., 1993). Yet, PDGFR-β is fully functional in SYF cells, deficient for Src family kinases (Klinghoffer et al., 1999). This argues that RTK signaling induces activation of signaling proteins with an overlapping role in vivo and thus the role of individual docking sites may be compensated for by the presence of other docking sites.

Further analysis of the carboxyl terminus of VEGFR-2 revealed that this region is engaged in VEGFR-2 activation in multiple ways. First, the carboxyl terminus of VEGFR-2 contains several tyrosine phosphorylation sites including tyrosine 1212, 1173 and 1221. Tyrosines 1212 and 1221 are phosphorylated but the identity of signaling proteins that are recruited to these sites is not known (Meyer et al., 2002; and our unpublished data). As discussed earlier, the presence of tyrosine 1212 is required for full autophosphorylation of VEGFR-2 (Meyer et al., 2002). Tyrosine 1173 is phosphorylated in vivo and recruits p85 of PI3 kinase (Dayanir et al., 2001), PLCγ1 (Takahashi et al., 2001; Meyer et al., 2003) and regulate phosphorylation of c-Cbl (our unpublished data). In addition to possessing multiple tyrosine phosphorylation sites, the carboxyl terminus of VEGFR-2 also contains putative serine phosphorylation sites. Mutation of serines 1188 and 1191 in the carboxyl terminus of VEGFR-2 is shown to impair the ligand-dependent down regulation of VEGFR-2 (Singh et al., 2005). This might explain why deletion of carboxyl terminus impairs the VEGFR's ability to undergo ligand-dependent downregulation (Meyer et al., 2004a, 2004b). Finally, deletion of the entire carboxyl terminus of VEGFR-2 is shown to impair its ligand-dependent autophosphorylation. It appears that this role of carboxyl terminus is independent of tyrosine 1212 and may involve residues other than tyrosines (Meyer et al., 2004a, 2004b). Altogether, the current literature provides a framework for understanding of regulation of VEGFR-2 activation and further demonstrates that the carboxyl terminus plays various important roles in VEGFR-2 functions ranging from its ability to regulate autophosphorylation and recruitment of signaling proteins to ligand-dependent downregulation. Future work to characterize function of the VEGFR-2 carboxyl terminus will require a detailed analysis including: identification of tyrosine and serine phosphorylation sites and signaling proteins that might interact with these sites. Finally, resolving the crystal structure of VEGFR-2 with its carboxyl terminus intact may provide further insight into regulation of this important protein.

4.2. Role of phosphoinositide 3-kinase in VEGFR-2 signaling and angiogenesis

In the last few years, the phosphoinositide 3-kinase (PI3K) signal transduction pathway has emerged as one of the main signal routes that VEGFR-2 employs to stimulate endothelial cell survival and proliferation. PI3 kinase is a lipid kinase that converts the plasma membrane lipid phosphatidylinositol 4,5-bisphosphate (PIP_2) to phosphatidylinositol-3,4,5-triphosphate (PIP_3). Proteins with pleckstrin-homology (PH) domains, such as protein kinase B (PKB/Akt), phosphoinositide-dependent kinase-1 (PDK-1) and PDK-2, bind to PIP_3. Akt is activated by PIP_3, PDK1 and PDK2 leading to phosphorylation of a host of other proteins that affect cell proliferation, cell cycle progression and cell survival (Rameh and Cantley, 1999; Cantley, 2002).

Various experiments using several in vivo and in vitro systems have demonstrated that activation of PI3 kinase by VEGFR-2 promotes endothelial cell survival, proliferation and angiogenesis (Fig. 3). First, Wortmannnin and LY294002, the PI3 kinase specific inhibitors and a dominant negative form of Akt, a downstream target of PI3 kinase, all are able to inhibit VEGF-stimulated endothelial cell survival (Gerber et al., 1998). Second, inhibition of PI3 kinase by overexpression of a dominant negative form of p85 of PI3 kinase inhibits endothelial cell proliferation and induction of c-fos (Thakker et al., 1999). Similarly, overexpression of PTEN, a lipid phosphatase that reverses PI3 kinase function by dephosphorylating its phospholipid products, inhibits VEGF-mediated endothelial cell proliferation. Overexpression of phosphatase inactive form of PTEN enhances VEGF-mediated endothelial cell proliferation (Huang and Kontos, 2002). Third, expression of a viral form of PI3 kinase and its target Akt promotes angiogenesis and VEGF expression in chicken embryo (Jiang et al., 2000). The most recent study on PI3 kinase also suggests that it may regulate angiogenesis by regulating expression of Tie-2 receptor (Lelievre et al., 2005).

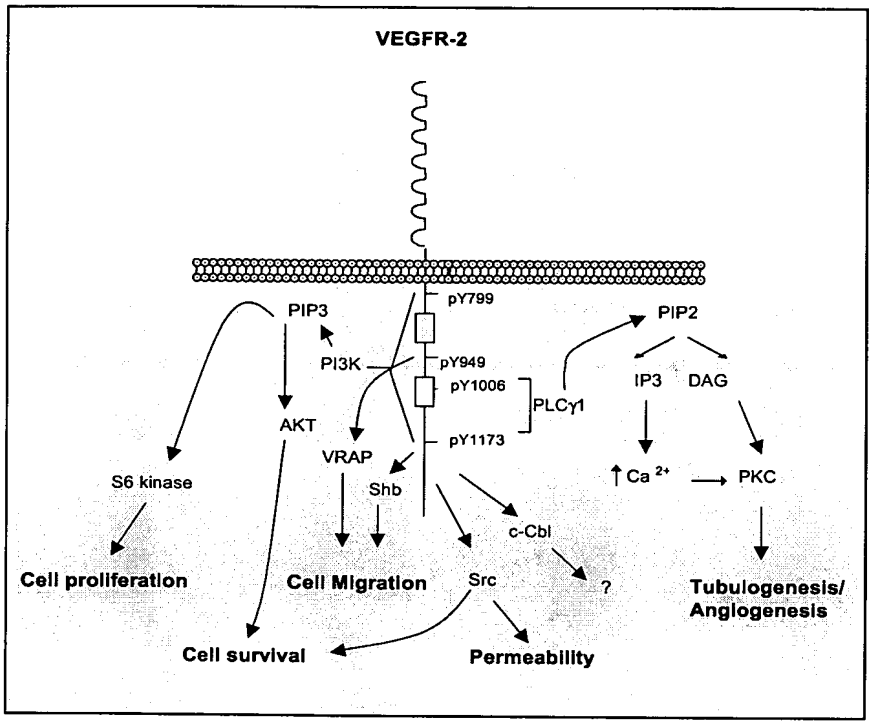

Fig. 3. Schematic representation of VEGFR-2 mediated signal transduction and their role in endothelial biology: VEGFR-2 activation induces tyrosine phosphorylation and activation PLCγ1 via tyrosines 1006 and 1173. Activation of PLCγ1 leads to tubulogenesis and proliferation of endothelial cells. Activation of PI3 kinase by VEGFR-2 is mediated by tyrosines 799 and 1173 and is involved in proliferation and survival of endothelial cells. Tyrosine 1173 of VEGFR-2 also associates with the adaptor protein, Shb. Src family kinases and c-Cbl are also activated by VEGFR-2. Activation of Src is linked to endothelial cell survival and permeability (see text for details). Phosphorylation of tyrosine 1049 in the kinase insert region of VEGFR-2 binds to VRAP (Matsumoto et al., 2005).

A mechanistic explanation on how PI3 kinase is activated by VEGFR-2 is demonstrated by a chimeric VEGFR-2 system in which the PI3 kinase binding sites were mutated and its role in VEGFR-2-mediated endothelial cell proliferation was tested. The tyrosine mutant chimeric VEGFR-2 (where tyrosines 799 and 1173 of mouse VEGFR-2 were mutated) abolished the ability of VEGFR-2 to stimulate PI3 kinase activity and cell proliferation (Dayanir et al., 2001). Also, PI3 kinase-dependent proliferation of endothelial cells is linked to activation of S6 kinase. This is supported by the observation that a mutant chimeric receptor that fails to activate PI3 kinase also fails to activate S6 kinase (Dayanir et al., 2001). Consistent with this observation, selective inhibition of S6 kinase inhibits VEGF-induced endothelial cell proliferation and in vivo angiogenesis (Guba et al., 2002; Yamazaki et al., 2005). In agreement with a critical role of PI3 kinase activation in growth and survival of endothelial cells, a recent study also demonstrated that tumstatin, a naturally occurring angiogenesis inhibitor, promotes apoptosis of endothelial cells by inhibiting the PI3 kinase pathway (Sudhakar et al., 2003).

4.3. Role of phospholipase Cγ1 in VEGFR-2 signaling and angiogenesis

Phospholipase Cγ1 (PLCγ1) hydrolyzes phosphoinositides to generate the second messengers, inositol 1,4,5-trisphosphate (IP_3) and diacylglycerol (DAG). IP_3 increases intracellular Ca^{2+} levels and DAG activates protein kinase C (PKC) leading to variety of cellular responses (Sekiya et al., 1999). Several lines of evidences indicate that activation of PLC-γ1 plays a pivotal role in angiogenesis and VEGFR-2 signal transduction (Fig. 3). First, a genetic study shows that lack of PLCγ1 in mice results in significantly diminished vasculogenesis and erythropoiesis (Liao et al., 2002). Second, in transgenic zebrafish the PLC-γ1deficiency shows defects in arterial formation. The PLC-γ1 deficient embryos also failed to respond to exogenous VEGF, highlighting the importance of PLC-γ1 for VEGFR-2-mediated signal transduction relay (Lawson et al., 2003). However, the exact role of PLCγ1 in angiogenesis is not clear. VEGFR-2-mediated activation of PLC-γ1 in a certain endothelial cellular background is suggested to stimulate cell proliferation and in other endothelial cells to stimulate differentiation and tubulogenesis (Rahimi et al., 2000; Takahashi et al., 2001; Meyer et al., 2003). Phosphorylation of tyrosines 1006 and 1173 (Y1006 and 1173 correspond to Y1008 and 1175 in human VEGFR-2, respectively) are important for recruitment of PLCγ1 by VEGFR-2 (Takahashi et al., 2001; Meyer et al., 2003). The tyrosine mutant VEGFR-2 that fails to activate PLCγ1 also fails to stimulate tubulogenesis in vitro (Meyer et al., 2003). A recent knockin approach in mice showed that mutation of tyrosine 1173 of VEGFR-2 abrogates its ability to promote angiogenesis

(Sakkurai et al., 2004). Although this finding suggests an essential role for tyrosine 1173 in the regulation of angiogenesis, it is not clear whether the defect is exclusively linked with the inability of the tyrosine 1173 mutant VEGFR-2 to activate PLCγ1. Tyrosine 1173 of VEGFR-2 is also known to recruit other signaling proteins such as p85 of PI3 kinase (Dayanir et al., 2001) and Shb (Holmqvist et al., 2004).

4.4. Role of Src kinases in VEGFR-2 signaling and angiogenesis

Activation of Src kinases have been implicated in the regulation of a variety of biological responses including cell proliferation, migration, differentiation and cell survival (Bromann et al., 2004). Activation of many RTKs leads to stimulation of Src family kinase activity via tyrosine phosphorylated docking sites on RTKs and the SH2 domain of Src kinases (Boggon and Eck, 2004). Selective activation of VEGFR-2 stimulates Src phosphorylation in endothelial cells (Meyer et al., 2002). However, the precise mechanism involved is not established. In particular, Src binding sites on VEGFR-2 and biological importance of Src in VEGFR-2-mediated signal transduction is not fully understood. A recent study demonstrated that Src kinase activity is required to protect endothelial cells from apoptosis and it appears that Src elicits its anti-apoptotic function via Raf-1 activation (Alavi et al., 2003). It has also been shown that the ability of VEGF to induce vascular permeability requires Src kinases. Curiously, angiogenesis is normal in mice deficient for Src and Yes (Eliceiri et al., 1999). Src activation also is implicated in GPCR (such as nucleotide receptor P2Y2)-mediated transactivation of VEGFR-2 but not in ligand-mediated VEGFR-2 activation (Meyer et al., 2002; Seye et al., 2004). Indeed, ligand-dependent autophosphorylation of VEGFR-2 is not compromised in SYF cells, deficient in Src, Yes and Fyn and also over-expression of a dominant negative form of Src in endothelial cells has no apparent effect on the ligand-stimulated VEGFR-2 autophosphorylation (Meyer et al., 2002). In addition to the role of c-Src in VEGFR-2-mediated signal transduction, Src also plays a key role in angiogenesis by promoting expression of VEGF in response to hypoxia (Mukhopadhyay et al., 1995). Further studies are required to delineate exact role of Src in VEGFR-2 signal transduction, in particular, its association with VEGFR-2 and tyrosine phosphorylation site on VEGFR-2 that might be involved in recruitment of Src to VEGFR-2.

4.5. Role of serine phosphorylation in VEGFR-2 signaling and angiogenesis

In addition to activating positive signaling pathways, activation of RTKs also induces negative feedback signaling pathways that attenuate or antagonize positive signaling. One mechanism that attenuates RTKs signaling is a rapid depletion of the cellular receptor pool, a phenomenon termed downregulation (Soldi et al., 1999). Recent study indicates that VEGFR-2 undergoes ligand-dependent downregulation and degradation in a novel mechanism involving non-classical PKCs. Singh et al. (2005) demonstrated that the carboxyl terminus is required for PKC-dependent downregulation of VEGFR-2. Surprisingly, the ligand-dependent downregulation and degradation of VEGFR-2 proceeds without involvement of its ectodomain and engagement of γ-secretase activity. Mutation of serine sites at 1188 and 1191 compromised the ability of VEGFR-2 to undergo efficient ligand-dependent downregulation. These findings suggest that serines 1188 and 1191 of VEGFR-2 are phosphorylated either directly by PKC or by serine kinases whose activity is regulated by PKCs. Upon phosphorylation of these sites they may recruit an E3 ligase to VEGFR-2, leading to ubiquitinylation and degradation of VEGFR-2. The identity of the E3 ligase responsible for ubiquitinylation of VEGFR-2 is not known. It appears, however, that c-Cbl is not the E3 ligase that involved in ubiquitinylation and downregulation of VEGFR-2, although it is phosphorylated upon VEGFR-2 stimulation with ligand (Singh et al., 2005). Since c-Cbl is activated by VEGFR-2 it is interesting to know what role it plays in angiogenesis.

4.6. VEGF, VEGF receptors and ocular angiogenesis

Vascular endothelial growth factor (VEGF) is normally expressed by many cell types of the retina, including retinal pigment epithelium (RPE) cells and ganglion cells (Miller et al., 1997; Ida et al., 2003). VEGF-A is the most potent angiogenic protein known and its expression is abnormally elevated in patients with age-related macular degeneration (AMD), diabetic retinopathy, and retinopathy of prematurity (Campochiaro et al., 1999; Witmer et al., 2003). Expression of VEGF-A and its receptors, VEGFR-1 and VEGFR-2 also play critical role during the embryonic development of retinal, choroidal vasculatures and neural retinal development (Robinson et al., 2001; Fruttiger, 2002).

The survey of current literature indicates that VEGF not only plays a functional role during ocular development but also is involved in normal function of the retina and pathological conditions associated with it. Studies suggest that in Type I diabetes expression of VEGF is altered due to metabolic abnormalities including hyperglycemia, which represent major vascular complications of Type I diabetes (Chiarelli et al., 2000). Aberrant angiogenesis in diabetes is most clinically apparent in proliferative diabetic retinopathy. Hypoxia-induced expression of VEGF and other pro-angiogenic factors leads to altered angiogenesis, which causes major damage to pericytes. These aberrant conditions lead to increased permeability and rupture of retinal vessels (Caldwell et al., 2005). Although the role of angiogenesis is well documented in diabetic retinopathy, altered angiogenesis may also play a key role in diabetic neuropathy, diabetic nephropathy and diabetic wound healing (Isner et al., 2001; Kim et al., 2005). Furthermore, evidence now suggests that VEGF-A also promotes retinal vascular permeability and its presence is associated with the leakiness of retinal vessels in non-proliferative diabetic retinopathy (Murata et al., 1995). While the role of individual VEGF receptors involved in mediating vascular permeability

is not fully understood, recent studies suggest that VEGFR-2 may play a prominent role in mediating the ability of VEGF to promote permeability of vascular endothelial cells (Joukov et al., 1998; Stacker et al., 1999). Elevated expression of VEGF-A due to hypoxia is considered to be the primary cause of retinopathy of prematurity (Smith, 2004). In addition, recent study suggests that PlGF, a VEGFR-1 specific ligand may protect against oxygen-induced vessel loss without stimulating angiogenesis (Shih et al., 2003). This finding implies that selective activation of VEGFR-1 but not VEGFR-2 may promote survival of retinal endothelial cells without promoting angiogenesis. It has been shown that VEGF-A plays a key role in choroidal angiogenesis, a major cause of visual loss in AMD. VEGF-A expression found to be significantly higher in patients with AMD (Zarbin, 2004) and its expression is also elevated in RPE cells in patients with AMD and in experimental animal models (Schwesinger et al., 2001).

Altogether, the above-mentioned studies provide ample evidence for the central role of VEGF and its receptors in ocular angiogenesis. Further studies, however, are needed to delineate the exact role of VEGF-A and possible involvement of other VEGF family proteins in ocular angiogenesis. It is also essential to establish the relative contribution of VEGF receptors in the development of these conditions. Finally, it should be noted that signal transduction pathways activated by VEGF receptors in pathological angiogenesis, in particular, in ocular angiogenesis is largely unknown. Thus, it is critical to dissect the molecular mechanisms of signaling aspects of VEGF receptors in various pathological conditions and this certainly will be an important direction for future studies and ultimately new strategies for clinical application.

4.7. Ocular diseases and anti-angiogenesis therapy

Although the idea of angiogenesis therapy was proposed over three decades ago (Folkman, 1971), the use of angiogenesis therapy was only realized in the last few years. Now, angiogenesis therapy is being considered for patients with cancer, age-related macular degeneration, heart diseases and others (Liu and Regillo, 2004; Annex and Simons, 2005; Neri and Bicknell, 2005; Wegewitz et al., 2005). The primary causes of vision loss in Western countries are macular degeneration and diabetic retinopathy. Although the mechanisms of each disease are distinct, they both involve abnormal angiogenesis. In addition, retinopathy of prematurity, a major cause of blindness in children, is associated with abnormal angiogenesis due to oxygen supplementation in the premature infants (Shih et al., 2003). In recent years several classes of anti-angiogenesis agents have been under development, many of these agents either target VEGF (e.g., VEGF antibodies) or VEGFRs (e.g., small molecule kinase inhibitors). Bevacizumab (Avastin; Genentech Inc., South San Francisco, CA) is a humanized monoclonal anti-VEGF-A antibody (Rosen, 2005). Avastin represents the first anti-angiogenesis drug that has recently been approved by the FDA for use in combination with standard chemotherapy in patients with advanced colorectal cancer. Another class of anti-angiogenesis inhibitors that are currently in clinical trails are the small molecule kinase inhibitors such as PTK787, SU11248 and ZD6474 which are potent inhibitors of VEGFR-1 and VEGFR-2 (Kerbel and Folkman, 2002; Rosen, 2005).

To date, the anti-angiogenesis therapy for ocular diseases that have been evaluated are angiogenesis inhibitors that mainly bind to VEGF such as pegaptanib (Macugen), and VEGF-Trap (Saishin et al., 2003; Gragoudas et al., 2004; Zakarija and Soff, 2005). Pegaptanib and VEGF-Trap like Avastin bind to VEGF and prevent binding of VEGF to VEGF receptors. Survey of current anti-angiogenesis therapies indicate that these therapies may in some cases reduces disease progression but by and large they are ineffective in stopping or reversing the diseases that are being tested (Stacker et al., 1999; Kerbel and Folkman, 2002). Another challenge facing the application of these anti-angiogenesis therapies to ocular angiogenesis in diseases such as AMD is the requirement of repeated injection of these drugs into the patient's eye. This represents a serious setback for usefulness of these drugs for patients with AMD. It appears that anti-angiogenesis therapy for ocular diseases may require a long-term administration of anti-angiogenesis drugs. Thus, preparation of these drugs in a sustained-release format may dramatically improve not only their efficacy but also the convenience of their application into the patients' eye. In addition, other strategies such as gene therapy may overcome limitations of the aforementioned anti-angiogenesis drugs. Recent studies using viral vector-mediated delivery of anti-angiogenesis proteins in rodent models provide a new and possibly more effective strategy for treatment of ocular angiogenesis (Reich and Bennett, 2003). Thus, it is clear that further work on the efficacy and safety of these agents as well as the development of more selective, potent and safer anti-angiogenesis agents certainly will provide substantial advances for the treatment of angiogenesis-associated ocular diseases. One avenue toward the development of more selective and better anti-angiogenesis drugs is to target a specific signaling pathway of VEGF receptors.

5. Conclusions

Abnormal angiogenesis is associated with pathology of many diseases including cancer, age-related macular degeneration (AMD), proliferative diabetic retinopathy (PDR), and retinopathy of prematurity (ROP). What is clear is that the more we learn about molecular mechanisms of VEGFR-1 and VEGFR-2 regulation and their signal transduction, the more we continue to learn about angiogenesis and molecules that regulate it. The emerging scenario in VEGFR-1 and VEGFR-2 activation is that the complexity of blood vessel development necessitated more stringent control over VEGFR-1. On one hand VEGFR-1 evolved to have a higher affinity to various ligands, on the other hand VEGFR-1 lost its potency in enzymatic activity, creating a unique mechanism to control its function. VEGFR-2 plays a broader role in angiogenesis; its activity regulates endothelial cell growth, differentiation, migration and tubulogenesis. The carboxyl terminus of

VEGFR-2 plays a central role in its activation, ability to recruit signaling proteins, to undergo downregulation and to promote angiogenesis.

Finally it should be noted that activation and signaling of VEGF receptors appear to be regulated not only by each other in both negative and positive manners but also by other receptors including integrins (Soldi et al., 1999; Yeynolds et al., 2004), cadherins (Rahimi and Kazlauskas, 1999; Bussolino et al., 2001) and neuropilins (Klagsbrun et al., 2002). In addition, the fact that multiple VEGF ligands with different preference and capability bind to VEGFRs and activate them in homo- and heterodimeric manners presents a challenge to study their selective biochemical and cellular signaling in endothelial cell background. Although characterization of specific functions of VEGFR-1 and VEGFR-2 and their signal transduction relays has been a frustrating task, it has nevertheless been illuminating. Continued research into the function of VEGFRs as well as techniques involving creating chimeric VEGFRs in which the extracellular domain of each VEGFR is replaced with that of CSF-1R (Rahimi et al., 2000), and mutant VEGFs that selectively bind to VEGFRs (Keyt et al., 1996; Stacker et al., 1999) continue to provide insight into their specific roles in angiogenesis. Evaluation of targeted mouse knockouts (Fong et al., 1995) and knockin (Sakurai et al., 2005) and the use of RNA interference may provide further insight into the function of this important family of receptors.

Acknowledgements

This work was supported in part through grants from The National Institutes of Health (NIH) EY0137061, EY012997 and a grant from Massachusetts Lions Foundation to N.R. I thank Amrik J. Singh and Rosana D. Meyer for their comments and reading the manuscript.

References

Alavi, A., Hood, J.D., Frausto, R., Stupack, D.G., Cheresh, D.A., 2003. Role of Raf in vascular protection from distinct apoptotic stimuli. Science 301, 94–96.

Annex, B.H., Simons, M., 2005. Growth factor-induced therapeutic angiogenesis in the heart: protein therapy (Review). Cardiovasc. Res. 65, 649–655.

Athanassiades, A., Lala, P.K., 1998. Role of placenta growth factor (PIGF) in human extravillous trophoblast proliferation, migration and invasiveness. Placenta 19, 465–473.

Autiero, M., Waltenberger, J., Communi, D., Kranz, A., Moons, L., Lambrechts, D., Kroll, J., Plaisance, S., De Mol, M., Bono, F., Kliche, S., Fellbrich, G., Ballmer-Hofer, K., Maglione, D., Mayr-Beyrle, U., Dewerchin, M., Dombrowski, S., Stanimirovic, D., Van Hummelen, P., Dehio, C., Hicklin, D.J., Persico, G., Herbert, J.M., Communi, D., Shibuya, M., Collen, D., Conway, E.M., Carmeliet, P., 2003. Role of PlGF in the intra- and intermolecular cross talk between the VEGF receptors Flt1 and Flk1. Nat. Med. 9, 936–943.

Blume-Jensen, P., Hunter, T., 2001. Oncogenic kinase signalling (Review). Nature 411, 355–365.

Boggon, T.J., Eck, M.J., 2004. Structure and regulation of Src family kinases (Review). Oncogene 23, 7918–7927.

Bromann, P.A., Korkaya, H., Courtneidge, S.A., 2004. The interplay between Src family kinases and receptor tyrosine kinases (Review). Oncogene 23, 7957–7968.

Bussolino, F., Serini, G., Mitola, S., Bazzoni, G., Dejana, E., 2001. Dynamic modules and heterogeneity of function: a lesson from tyrosine kinase receptors in endothelial cells (Review). EMBO Rep. 2, 763–767.

Caldwell, R.B., Bartoli, M., Behzadian, M.A., El-Remessy, A.E., Al-Shabrawey, M., Platt, D.H., Liou, G.I., Caldwell, R.W., 2005. Vascular endothelial growth factor and diabetic retinopathy: role of oxidative stress. Curr. Drug Targets 6, 511–524.

Campochiaro, P.A., Soloway, P., Ryan, S.J., Miller, J.W., 1999. The pathogenesis of choroidal neovascularization in patients with age-related macular degeneration (Review). Mol. Vis. 5, 34–38.

Cantley, L.C., 2002. The phosphoinositide 3-kinase pathway (Review). Science 296, 1655–1657.

Carmeliet, P., 2003. Angiogenesis in health and disease (Review). Nat. Med. 9, 653–660.

Chiarelli, F., Spagnoli, A., Basciani, F., Tumini, S., Mezzetti, A., Cipollone, F., Cuccurullo, F., Morgese, G., Verrotti, A., 2000. Vascular endothelial growth factor (VEGF) in children, adolescents and young adults with Type 1 diabetes mellitus: relation to glycaemic control and microvascular complications. Diabetes Med. 17, 650–656.

Chou, Y.H., Hayman, M.J., 1991. Characterization of a member of the immunoglobulin gene superfamily that possibly represents an additional class of growth factor receptor. Proc. Natl. Acad. Sci. USA 88, 4897–4901.

Citri, A., Skaria, K.B., Yarden, Y., 2003. The deaf and the dumb: the biology of ErbB-2 and ErbB-3 (Review). Exp. Cell Res. 284, 54–65.

Clauss, M., Weich, H., Breier, G., Knies, U., Rockl, W., Waltenberger, J., Risau, W., 1996. The vascular endothelial growth factor receptor Flt-1 mediates biological activities. Implications for a functional role of placenta growth factor in monocyte activation and chemotaxis. J. Biol. Chem. 271, 17629–17634.

Cleaver, O., Melton, D.A., 2003. Endothelial signaling during development (Review). Nat. Med. 9, 661–668.

Dayanir, V., Meyer, R.D., Lashkari, K., Rahimi, N., 2001. Identification of tyrosine residues in vascular endothelial growth factor receptor-2/FLK-1 involved in activation of phosphatidylinositol 3-kinase and cell proliferation. J. Biol. Chem. 276, 17686–17692.

de Vries, C., Escobedo, J.A., Ueno, H., Houck, K., Ferrara, N., Williams, L.T., 1992. The fms-like tyrosine kinase, a receptor for vascular endothelial growth factor. Science 255, 989–991.

Dikov, M.M., Ohm, J.E., Ray, N., Tchekneva, E.E., Burlison, J., Moghanaki, D., Nadaf, S., Carbone, D.F., 2005. Differential roles of vascular endothelial growth factor receptors 1 and 2 in dendritic cell differentiation. J. Immunol. 174, 215–222.

Dixelius, J., Makinen, T., Wirzenius, M., Karkkainen, M.J., Wernstedt, C., Alitalo, K., Claesson-Welsh, L., 2003. Ligand-induced vascular endothelial growth factor receptor-3 (VEGFR-3) heterodimerization with VEGFR-2 in primary lymphatic endothelial cells regulates tyrosine phosphorylation sites. J. Biol. Chem. 278, 40973–40979.

Eliceiri, B.P., Paul, R., Schwartzberg, P.L., Hood, J.D., Leng, J., Cheresh, D.A., 1999. Selective requirement for Src kinases during VEGF-induced angiogenesis and vascular permeability. Mol. Cell 4, 915–924.

Fambrough, D., McClure, K., Kazlauskas, A., Lander, E.S., 1999. Diverse signaling pathways activated by growth factor receptors induce broadly overlapping, rather than independent, sets of genes. Cell 97, 727–741.

Folkman, J., 1971. Tumor angiogenesis: therapeutic implications (Review). N. Engl. J. Med. 285, 1182–1186.

Fong, G.H., Rossant, J., Gertsenstein, M., Breitman, M.L., 1995. Role of the Flt-1 receptor tyrosine kinase in regulating the assembly of vascular endothelium. Nature 376, 66–70.

Fong, G.H., Zhang, L., Bryce, D.M., Peng, J., 1999. Increased hemangioblast commitment, not vascular disorganization, is the primary defect in flt-1 knock-out mice. Development 126, 3015–3025.

Fruttiger, M., 2002. Development of the mouse retinal vasculature: angiogenesis versus vasculogenesis (Review). Invest. Ophthalmol. Vis. Sci. 43, 522–527.

Gerber, H.P., McMurtrey, A., Kowalski, J., Yan, M., Keyt, B.A., Dixit, V., Ferrara, N., 1998. Vascular endothelial growth factor regulates endothelial

cell survival through the phosphatidylinositol 3′-kinase/Akt signal transduction pathway. Requirement for Flk-1/KDR activation. J. Biol. Chem. 273, 30336–30343.

Gille, H., Kowalski, J., Yu, L., Chen, H., Pisabarro, M.T., Davis-Smyth, T., Ferrara, N., 2000. A repressor sequence in the juxtamembrane domain of Flt-1 (VEGFR-1) constitutively inhibits vascular endothelial growth factor-dependent phosphatidylinositol 3′-kinase activation and endothelial cell migration. EMBO J. 19, 4064–4073.

Gragoudas, E.S., Adamis, A.P., Cunningham Jr., E.T., Feinsod, M., Guyer, D.R., 2004. VEGF Inhibition Study in Ocular Neovascularization Clinical Trial Group. Pegaptanib for neovascular age-related macular degeneration. N. Engl. J. Med. 351, 2805–2816.

Guba, M., von Breitenbuch, P., Steinbauer, M., Koehl, G., Flegel, S., Hornung, M., Bruns, C.J., Zuelke, C., Farkas, S., Anthuber, M., Jauch, K.W., Geissler, E.R., 2002. Rapamycin inhibits primary and metastatic tumor growth by antiangiogenesis: involvement of vascular endothelial growth factor. Nat. Med. 8, 128–135.

Guy, P.M., Platko, J.V., Cantley, L.C., Cerione, R.A., Carraway 3rd, K.L., 1994. Insect cell-expressed p180erbB3 possesses an impaired tyrosine kinase activity. Proc. Natl. Acad. Sci. USA 91, 8132–8136.

Hanks, S.K., Quinn, A.M., 1991. Protein kinase catalytic domain sequence database: identification of conserved features of primary structure and classification of family members (Review). Methods Enzymol. 200, 38–62.

Hiratsuka, S., Minowa, O., Kuno, J., Noda, T., Shibuya, M., 1998. Flt-1 lacking the tyrosine kinase domain is sufficient for normal development and angiogenesis in mice. Proc. Natl. Acad. Sci. USA 95, 9349–9354.

Holmqvist, K., Cross, M.J., Rolny, C., Hagerkvist, R., Rahimi, N., Matsumoto, T., Claesson-Welsh, L., Welsh, M., 2004. The adaptor protein shb binds to tyrosine 1175 in vascular endothelial growth factor (VEGF) receptor-2 and regulates VEGF-dependent cellular migration. J. Biol. Chem. 279, 22267–22275.

Huang, J., Kontos, C.D., 2002. PTEN modulates vascular endothelial growth factor-mediated signaling and angiogenic effects. J. Biol. Chem. 277, 10760–10766.

Hubbard, S.R., Mohammadi, M., Schlessinger, J., 1998. Autoregulatory mechanisms in protein-tyrosine kinases (Review). J. Biol. Chem. 273, 11987–11990.

Ida, H., Tobe, T., Nambu, H., Matsumura, M., Uyama, M., Campochiaro, P.A., 2003. RPE cells modulate subretinal neovascularization, but do not cause regression in mice with sustained expression of VEGF. Invest. Ophthalmol. Vis. Sci. 44, 5430–5437.

Isner, J.M., Ropper, A., Hirst, K., 2001. VEGF gene transfer for diabetic neuropathy. Hum. Gene. Ther. 12, 1593–15104.

Jain, R.K., 2003. Molecular regulation of vessel maturation (Review). Nat. Med. 9, 685–693.

Jiang, B.H., Zheng, J.Z., Aoki, M., Vogt, P.K., 2000. Phosphatidylinositol 3-kinase signaling mediates angiogenesis and expression of vascular endothelial growth factor in endothelial cells. Proc. Natl. Acad. Sci. USA 97, 1749–1753.

Joukov, V., Kumar, V., Sorsa, T., Arighi, E., Weich, H., Saksela, O., Alitalo, K., 1998. A recombinant mutant vascular endothelial growth factor-C that has lost vascular endothelial growth factor receptor-2 binding, activation, and vascular permeability activities. J. Biol. Chem. 273, 6599–6602.

Jussila, L., Alitalo, K., 2000. Vascular growth factors and lymphangiogenesis (Review). Physiol. Rev. 82, 673–700.

Kearney, J.B., Ambler, C.A., Monaco, K.A., Johnson, N., Rapoport, R.G., Bautch, V.L., 2002. Vascular endothelial growth factor receptor Flt-1 negatively regulates developmental blood vessel formation by modulating endothelial cell division. Blood 99, 2397–2407.

Kearney, J.B., Kappas, N.C., Ellerstrom, C., DiPaola, F.W., Bautch, V.L., 2004. The VEGF receptor flt-1 (VEGFR-1) is a positive modulator of vascular sprout formation and branching morphogenesis. Blood 103, 4527–4535.

Kerbel, R., Folkman, J., 2002. Clinical translation of angiogenesis inhibitors (Review). Nat. Rev. Cancer 2, 727–739.

Keyt, B.A., Nguyen, H.V., Berleau, L.T., Duarte, C.M., Park, J., Chen, H., Ferrara, N., 1996. Identification of vascular endothelial growth factor determinants for binding KDR and FLT-1 receptors. Generation of receptor-selective VEGF variants by site-directed mutagenesis. J. Biol. Chem. 271, 5638–5646.

Kim, N.H., Oh, J.H., Seo, J.A., Lee, K.W., Kim, S.G., Choi, K.M., Baik, S.H., Choi, D.S., Kang, Y.S., Han, S.Y., Han, K.H., Ji, Y.H., Cha, D.R., 2005. Vascular endothelial growth factor (VEGF) and soluble VEGF receptor FLT-1 in diabetic nephropathy. Kidney Int. 67, 167–177.

Klagsbrun, M., Takashima, S., Mamluk, R., 2002. The role of neuropilin in vascular and tumor biology (Review). Adv. Exp. Med. Biol. 515, 33–48.

Klinghoffer, R.A., Sachsenmaier, C., Cooper, J.A., Soriano, P., 1999. Src family kinases are required for integrin but not PDGFR signal transduction. EMBO J. 18, 2459–2471.

Lawson, N.D., Mugford, J.W., Diamond, B.A., Weinstein, B.M., 2003. Phospholipase C gamma-1 is required downstream of vascular endothelial growth factor during arterial development. Genes Dev. 17, 1346–1351.

Lelievre, E., Bourbon, P.M., Duan, L.J., Nussbaum, R.L., Fong, G.H., 2005. Deficiency in the p110{alpha} subunit of PI 3-kinase results in diminished Tie-2 expression and Tie-2−/− like vascular defects in mice. Blood 105, 3935–3938.

Liao, H.J., Kume, T., McKay, C., Xu, M.J., Ihle, J.N., Carpenter, G., 2002. Absence of erythrogenesis and vasculogenesis in Plcg1-deficient mice. J. Biol. Chem. 277, 9335–9341.

Liu, M., Regillo, C.D., 2004. A review of treatments for macular degeneration: a synopsis of currently approved treatments and ongoing clinical trials. Curr. Opin. Ophthalmol. 15, 221–226.

Matsumoto, T., Bohman, S., Dixelius, J., Berge, T., Dimberg, A., Magnusson, P., Wang, L., Wikner, C., Qi, J.H., Wernstedt, C., Wu, J., Bruheim, S., Mugishima, H., Mukhopadhyay, D., Spurkland, A., Claesson-Welsh, L., 2005. VEGF receptor-2 Y951 signaling and a role for the adapter molecule TSAd in tumor angiogenesis. EMBO J. 24, 2342–2353.

McTigue, M.A., Wickersham, J.A., Pinko, C., Showalter, R.E., Parast, C.V., Tempczyk-Russell, A., Gehring, M.R., Mroczkowski, B., Kan, C.C., Villafranca, J.E., Appelt, K., 1999. Crystal structure of the kinase domain of human vascular endothelial growth factor receptor 2: a key enzyme in angiogenesis. Structure 7, 319–330.

Meyer, R.D., Rahimi, N., 2003. Comparative structure-function analysis of VEGFR-1 and VEGFR-2: What have we learned from chimeric systems? (Review). Ann. N.Y. Acad. Sci. 995, 200–207.

Meyer, R.D., Dayanir, V., Majnoun, F., Rahimi, N., 2002. The presence of a single tyrosine residue at the carboxyl domain of vascular endothelial growth factor receptor-2/FLK-1 regulates its autophosphorylation and activation of signaling molecules. J. Biol. Chem. 277, 27081–27087.

Meyer, R.D., Latz, C., Rahimi, N., 2003. Recruitment and activation of phospholipase Cgamma1 by vascular endothelial growth factor receptor-2 are required for tubulogenesis and differentiation of endothelial cells. J. Biol. Chem. 278, 16347–16355.

Meyer, R.D., Singh, A., Majnoun, F., Latz, C., Lashkari, K., Rahimi, N., 2004a. Substitution of C-terminus of VEGFR-2 with VEGFR-1 promotes VEGFR-1 activation and endothelial cell proliferation. Oncogene 23, 5523–5531.

Meyer, R.D., Singh, A.J., Rahimi, N., 2004b. The carboxyl terminus controls ligand-dependent activation of VEGFR-2 and its signaling. J. Biol. Chem. 279, 735–742.

Meyer, R.D., Mohammadi, M., Rahimi, N., 2006. A single amino acid substitution in the activation loop defines the decoy characteristic of VEGFR-1/FLT-1. J. Biol. Chem. 281, 867–875.

Miller, J.W., Adamis, A.P., Aiello, L.P., 1997. Vascular endothelial growth factor in ocular neovascularization and proliferative diabetic retinopathy (Review). Diabetes Metab. Rev. 13, 37–50.

Mori, S., Ronnstrand, L., Yokote, K., Engstrom, A., Courtneidge, S.A., Claesson-Welsh, L., Heldin, C.H., 1993. Identification of two juxtamembrane autophosphorylation sites in the PDGF beta-receptor; involvement in the interaction with Src family tyrosine kinases. EMBO J. 12, 2257–2264.

Mossie, K., Jallal, B., Alves, F., Sures, I., Plowman, G.D., Ullrich, A., 1995. Colon carcinoma kinase-4 defines a new subclass of the receptor tyrosine kinase family. Oncogene 11, 2179–2184.

Mukhopadhyay, D., Tsiokas, L., Zhou, X.M., Foster, D., Brugge, J.S., Sukhatme, V.P., 1995. Hypoxic induction of human vascular endothelial growth factor expression through c-Src activation. Nature 375, 577–581.

Murata, T., Ishibashi, T., Khalil, A., Hata, Y., Yoshikawa, H., Inomata, H., 1995. Vascular endothelial growth factor plays a role in hyperpermeability of diabetic retinal vessels. Ophthalmic Res. 27, 48–52.

Neagoe, P.E., Lemieux, C., Sirois, M.G., 2005. Vascular endothelial growth factor (VEGF)-A165-induced prostacyclin synthesis requires the activation of VEGF receptor-1 and -2 heterodimer. J. Biol. Chem. 280, 9904–9912.

Neri, D., Bicknell, R., 2005. Tumour vascular targeting (Review). Nat. Rev. Cancer 5, 436–446.

Neufeld, G., Cohen, T., Gengrinovitch, S., Poltorak, Z., 1999. Vascular endothelial growth factor (VEGF) and its receptors (Review). FASEB J. 13, 9–22.

Niu, X.L., Peters, K.G., Kontos, C.D., 2002. Deletion of the carboxyl terminus of Tie2 enhances kinase activity, signaling, and function. Evidence for an autoinhibitory mechanism. J. Biol. Chem. 277, 31768–31773.

Odorisio, T., Schietroma, C., Zaccaria, M.L., Cianfarani, F., Tiveron, C., Tatangelo, L., Failla, C.M., Zambruno, G., 2002. Mice overexpressing placenta growth factor exhibit increased vascularization and vessel permeability. J. Cell Sci. 115, 2559–2567.

Pawson, T., 2004. Specificity in signal transduction: from phosphotyrosine-SH2 domain interactions to complex cellular systems (Review). Cell 116, 191–203.

Pinkas-Kramarski, R., Soussan, L., Waterman, H., Levkowitz, G., Alroy, I., Klapper, L., Lavi, S., Seger, R., Ratzkin, B.J., Sela, M., Yarden, Y., 1996. Diversification of Neu differentiation factor and epidermal growth factor signaling by combinatorial receptor interactions. EMBO J. 15, 2452–2467.

Rahimi, N., 2006. VEGFR-1 and VEGFR-2: two non-identical twins with a unique physiognomy. Front. Biosci. 11, 818–829.

Rahimi, N., Kazlauskas, A., 1999. A role for cadherin-5 in regulation of vascular endothelial growth factor receptor 2 activity in endothelial cells. Mol. Biol. Cell 10, 3401–3407.

Rahimi, N., Dayanir, V., Lashkari, K., 2000. Receptor chimeras indicate that the vascular endothelial growth factor receptor-1 (VEGFR-1) modulates mitogenic activity of VEGFR-2 in endothelial cells. J. Biol. Chem. 275, 16986–16992.

Rameh, L.E., Cantley, L.C., 1999. The role of phosphoinositide 3-kinase lipid products in cell function (Review). J. Biol. Chem. 274, 8347–8350.

Reich, S.J., Bennett, J., 2003. Gene therapy for ocular neovascularization: a cure in sight (Review). Curr. Opin. Genet. Dev. 13, 317–322.

Robinson, G.S., Ju, M., Shih, S.C., Xu, X., McMahon, G., Caldwell, R.B., Smith, L.E., 2001. Nonvascular role for VEGF: VEGFR-1, 2 activity is critical for neural retinal development. FASEB J. 15, 1215–1217.

Rosen, L.S., 2005. VEGF-targeted therapy: therapeutic potential and recent advances (Review). Oncologist 10, 382–391.

Saishin, Y., Saishin, Y., Takahashi, K., Lima e Silva, R., Hylton, D., Rudge, J.S., Wiegand, S.J., Campochiaro, P.A., 2003. VEGF-TRAP(R1R2) suppresses choroidal neovascularization and VEGF-induced breakdown of the blood-retinal barrier. J. Cell Physiol. 195, 241–248.

Sakurai, Y., Ohgimoto, K., Kataoka, Y., Yoshida, N., Shibuya, M., 2005. Essential role of Flk-1 (VEGF receptor 2) tyrosine residue 1173 in vasculogenesis in mice. Proc. Natl. Acad. Sci. USA 102, 1076–1081.

Schlessinger, J., 2000. Cell signaling by receptor tyrosine kinases. Cell 103, 211–215.

Schlessinger, J., 2003. Signal transduction. Autoinhibition control. Science 300, 750–752.

Schwesinger, C., Yee, C., Rohan, R.M., Joussen, A.M., Fernandez, A., Meyer, T.N., Poulaki, V., Ma, J.J., Redmond, T.M., Liu, S., Adamis, A.P., D'Amato, R.J., 2001. Intrachoroidal neovascularization in transgenic mice overexpressing vascular endothelial growth factor in the retinal pigment epithelium. Am. J. Pathol. 158, 1161–1172.

Sekiya, F., Bae, Y.S., Rhee, S.G., 1999. Regulation of phospholipase C isozymes: activation of phospholipase C-gamma in the absence of tyrosine-phosphorylation (Review). Chem. Phys. Lipids. 98, 3–11.

Seye, C.I., Yu, N., Gonzalez, F.A., Erb, L., Weisman, G.A., 2004. The P2Y2 nucleotide receptor mediates vascular cell adhesion molecule-1 expression through interaction with VEGF receptor-2 (KDR/Flk-1). J. Biol. Chem. 279, 35679–35686.

Shih, S.C., Ju, M., Liu, N., Smith, L.E., 2003. Selective stimulation of VEGFR-1 prevents oxygen-induced retinal vascular degeneration in retinopathy of prematurity. J. Clin. Invest. 112, 50–57.

Singh, A.J., Meyer, R.D., Band, H., Rahimi, N., 2005. The carboxyl terminus of VEGFR-2 is required for PKC-mediated down-regulation. Mol. Biol. Cell 16, 2106–2118.

Smith, L.E., 2004. Pathogenesis of retinopathy of prematurity. Growth Horm. IGF Res. 14 (Suppl. A), S140–S144.

Soldi, R., Mitola, S., Strasly, M., Defilippi, P., Tarone, G., Bussolino, F., 1999. Role of alphavbeta3 integrin in the activation of vascular endothelial growth factor receptor-2. EMBO J. 18, 882–892.

Stacker, S.A., Vitali, A., Caesar, C., Domagala, T., Groenen, L.C., Nice, E., Achen, M.G., Wilks, A.F., 1999. A mutant form of vascular endothelial growth factor (VEGF) that lacks VEGF receptor-2 activation retains the ability to induce vascular permeability. J. Biol. Chem. 274, 34884–34892.

Sudhakar, A., Sugimoto, H., Yang, C., Lively, J., Zeisberg, M., Kalluri, R., 2003. Human tumstatin and human endostatin exhibit distinct antiangiogenic activities mediated by alpha v beta 3 and alpha 5 beta 1 integrins. Proc. Natl. Acad. Sci. USA 100, 4766–4771.

Takahashi, T., Yamaguchi, S., Chida, K., Shibuya, M., 2001. A single autophosphorylation site on KDR/Flk-1 is essential for VEGF-A-dependent activation of PLC-gamma and DNA synthesis in vascular endothelial cells. EMBO J. 20, 2768–2778.

Tammela, T., Enholm, B., Alitalo, K., Paavonen, K., 2005. The biology of vascular endothelial growth factors (Review). Cardiovasc. Res. 65, 550–563.

Thakker, G.D., Hajjar, D.P., Muller, W.A., Rosengart, T.K., 1999. The role of phosphatidylinositol 3-kinase in vascular endothelial growth factor signaling. J. Biol. Chem. 274, 10002–10007.

Till, J.H., Becerra, M., Watty, A., Lu, Y., Ma, Y., Neubert, T.A., Burden, S.J., Hubbard, S.R., 2002. Crystal structure of the MuSK tyrosine kinase: insights into receptor autoregulation. Structure (Camb.) 10, 1187–1196.

Waltenberger, J., Claesson-Welsh, L., Siegbahn, A., Shibuya, M., Heldin, C.H., 1994. Different signal transduction properties of KDR and Flt1, two receptors for vascular endothelial growth factor. J. Biol. Chem. 269, 26988–26995.

Wegewitz, U., Gohring, I., Spranger, J., 2005. Novel approaches in the treatment of angiogenic eye disease (Review). Curr. Pharm. Des. 11, 2311–2330.

Wey, J.S., Fan, F., Gray, M.J., Bauer, T.W., McCarty, M.F., Somcio, R., Liu, W., Evans, D.B., Wu, Y., Hicklin, D.J., Ellis, L.M., 2005. Vascular endothelial growth factor receptor-1 promotes migration and invasion in pancreatic carcinoma cell lines. Cancer 104, 427–438.

Wiesmann, C., Fuh, G., Christinger, H.W., Eigenbrot, C., Wells, J.A., de Vos, A.M., 1997. Crystal structure at 1.7 A resolution of VEGF in complex with domain 2 of the Flt-1 receptor. Cell 91, 695–704.

Witmer, A.N., Vrensen, G.F., Van Noorden, C.J., Schlingemann, R.O., 2003. Vascular endothelial growth factors and angiogenesis in eye disease (Review). Prog. Retin. Eye Res. 22, 1–29.

Wybenga-Groot, L.E., Baskin, B., Ong, S.H., Tong, J., Pawson, T., Sicheri, F., 2001. Structural basis for autoinhibition of the Ephb2 receptor tyrosine kinase by the unphosphorylated juxtamembrane region. Cell 106, 745–757.

Yamazaki, T., Akada, T., Niizeki, O., Suzuki, T., Miyashita, H., Sato, Y., 2005. Puromycin-insensitive leucyl-specific aminopeptidase (PILSAP) binds and catalyzes PDK1, allowing VEGF-stimulated activation of S6K for endothelial cell proliferation and angiogenesis. Blood 104, 2345–2352.

Yancopoulos, G.D., Davis, S., Gale, N.W., Rudge, J.S., Wiegand, S.J., Holash, J., 2000. Vascular-specific growth factors and blood vessel formation (Review). Nature 407, 242–248.

Yeynolds, A.R., Reynolds, L.E., Nagel, T.E., Lively, J.C., Robinson, S.D., Hicklin, D.J., Bodary, S.C., Hodivala-Dilke, K.M., 2004. Elevated Flk1 (vascular endothelial growth factor receptor 2) signaling mediates enhanced angiogenesis in beta3-integrin-deficient mice. Cancer Res. 64, 8643–8650.

Yoshikawa, S., Bonkowsky, J.L., Kokel, M., Shyn, S., Thomas, J.B., 2001. The derailed guidance receptor does not require kinase activity in vivo. J. Neurosci. 21, RC119–RC121.

Zakarija, A., Soff, G., 2005. Update on angiogenesis inhibitors (Review). Curr. Opin. Oncol. 17, 578–583.

Zarbin, M.A., 2004. Current concepts in the pathogenesis of age-related macular degeneration. Arch. Ophthalmol. 122, 598–614.

Zeng, H., Dvorak, H.F., Mukhopadhyay, D., 2001. Vascular permeability factor (VPF)/vascular endothelial growth factor (VEGF) peceptor-1 down-modulates VPF/VEGF receptor-2-mediated endothelial cell proliferation, but not migration, through phosphatidylinositol 3-kinase-dependent pathways. J. Biol. Chem. 276, 26969–26979.

THE JOURNAL OF BIOLOGICAL CHEMISTRY
© 1991 by The American Society for Biochemistry and Molecular Biology, Inc.

Vol. 266, No. 18, Issue of June 25, pp. 11947-11954, 1991
Printed in U.S.A.

The Human Gene for Vascular Endothelial Growth Factor

MULTIPLE PROTEIN FORMS ARE ENCODED THROUGH ALTERNATIVE EXON SPLICING*

(Received for publication, December 13, 1990)

Edmund Tischer, Richard Mitchell‡, Taymar Hartman, Maria Silva, Denis Gospodarowicz§, John C. Fiddes, and Judith A. Abraham¶

From California Biotechnology Inc., Mountain View, California 94043 and the §Cancer Research Institute, School of Medicine, University of California, San Francisco, California 94143

Vascular endothelial growth factor (VEGF) is an apparently endothelial cell-specific mitogen that is structurally related to platelet-derived growth factor. By Northern blot and protein analyses, we show that VEGF is produced by cultured vascular smooth muscle cells. Analysis of VEGF transcripts in these cells by polymerase chain reaction and cDNA cloning revealed three different forms of the VEGF coding region, as had been reported in HL60 cells. The three forms of the human VEGF protein chain predicted from these coding regions are 189, 165, and 121 amino acids in length. Comparison of cDNA nucleotide sequences with sequences derived from human VEGF genomic clones indicates that the VEGF gene is split among eight exons and that the various VEGF coding region forms arise from this gene by alternative splicing: the 165-amino-acid form of the protein is missing the residues encoded by exon 6, whereas the 121-amino-acid form is missing the residues encoded by exons 6 and 7. Analysis of the VEGF gene promoter region revealed a single major transcription start, which lies near a cluster of potential Sp1 factor binding sites. The promoter region also contains several potential binding sites for the transcription factors AP-1 and AP-2; consistent with the presence of these sites, Northern blot analysis demonstrated that the level of VEGF transcripts is elevated in cultured vascular smooth muscle cells after treatment with the phorbol ester 12-*O*-tetradecanoyl-phorbol-13-acetate.

Many polypeptide mitogens such as basic fibroblast growth factor (bFGF)[1] and platelet-derived growth factor (PDGF) are active on a wide range of different cell types. In contrast, the recently identified vascular endothelial growth factor (VEGF) is a mitogen primarily for vascular endothelial cells; it appears to be inactive on fibroblasts, keratinocytes, vascular smooth muscle cells, lens epithelial cells, corneal endothelial cells, adrenal cortical cells, and granulosa cells (Gospodarowicz *et al.*, 1989; Ferrara and Henzel, 1989). Consistent with its endothelial cell mitogenicity, VEGF has also been shown to be angiogenic in the chick chorioallantoic membrane assay (Plouët *et al.*, 1989; Leung *et al.*, 1989).

VEGF was purified by Gospodarowicz *et al.* (1989) and Ferrara and Henzel (1989) from the conditioned medium of bovine pituitary folliculo stellate cells, utilizing an endothelial cell proliferation assay to monitor the biological activity of the protein. Use of a completely different assay, the stimulation of vascular permeability in guinea pig skin, resulted in the identification of a vascular permeability factor in tumor ascites fluid and in the conditioned medium from several tumor cell lines such as guinea pig line 10 hepatocarcinoma cells and the human histiocytic lymphoma cell line U-937 (Senger *et al.*, 1983, 1986; Connolly *et al.*, 1989a). Vascular permeability factor was subsequently found to be an angiogenic endothelial cell mitogen, and structural characterization by protein sequencing and cDNA cloning showed it to be identical to VEGF (Connolly *et al.*, 1989a, 1989b; Keck *et al.*, 1989). The range of cell types producing VEGF has now been extended to include a rat glioma cell line GS-9L (Conn *et al.*, 1990a), a mouse neuroblastoma cell line NB41 (Levy *et al.*, 1989), and the mouse pituitary cell line AtT-20 (Plouët *et al.*, 1989).

Purified VEGF is an approximately 46-kDa protein which dissociates upon reduction into two apparently identical 23-kDa subunits (Gospodarowicz *et al.*, 1989; Ferrara and Henzel, 1989; Connolly *et al.*, 1989b). Analysis of cDNA clones revealed heterogeneity in the VEGF coding region, and predicted the existence of 189-, 165-, and 121-residue forms of the mature human VEGF subunit, as well as 164- and 120-residue forms of the mature bovine VEGF subunit (Leung *et al.*, 1989; Keck *et al.*, 1989; Tischer *et al.*, 1989). Recently, a 164-residue form of the rat VEGF subunit has also been identified by amino acid sequencing and cDNA cloning (Conn *et al.*, 1990b). Taking into account the single site in VEGF for *N*-linked glycosylation, the 23-kDa subunit appears to correspond most closely to the size predicted for the 165 (164)-residue chain. Comparison of the amino acid sequences predicted from the cDNA clones with protein databases showed that VEGF is distantly related to both the A and B chains of PDGF, with complete conservation of the 8 cysteines involved in inter- and intra-chain disulfides in PDGF.

Here, we identify vascular smooth muscle (VSM) cells as an additional source of both VEGF mRNA and protein and

* This work was supported in part by Small Business Innovation Research Grant HL44832-01 from the National Heart, Lung, and Blood Institute. The costs of publication of this article were defrayed in part by the payment of page charges. This article must therefore be hereby marked "*advertisement*" in accordance with 18 U.S.C. Section 1734 solely to indicate this fact.

The nucleotide sequence(s) reported in this paper has been submitted to the GenBank™/EMBL Data Bank with accession number(s) M63971-M63978.

‡ Present address: Panlabs, Bothell, WA 98001.

¶ To whom correspondence should be addressed: California Biotechnology Inc., 2450 Bayshore Parkway, Mountain View, CA 94043. Tel.: 415-966-1550; Fax: 415-968-2438.

[1] The abbreviations used are: bFGF, basic fibroblast growth factor; PDGF, platelet-derived growth factor; VEGF, vascular endothelial growth factor; VSM, vascular smooth muscle; PCR, polymerase chain reaction; DMEM, Dulbecco's modified Eagle's medium; TPA, 12-*O*-tetradecanoyl-phorbol-13-acetate; HPLC, high-performance liquid chromatography; SDS, sodium dodecyl sulfate; bp, base pair(s); kb, kilobase(s); HEPES, 4-(2-hydroxyethyl)-1-piperazineethanesulfonic acid; PIPES, 1,4-piperazinebis(ethanesulfonic acid).

EXHIBIT C

characterize the multiple VEGF mRNA forms observed in VSM cells by polymerase chain reaction (PCR) and by cDNA cloning. Comparison of the cDNAs with the structure of the cloned human VEGF gene reported here shows that the VEGF protein coding region is split among eight exons and that the three forms of the coding region arise by alternative exon splicing. The intron-exon pattern determined for the VEGF gene is somewhat related to that of the genes encoding the PDGF A and B chains.

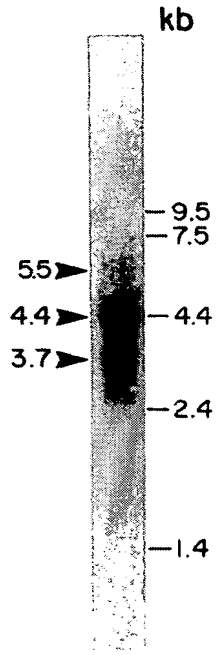

FIG. 1. **Northern blot analysis of VEGF transcripts in fetal human VSM cells.** Polyadenylated RNA (5 μg) was fractionated on a 1.2% agarose-formaldehyde gel and transferred to a Hybond-N nylon membrane. The membrane was probed with a ^{32}P-labeled 0.35-kb *Eco*RI-*Hpa*II coding region fragment isolated from the bovine VEGF cDNA clone, λST800 (Tischer *et al.*, 1989). The hybridization was carried out in Rapid Hybridization Buffer (Amersham Corp.). The membrane was then washed at 52 °C in 0.15 M NaCl, 15 mM sodium citrate, 0.1% SDS prior to autoradiography. VEGF mRNA species of 5.5, 4.4, and 3.7 kb were detected. Sizes of RNA markers (GIBCO-Bethesda Research Laboratories) are given in kilobases.

EXPERIMENTAL PROCEDURES

RNA Isolation and Northern Blot Analysis—Fetal human VSM cells (Gospodarowicz, 1990) were grown to confluence in Dulbecco's modified Eagle's medium (DMEM) containing 10% fetal bovine serum, 2 mM L-glutamine, 50 units/ml penicillin, and 50 μg/ml streptomycin sulfate; during growth of the cells, the medium was supplemented every other day with 1 ng/ml bFGF. U-937 cells obtained from the American Type Culture Collection (ATCC CRL 1593) were cultured in RPMI 1640 containing 10% fetal bovine serum, L-glutamine, and antibiotics as above to a density of 4×10^6 cells/ml. The U-937 cells were then diluted in growth medium to a density of 5×10^6 cells/ml and incubated with 20 ng/ml 12-*O*-tetradecanoylphorbol-13-acetate (TPA) for 3 days prior to RNA isolation.

To examine the effect of phorbol ester treatment on the level of VEGF transcripts in the fetal human VSM cells, 20 ng/ml of TPA were added to flasks of these cells at 3 days post-confluence (and 3 days past the last addition of bFGF). RNA was harvested from the cells either prior to TPA addition (control) or at various time intervals after TPA addition.

Total RNA was isolated from the cells by the guanidine thiocyanate method (Chirgwin *et al.*, 1979). Polyadenylated RNA was obtained by fractionation of the total RNA on oligo(dT)-cellulose (Type 3; Collaborative Research Inc.). Aliquots of total or polyadenylated RNA were subjected to denaturing electrophoresis on agarose-formaldehyde gels (Lehrach *et al.*, 1977) and transferred to either nitrocellulose filters (Schleicher & Schuell) or Hybond-N nylon membranes (Amersham Corp.), prior to hybridization to the nick-translated probes noted in the figure legends.

Protein Purification—Primary cultures of adult bovine VSM cells derived from the aorta were established as described previously (Gospodarowicz *et al.*, 1977, 1988). For large-scale culture of the cells in 530-cm^2 plates, seeding was at an initial cell density of 6×10^6 cells/plate in DMEM supplemented with 0.25 μg/ml Fungizone, 50 μg/ml gentamicin, 10% calf serum, and 1 ng/ml bFGF. Confluent monolayers were washed twice with DMEM alone prior to the addition of 150 ml/plate of DMEM supplemented with 2.5 μg/ml Fungizone, 50 μg/ml gentamicin, 5 μg/ml insulin, 10 μg/ml transferrin, and 0.1 ng/ml bFGF. After 48 h, culture fluids were collected and replaced with the same amount of fresh serum-free medium. Collections were made for two weeks without visible deterioration of the monolayer. VEGF

```
                                  70                                  80                                  90
                    Glu Cys Val Pro Thr Glu Glu Ser Asn Ile Thr Met Gln Ile Met Arg Ile Lys Pro His Gln Gly Gln His Ile
PCR-1    aagctt gag tgt gtg ccc act gag gag tcc aac atc acc atg cag ATT ATG CGG ATC AAA CCT CAC CAA GGC CAG CAC ATA
PCR-2    aagctt gag tgt gtg ccc act gag gag tcc aac atc acc atg cag ATT ATG CGG ATC AAA CCT CAC CAA GGC CAG CAC ATA
PCR-3    aagctt gag tgt gtg ccc act gag gag tcc aac atc acc atg cag ATT ATG CGG ATC AAA CCT CAC CAA GGC CAG CAC ATA

                                 100                                 110
    Gly Glu Met Ser Phe Leu Gln His Asn Lys Cys Glu Cys Arg Pro Lys Lys Asp Arg Ala Arg Gln Glu Lys Lys Ser Val
PCR-1    GGA GAG ATG AGC TTC CTA CAG CAC AAC AAA TGT GAA TGC AGA CCA AAG AAG GAT AGA GCA AGA CAA GAA AAA AAA TCA GTT
PCR-2    GGA GAG ATG AGC TTC CTA CAG CAC AAC AAA TGT GAA TGC AGA CCA AAG AAA GAT AGA GCA AGA CAA GAA AA ------------
PCR-3    GGA GAG ATG AGC TTC CTA CAG CAC AAC AAA TGT GAA TGC AGA CCA AAG AAA GAT AGA GCA AGA CAA GAA AA ------------
                                                                  *
        120                                 130                                 140
    Arg Gly Lys Gly Lys Gly Gln Lys Arg Lys Arg Lys Lys Ser Arg Tyr Lys Ser Trp Ser Val Pro Cys Gly Pro Cys Ser
PCR-1    CGA GGA AAG GGA AAG GGG CAA AAA CGA AAG CGC AAG AAA TCC CGG TAT AAG TCC TGG AGC GTT CCC TGT GGG CCT TGC TCA
PCR-2    ---------------------------------------------------------------------- T CCC TGT GGG CCT TGC TCA
PCR-3    ----------------------------------------------------------------------------------------------------

                    150                                 160                                 170
    Glu Arg Arg Lys His Leu Phe Val Gln Asp Pro Gln Thr Cys Lys Cys Ser Cys Lys Asn Thr Asp Ser Arg Cys Lys Ala
PCR-1    GAG CGG AGA AAG CAT TTG TTT GTA CAA GAT CCG CAG ACG TGT AAA TGT TCC TGC AAA AAC ACA GAC TCG CGT TGC AAG GCG
PCR-2    GAG CGG AGA AAG CAT TTG TTT GTA CAA GAT CCG CAG ACG TGT AAA TGT TCC TGC AAA AAC ACA GAC TCG CGT TGC AAG GCG
PCR-3    ----------------------------------------------------------------------------------------------------

                                 180                                 189
    Arg Gln Leu Glu Leu Asn Glu Arg Thr Cys Arg Cys Asp Lys Pro Arg Arg .
PCR-1    AGG CAG CTT GAG TTA AAC GAA CGT ACT TGC AGA tgt gac aag ccg agg cgg tga gccgggcaggagcaagctt
PCR-2    AGG CAG CTT GAG TTA AAC GAA CGT ACT TGC AGA tgt gac aag ccg agg cgg tga gccgggcaggagcaagctt
PCR-3    ------------------------------------ A tgt gac aag ccg agg cgg tga gccgggcaggagcaagctt
```

FIG. 2. **DNA sequences of products obtained from PCR amplification of the variable (carboxyl-terminal) portion of the VEGF coding region in fetal human VSM polyadenylated RNA.** The PCR products shown have the sequences expected for amplified copies of the carboxyl-terminal portion of the coding regions for $VEGF_{189}$ (*PCR-1*), $VEGF_{165}$ (*PCR-2*), and $VEGF_{121}$ (*PCR-3*). Primer sequences are shown in *lower case letters*, with the *Hin*dIII sites *underlined*. *Dashes* in the amplified sequences indicate nucleotides missing in PCR-2 and PCR-3 when compared with PCR-1. Predicted amino acids are numbered as in Keck *et al.* (1989) for the 189-residue form of VEGF (the PCR-2 nucleotide sequence encodes an asparagine at amino acid position 115, rather than lysine as in PCR-1 and PCR-3). The *asterisk* indicates an apparent polymorphism in the codon encoding amino acid 108.

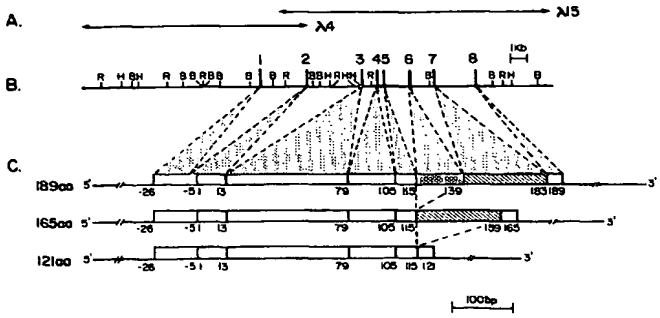

FIG. 3. **Human VEGF gene structure.** *A*, extents of the genomic DNA inserts contained in the clones λ4 and λ15. *B*, restriction map of the human VEGF gene and flanking regions, as established from clones λ4 and λ15. Sites are marked for the enzymes *Eco*RI (*R*), *Hin*dIII (*H*), and *Bam*HI (*B*). The locations of exons 2–7 and of the coding region portions of exons 1 and 8 are indicated. *C*, the 189-, 165-, and 121-amino acid (*aa*) forms of VEGF arise by alternative splicing. Amino acids in each form are numbered below the schematic diagrams, starting with the mature amino terminus. The signal peptide is indicated by *solid shading*. Exon 6, which is only present in $VEGF_{189}$, is marked by *cross-hatching*; exon 7, present in $VEGF_{189}$ and $VEGF_{165}$, is indicated by *diagonal lines*.

protein was partially purified from the conditioned medium by a combination of heparin-Sepharose affinity chromatography and C_4 reversed-phase high-performance liquid chromatography (HPLC) as described (Gospodarowicz *et al.*, 1989). The proteins in the peak activity fractions from the HPLC column were electrophoresed on a reducing 12.5% acrylamide, sodium dodecyl sulfate (SDS) gel (Laemmli, 1970), transferred to a polyvinylidene difluoride membrane (Millipore), and sequenced on an Applied Biosystems 477A gas-phase protein sequencer with an on-line model 120A PTH Analyzer for amino acid identification.

PCR Analysis—By using the antisense primer 5′ GCCAAGCTTGCTCCTGCCCGGCTCACCGCCTCGGCTTGTCACA 3′ and a cDNA synthesis kit (Boehringer Mannheim), cDNA was synthesized from 5 μg of fetal human VSM cell polyadenylated RNA. Following first strand cDNA synthesis, the reaction was extracted with phenol and chloroform and precipitated with ethanol. The cDNA was then amplified by 30 rounds of PCR (Saiki *et al.*, 1988) in a Perkin-Elmer Cetus DNA Thermal Cycler using the antisense primer above and a sense strand primer, 5′ GCCAAGCTTGAGTGTGTGCCCACTGAGGAGTCCAACATCACCATGCAG 3′. Each primer contained a *Hin*dIII site near its 5′ end, and the products of the PCR were digested with *Hin*dIII prior to fractionation on a 3% agarose gel. Fragments detected by ethidium bromide staining of the gel were eluted and cloned into the *Hin*dIII site in M13mp18 (Yanisch-Perron *et al.*, 1985) for sequence analysis by the dideoxynucleotide method (Sanger *et al.*, 1980).

Isolation of Genomic Clones—A human lung fibroblast genomic library in λ FIX (Stratagene) was screened on nitrocellulose filters by hybridization to the 789-base pair (bp) cDNA insert in clone λST800, which encodes a portion of bovine $VEGF_{120}$ (Tischer *et al.*, 1989). Hybridization was overnight at 37 °C in 40% formamide, 50 mM HEPES, pH 7.0, 0.1% Ficoll, 0.1% polyvinylpyrrolidone, 0.1% bovine serum albumin, 0.75 M NaCl, 75 mM sodium citrate, and 50 μg/ml sheared salmon sperm DNA. The filters were washed at 50 °C in 0.15 M NaCl, 15 mM sodium citrate, 0.1% SDS. An additional screening to search for the 5′-most coding region of VEGF was carried out with a ^{32}P-labeled 54-base oligonucleotide, 5′ CTCTCTTGGGTACATTGGAGCCTTGCCTTGCTGCTCTACCTTCACCATGCCAAG 3′, designed based on the sequence of a bovine cDNA clone generated by primer extension across the 5′ end of the bovine VEGF coding region. Hybridizations with the oligonucleotide and filter washes were as above, except that the hybridizations were carried out at room temperature in buffer lacking formamide. DNA from hybridizing phage was purified and subcloned into appropriate M13 cloning vectors for nucleotide sequencing (Sanger *et al.*, 1980) of both strands.

Primer Extension Analysis—Two synthetic antisense oligonucleotides, 5117 (5′ CCTCTTTCTGCTGGTTTCCAAAATCCACAG 3′) and 5118 (5′ CCTCGACTTCTCTCTGGAGCTCTTGCTACC 3′), were labeled with [γ-^{32}P]ATP and polynucleotide kinase to 5 × 10^6 cpm/μg. In each primer extension reaction, approximately 5 × 10^5 cpm of one of the oligonucleotides was co-precipitated in ethanol with 1 μg of U-937 cell polyadenylated RNA. In control reactions, the oligonucleotides were co-precipitated with 4 μg of U-937 RNA which had been depleted of polyadenylated RNA by passage over oligo(dT)-cellulose. The samples were resuspended in 50 μl of 40 mM PIPES, pH 6.4, 0.4 M NaCl, 1 mM EDTA, heated to 95 °C for 5 min, and annealed at 50 °C for 8 h. Following precipitation with ethanol, the samples were resuspended in 60 μl of 33 mM KCl, 9 mM $MgCl_2$, 40 mM Tris-Cl, pH 8.5, and 0.7 mM each dATP, dCTP, dGTP, and dTTP. RNasin (60 units) and avian myeloblastosis virus reverse transcriptase (25 units; Boehringer Mannheim) were then added, and the reactions were incubated at 42 °C for 45 min. After extraction with phenol and chloroform and precipitation with ethanol, the products of each reaction were fractionated on a 6% polyacrylamide, 8 M urea gel alongside the products of a set of dideoxy sequencing reactions. The dideoxy sequence ladder was generated from a genomic subclone containing the 5′ end of the VEGF gene, using as a sequencing primer the same oligonucleotide as was used for the primer extension.

RESULTS

Synthesis of VEGF in Cultured Vascular Smooth Muscle Cells—Since VSM cells are in close proximity to endothelial cells in blood vessels, we sought to determine whether they represent a potential source of VEGF activity that could act in a paracrine fashion on the vascular endothelium. Messenger RNA was isolated from fetal human VSM cells and found by Northern blot analysis (Fig. 1) to contain VEGF transcripts of 5.5, 4.4, and 3.7 kilobases (kb). This result is in contrast to the reports that bovine pituitary folliculo stellate cells contain only a 3.7-kb mRNA (Leung *et al.*, 1989) or 4.2-, 3.7-, and 3.4-kb mRNAs (Tischer *et al.*, 1989), whereas U-937 cells express an approximately 3.8-kb transcript (Keck *et al.*, 1989). VEGF transcripts were not detected in similar blots using polyadenylated RNA isolated from cultured capillary endothelial cells (data not shown).

To confirm that VSM cells are capable of producing VEGF protein as well as mRNA, conditioned medium was collected from bovine VSM cells, and the endothelial cell mitogen present in the medium was purified using heparin-Sepharose chromatography and C_4 reversed-phase HPLC, followed by electrophoresis on a 12.5% acrylamide, SDS gel. The proteins fractionated on the gel were transferred onto a polyvinylidene difluoride membrane, and the region of the membrane carrying a protein migrating at the same apparent molecular weight as bovine pituitary folliculo stellate cell VEGF (Gospodarowicz *et al.*, 1989) was excised for sequencing. The amino-terminal sequence of the protein on the membrane was determined to be Ala-Pro-Met-Ala-Glu-*X*-Gly-Gln-, in agreement with the amino-terminal sequence reported previously for bovine VEGF (Ala-Pro-Met-Ala-Glu-Gly-Gly-Gln-; Gospodarowicz *et al.*, 1989; Tischer *et al.*, 1989; Leung *et al.*, 1989).

Expression of Multiple Forms of the VEGF Coding Region in VSM Cells—A cDNA clone encoding the 189-amino acid form of human VEGF ($VEGF_{189}$) has been isolated from U-937 cells (Keck *et al.*, 1989), whereas cDNA clones encoding $VEGF_{189}$ and the 165- and 121-amino acid forms of human VEGF ($VEGF_{165}$ and $VEGF_{121}$) have been isolated from phorbol ester-activated HL60 cells (Leung *et al.*, 1989). Compared with $VEGF_{121}$, $VEGF_{165}$ has an extra 44 residues located six amino acids from the carboxyl terminus, and $VEGF_{189}$ has an additional 24 amino acids located immediately upstream of the 44-residue insert. To investigate the occurrence of this VEGF coding region heterogeneity in a cell type other than the promyelocytic leukemia HL60 cells, a bovine VEGF cDNA probe (Tischer *et al.*, 1989) was used to isolate multiple VEGF clones from a fetal human VSM library. Although many of these clones were found by nucleotide sequence analysis to be

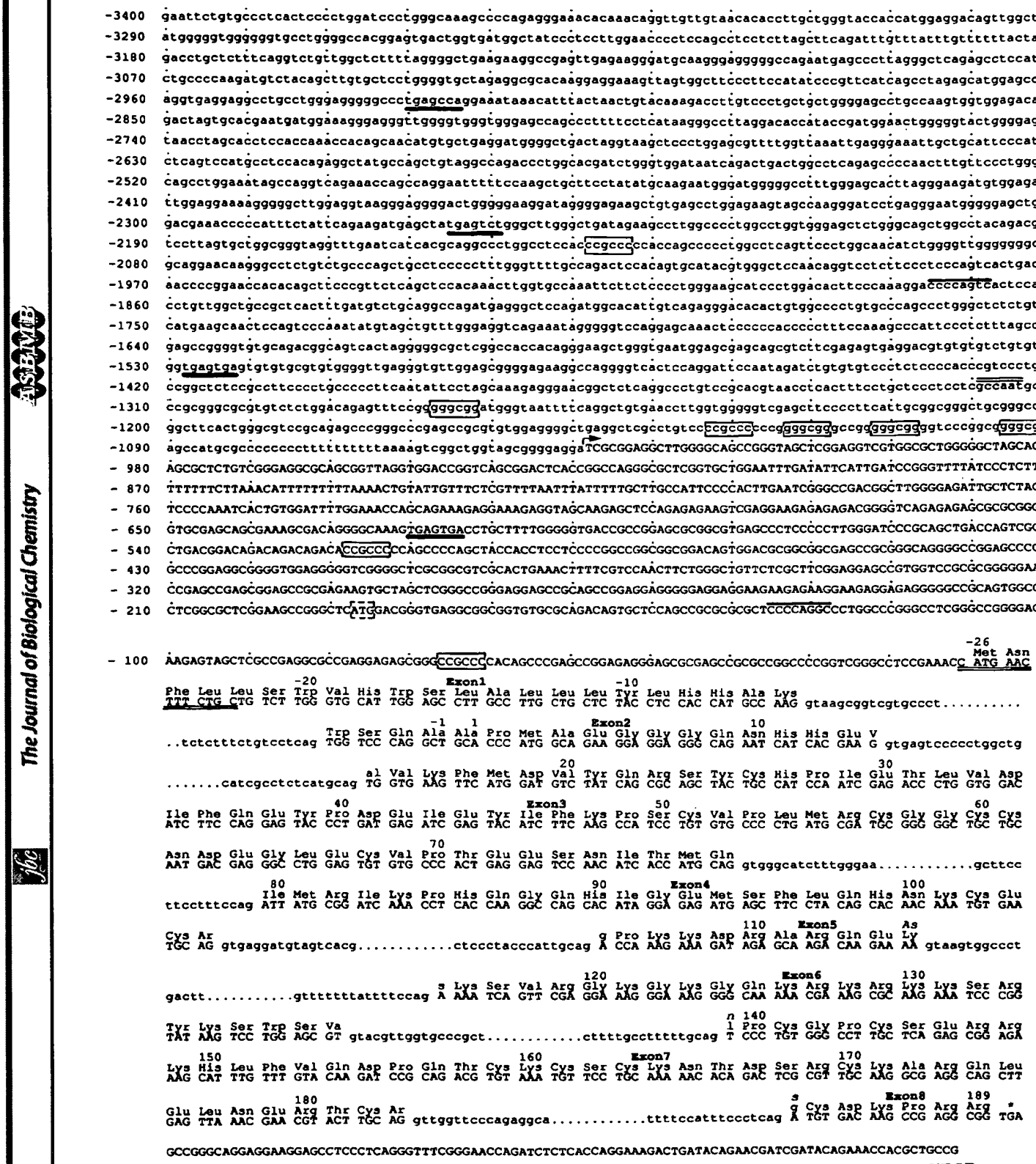

FIG. 4. **Partial nucleotide sequence of the human VEGF gene.** Nucleotides present in mature VEGF transcripts are shown in *upper case letters*; nucleotides present in the 5′-flanking region and introns are in *lower case*. Amino acids are numbered from the alanine residue corresponding to the amino terminus of the mature protein, and nucleotides are numbered from the translation start site. Regions closely matching transcriptional control consensus sequences are indicated as follows: *solid boxes*, Sp1 (5′ GGGCGG 3′ or 5′ CCGCCC 3′);

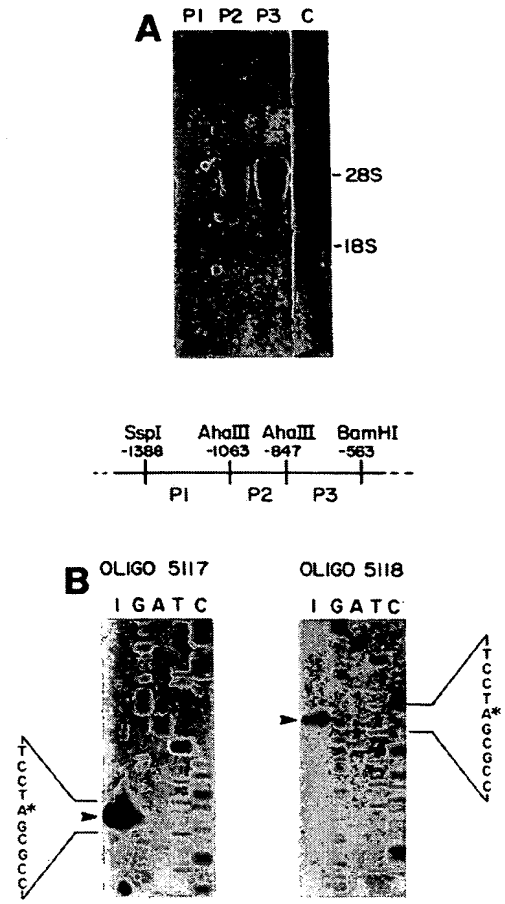

FIG. 5. **Mapping of the VEGF transcriptional start site in U-937 cells.** *A*, Northern blot analyses of total RNA (25 μg/lane) from U-937 cells. The RNA was fractionated on a 1.0% agarose-formaldehyde gel and transferred to nitrocellulose. The lanes were probed with one of three restriction fragments: P1 (a 325-bp *Ssp*I-*Aha*III fragment, nucleotides −1388 to −1064); P2 (a 216-bp *Aha*III fragment, nucleotides −1063 to −848); and P3 (a 284-bp *Aha*III-*Bam*HI fragment, nucleotides −847 to −564). Each of the probes was nick-translated to an approximately equal specific activity. Hybridization conditions were as described for the genomic library screening, except that 50% formamide was used. Washes were carried out at 50 °C in 15 mM NaCl, 1.5 mM sodium citrate, 0.1% SDS, prior to autoradiography. The control lane (*lane C*) was probed with a cDNA corresponding to the complete coding sequence for $VEGF_{165}$. *B*, primer extension analysis of VEGF mRNA. The primer extension products generated using oligonucleotide 5117 or 5118 were fractionated alongside a DNA sequencing ladder primed by the same oligonucleotide as was used for the primer extension. The location of the major primer extension product in each case is indicated by an *arrow*, and the A nucleotide complementary to the transcriptional start site (nucleotide −1038) is indicated by an *asterisk*. The primer extension products were not observed in reactions using control RNA (U-937 RNA that had been depleted of polyadenylated RNA by passage over an oligo(dT)-cellulose column).

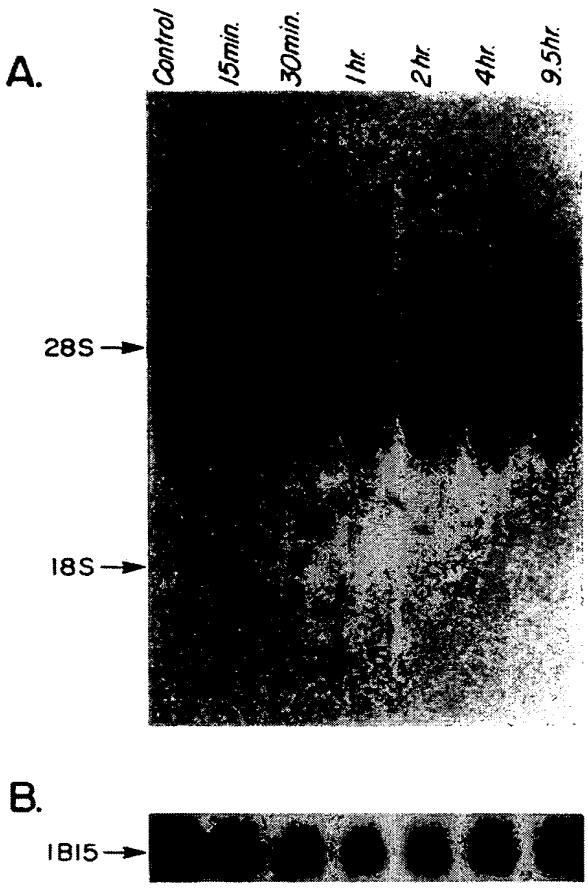

FIG. 6. **Northern blot analysis of polyadenylated RNA isolated from untreated (*Control*) fetal human VSM cells and from cells treated for various time periods with TPA.** *A*, VEGF transcripts detected in the RNA samples. The experimental procedures used were as in Fig. 1. Before blotting, the fractionated RNAs in the gel were stained with ethidium bromide to confirm that approximately equal amounts of RNA were loaded in each lane. The migration positions of the 28 and 18 S ribosomal RNA species in the samples are indicated to the left of the autoradiogram. *B*, level of cyclophilin RNA transcript in the RNA samples. To further confirm that the gel lanes were loaded with similar amounts of RNA, the Northern blot membrane in *A* was reprobed for the level of the constitutively expressed cyclophilin RNA (Sternfeld *et al.*, 1988) encoded by the 1B15 cDNA.

copies of partially unspliced mRNAs, the sequence analysis showed that the spliced portions of the clones represented copies of three different sequences, corresponding to the coding regions for $VEGF_{189}$, $VEGF_{165}$, or $VEGF_{121}$ (data not shown).

The occurrence of the coding region heterogeneity in the fetal human VSM cells was confirmed by PCR analysis. In this experiment, oligonucleotides flanking the variable (carboxyl-terminal) portion of the coding region were used to prime a PCR synthesis from fetal human VSM single-stranded cDNA. The various products of the PCR reaction visible after agarose gel electrophoresis and ethidium bromide staining were excised from the gel, subcloned into M13mp18, and sequenced. This analysis revealed three products that had the sequences predicted for the PCR copies of the $VEGF_{189}$, $VEGF_{165}$, and $VEGF_{121}$ coding regions (Fig. 2).

Like HL60 cells, then, cultured fetal human VSM cells express three different forms of the VEGF coding region.

bold underlines, AP-1 (5′ TGAC/GTCA 3′); *bold overlines*, AP-2 (5′ CCCCAGGC 3′); *double overline*, nuclear factor I (5′ GCCAAT 3′; Mitchell and Tjian, 1989); *double underline*, heat shock (5′ CXXGAAXXTTCXXG 3′; Bienz and Pelham, 1986). The *dashed box* in the 5′-untranslated region marks the upstream ATG codon. The major site of transcription initiation as identified by primer extension analysis is indicated by a *bent arrow*.

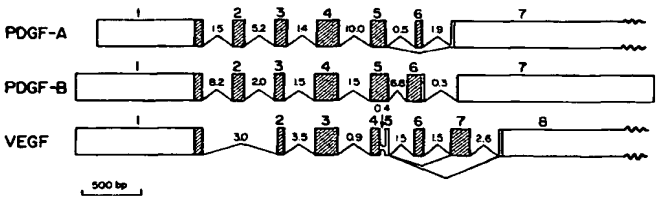

FIG. 7. **Comparison of the intron-exon structure of the VEGF gene with those of the PDGF A and B chain genes.** The number of each exon is given above each gene structure; coding regions are marked by *diagonal lines* and untranslated regions by *open boxes*. The precise lengths of the 3′-untranslated regions of PDGF A and VEGF are not known. Numbers between the exons refer to the size of each intron in kilobases. Both the normal and alternative exon splicing patterns are shown. The scale refers to the exon sequences only. Data for the PDGF A and B chains are from Rao *et al.* (1986) and Bonthron *et al.* (1988).

Similar PCR analyses using bovine folliculo stellate cell single-stranded cDNA as the template showed only the products corresponding to $VEGF_{164}$ and $VEGF_{120}$ (Tischer *et al.*, 1989), consistent with the fact that VEGF cDNA clones encoding a bovine equivalent to the 189-amino acid human form were not isolated from bovine folliculo stellate cDNA libraries (Leung *et al.*, 1989; Tischer *et al.*, 1989). This may be due to the different cell types analyzed, or it may indicate a species difference between human and bovine VEGF.

Isolation and Characterization of Human VEGF Genomic Clones—Two bacteriophage λ clones spanning portions of the human VEGF gene were isolated from a human lung fibroblast genomic library, using as probes either a bovine VEGF cDNA fragment or a synthetic oligonucleotide corresponding to the coding region for a portion of the secretion signal of bovine VEGF. The restriction enzyme maps for these two clones, λ4 and λ15, were determined for the enzymes *Hin*dIII, *Eco*RI, and *Bam*HI by a combination of single and double digests (Fig. 3). Restriction fragment lengths predicted from the maps were confirmed by Southern blot analysis of human genomic DNA (data not shown). The two genomic clones overlap (both contain exon 2) and define a contiguous stretch of approximately 28 kb. The coding domain for human VEGF is contained within approximately 14 kb.

The coding domains, intron-exon junctions, 5′-untranslated region, putative promoter region, and part of the 3′-untranslated region were sequenced (Fig. 4). A comparison of the sequence of the gene with that of the human cDNAs isolated previously (Keck *et al.*, 1989; Leung *et al.*, 1989), and characterized here from fetal human VSM cells, indicates that the coding sequence is interrupted by seven introns. The sequences of all intron-exon boundaries conform to the consensus splicing signals (Breathnach and Chambon, 1981). The locations of all of the exons except exons 6 and 8 on the genomic map shown in Fig. 3 were established directly from the nucleotide sequence analysis of subclones, in that the sequencing spanned restriction enzyme sites identified on the genomic map; exons 6 and 8 were located approximately through the use of exon-specific oligonucleotides to probe Southern blots of restriction enzyme-digested λ15 DNA. The absence of additional introns in the 5′-untranslated region was confirmed by PCR (data not shown).

Comparison of the cDNA cloning and PCR results with the human VEGF gene sequence also indicated that the three forms of the VEGF coding region arise by alternative exon splicing (see Figs. 2 and 4). The alternative splicing involves exons 6 and 7 (Fig. 3); if neither exon is removed, $VEGF_{189}$ is generated; if only exon 6 is removed, $VEGF_{165}$ (with a lysine-to-asparagine change at residue 115) is generated; and if both exons 6 and 7 are removed, $VEGF_{121}$ (with a lysine at residue 115) is generated. The 44-amino acid segment encoded by exon 7, which is present in both $VEGF_{189}$ and $VEGF_{165}$, contains 7 cysteines not found in the shortest VEGF form. This segment is also very basic in nature, containing 9 arginine and lysine residues. The 24-amino acid segment encoded by exon 6, present only in $VEGF_{189}$, is even more basic in nature, containing 12 lysine and arginine residues.

Analysis of the Human VEGF Gene Promoter—The 5′ end of the human VEGF mRNA was mapped by Northern blot analysis as well as by primer extension using synthetic oligonucleotides. Northern blots of U-937 cell total RNA probed with a series of genomic restriction fragment probes (Fig. 5*A*) defined the approximate location of the transcriptional start site. The results indicated that probe P2 (nucleotides −1063 to −848 in Fig. 4) is the 5′-most probe which still hybridizes to the VEGF mRNA; probe P1 (nucleotides −1388 to −1064) gave no detectable signal on the Northern blot and apparently corresponds, therefore, to nontranscribed sequences. Primer extension analysis was then carried out with two synthetic antisense oligonucleotides whose 5′ ends are 35 bases apart (nucleotides −749 to −720 and −714 to −685 in Fig. 4) to obtain a precise definition of the transcription start site. Results from this analysis (Fig. 5*B*) indicated that the human VEGF gene has a single major transcriptional start site, although several potential minor starts were also evident on longer exposures of the autoradiographs. By fractionating the primer extension products alongside matching DNA sequence ladders (Fig. 5*B*), the precise location of the major start site was found to be 1038 bp upstream from the ATG initiation codon.

VEGF Transcript Levels in VSM Cells Treated with TPA—The effect of phorbol ester treatment on the level of VEGF transcripts in fetal human VSM cells was assessed by exposing confluent cultures to 20 ng/ml TPA for various time periods. Polyadenylated RNA was then isolated, and the relative level of VEGF transcripts was determined by Northern blot analysis (Fig. 6). The results indicate that the amount of VEGF mRNA in the VSM cells rises in response to the TPA, reaching a maximum at 2–4 h.

DISCUSSION

Cultured VSM cells have been shown to synthesize VEGF mRNA and to secrete biologically active VEGF. This observation raises the possibility that VSM cells act as a source of VEGF that could function as a paracrine factor both to maintain the integrity of the vascular endothelium and to repair endothelial damage. Since VEGF binds heparin (although with a lower affinity than does bFGF; Gospodarowicz *et al.*, 1989; Ferrara and Henzel, 1989), locally synthesized VEGF might be stored in the extracellular matrix bound to heparin-like molecules, as appears to occur with bFGF (Vlodavsky *et al.*, 1987). Whether VSM cells make VEGF *in vivo* remains to be confirmed by *in situ* hybridization or by immunohistochemistry.

Structural characterization of the human VEGF gene shows that it comprises eight exons. Mature $VEGF_{189}$ retains coding sequence from exons 2–8 (exon 1 representing the majority of the secretion signal portion of the primary translation product), whereas $VEGF_{165}$ lacks the amino acids encoded by exon 6, and $VEGF_{121}$ lacks the residues encoded by exons 6 and 7. RNA species corresponding to all three forms have been detected in cultured VSM cells via cDNA cloning and PCR. VEGF protein isolated from various cell sources (Ferrara and Henzel, 1989; Gospodarowicz *et al.*, 1989; Connolly *et al.*, 1989a, 1989b) has been reported to have a subunit molecular

mass of between 18 and 24 kDa, but individual proteins corresponding to the 189-, 165-, and 121-amino acid forms have not been definitively characterized. There is therefore as yet no direct evidence that the three proteins encoded by the three different VEGF coding region forms are actually synthesized *in vivo*.

The physical properties of the proteins that are predicted from the three coding sequences differ considerably. Both $VEGF_{189}$ and $VEGF_{165}$ have 16 cysteines; 8 of those are encoded by exons 3 and 4 (common to all VEGF forms), 7 are encoded by exon 7 (not present in $VEGF_{121}$), and 1 is encoded by exon 8 (common to all VEGF forms). There are also significant charge differences: 12 of the 24 codons in exon 6 (not present in $VEGF_{165}$ and $VEGF_{121}$) encode basic amino acids, and 9 of the 44 codons in exon 7 (not present in $VEGF_{121}$) encode basic amino acids. Thus, in addition to significant structural changes, isoelectric point variations should result from these differences, in that the shorter forms of VEGF are predicted to be more acidic. No biological activity differences have yet been reported reflecting these altered physical properties.

The locations of the intron-exon junctions in VEGF are compared in Fig. 7 to those in the PDGF A and B chains. Both PDGF A and B have very similar gene structures (Rao *et al.*, 1986; Bonthron *et al.*, 1988). An overall similarity in gene structure can also be observed between VEGF and the PDGFs, but significant differences do exist which are consistent with the low level (20–25%) of amino acid sequence relatedness between VEGF and the PDGFs. Exon 1 in both VEGF and the PDGFs contains a relatively long (approximately 840–1030 bp) 5′-untranslated region as well as the majority of the hydrophobic signal peptide domain. Following this, exon 2 in VEGF, and exons 2 and 3 in the PDGFs, represent a region with no sequence similarity. Exons 3 in VEGF and 4 in PDGF are comparable and contain 6 of the 8 conserved cysteine residues, but the precise sequences at the intron-exon boundaries are not conserved. VEGF exons 4 and 5 appear to correspond to exon 5 in the PDGFs; this region contains the two other conserved cysteines but the overall sequence relatedness is minimal. Exon 6 is a highly basic region in both PDGFs and in VEGF, and there is more sequence similarity in this region between VEGF and the PDGF A chain than between the two PDGFs (see Bonthron *et al.*, 1988; Betsholtz *et al.*, 1990).

In the case of PDGF A, but not PDGF B, an alternatively spliced form is found which lacks the residues encoded by exon 6. In this respect VEGF is, therefore, like PDGF A, since both $VEGF_{165}$ and $VEGF_{121}$ lack the exon 6 amino acids. The short form of PDGF A appears to be the exclusive PDGF A gene product in endothelial cells, and the long form is made by several transformed lines (Betsholtz *et al.*, 1986; Tong *et al.*, 1987; Collins *et al.*, 1987). Both the long and the short forms of PDGF A appear to be equally active, but it has been reported that the short form may be less efficiently secreted and dimerized (Beckman *et al.*, 1988; Collins *et al.*, 1987). In the case of VEGF, both the 189- and 165-residue forms have been expressed recombinantly and shown to be biologically active (Leung *et al.*, 1989; Keck *et al.*, 1989), indicating that, as with PDGF A, the exon 6-encoded amino acids are not essential for VEGF activity.

Exon 7 in VEGF, which encodes the domain with 7 cysteines, appears to have no counterpart in either PDGF chain. It will be interesting to determine whether the presence of this region confers $VEGF_{189}$ and $VEGF_{165}$ with biological properties in addition to mitogenicity, such as the ability to induce permeability in the vascular endothelium. Finally, although there is no sequence similarity in this region, both PDGF A and VEGF have a short carboxyl-terminal coding region present in exons 7 and 8, respectively, followed by the 3′-untranslated region.

Similarly to both PDGF chains (Bonthron *et al.*, 1988; Rao *et al.*, 1986), the section of the 5′-untranslated region of VEGF immediately upstream of the translation initiation codon is very GC-rich. A GC-rich 5′-untranslated region has also been noted in other growth factor genes such as those encoding bFGF and transforming growth factor β (Abraham *et al.*, 1986; Derynck *et al.*, 1985) and may be involved in translational control. The 5′-untranslated region of VEGF contains a single ATG codon located 185–187 nucleotides upstream of the proposed initiating methionine codon. In this respect VEGF is again like the two PDGFs, both of which have three apparently nonutilized ATG codons in their 5′-untranslated regions. The significance of these ATGs is unknown but it has been proposed they might also have a role in translational control (Bonthron *et al.*, 1988).

Primer extension analysis mapped the single major transcriptional initiation site for the human VEGF gene to nucleotide −1038 (Fig. 4). Approximately 50 bp 5′ to this site there is a cluster of four GC box sequences (5′ GGGCGG 3′ or 5′ CCGCCC 3′) at nucleotides −1096 to −1091, −1112 to −1107, −1123 to −1118, and −1133 to −1128. GC box sequences located close to transcription start sites in other genes have been shown to bind the transcription factor Sp1 (Gidoni *et al.*, 1984; Kadonaga *et al.*, 1986). Three of these four GC boxes near the transcription start site in the VEGF gene are also perfect matches to a consensus sequence for "strong" Sp1 binding sites (5′ G/TGGGCGGG/AG/AC/T 3′ or its complement 5′ G/AC/TC/TCCGCCCC/A 3′; Kadonaga *et al.*, 1986). In addition, two other GC box sequences are found further upstream in the 5′-flanking region (nucleotides −1277 to −1272 and −2138 to −2133), and two more are present in the 5′-untranslated region (nucleotides −66 to −61 and −518 to −513). No TATA box-like promoter sequence (Corden *et al.*, 1980) is seen close to the start of transcription; the only match to this consensus sequence is found at nucleotides −2465 to −2461 in the 5′-flanking region, too far from the transcription start site to be of significance. The human VEGF gene, therefore, differs from the human PDGF genes which both have TATA box promoters (Rao *et al.*, 1986; Bonthron *et al.*, 1988). Also although the primer extension analysis carried out on the VEGF gene did reveal the possibility of several minor transcription start sites, it is unusual for a promoter with multiple closely spaced GC boxes as in the case of VEGF to have a single major transcription initiation site.

The sequence of the VEGF gene was scanned for additional consensus binding sites for other transcriptional control factors (reviewed in Mitchell and Tjian, 1989; Johnson and McKnight, 1989). The presence of four potential AP-1 binding sites (consensus 5′ TGAC/GTCA 3′) at nucleotides −620 to −614, −1528 to −1522, −2265 to −2258, and −2930 to −2924 (see Fig. 4) implied that the VEGF gene should be inducible by serum or by the phorbol ester TPA (Curran and Franza, 1988; Mitchell and Tjian, 1989). In addition, two potential AP-2 binding sites (consensus 5′ CCCCAGGC 3′ or 5′ T/CCCCCA/CNG/CC/GG/C 3′) at nucleotides −135 to −128 and −1875 to −1868 also indicated that VEGF gene expression should be inducible by TPA, as well as by cAMP (Imagawa *et al.*, 1987; Mitchell and Tjian, 1989). Consistent with these predictions, initial experiments with fetal human VSM cells indicate that TPA treatment indeed results in an increase in the level of VEGF mRNA (Fig. 6). The availability of cloned VEGF promoter sequences will allow a detailed examination

of this and other components involved in VEGF transcriptional regulation to take place.

Acknowledgments—We thank J. Iwasa for oligonucleotides, J. Miller for help with DNA sequencing, K. Wood for help with protein purification, K. Lau for protein sequencing, S. Pollitt and T. White for critical reading of the manuscript, E. Stoelting for artwork, and K. MacDonald for preparation of the manuscript.

REFERENCES

Abraham, J. A., Whang, J. L., Tumolo, A., Mergia, A., Friedman, J., Gospodarowicz, D., and Fiddes, J. C. (1986) *EMBO J.* **5,** 2523–2528

Beckman, M. P., Betsholtz, C., Heldin, C.-H., Westermark, B., DiMarco, E., DiFiore, P. P., Robbins, K. C., and Aaronson, S. A. (1988) *Science* **241,** 1346–1349

Betsholtz, C., Johnson, A., Heldin, C.-H., Westermark, B., Lind, P., Urdea, M. S., Eddy, R., Shows, T. B., Philpott, K., Mellor, A. L., Knott, T. J., and Scott, J. (1986) *Nature* **320,** 695–699

Betsholtz, C., Rorsman, F., Westermark, B., Ostman, A., and Heldin, C.-H. (1990) *Nature* **344,** 299

Bienz, M., and Pelham, H. R. B. (1986) *Cell* **45,** 753–760

Bonthron, D. T., Morton, C. C., Orkin, S. H., and Collins, T. (1988) *Proc. Natl. Acad. Sci. U. S. A.* **85,** 1492–1496

Breathnach, R., and Chambon, P. (1981) *Annu. Rev. Biochem.* **50,** 349–383

Chirgwin, J. M., Przybyla, A. E., MacDonald, R. J., and Rutter, W. J. (1979) *Biochemistry* **18,** 5294–5299

Collins, T., Bonthron, D. T., and Orkin, S. H. (1987) *Nature* **328,** 621–624

Conn, G., Soderman, D. D., Schaeffer, M.-T., Wile, M., Hatcher, V. B., and Thomas, K. A. (1990a) *Proc. Natl. Acad. Sci. U. S. A.* **87,** 1323–1327

Conn, G., Bayne, M. L., Soderman, D. D., Kwok, P. W., Sullivan, K. A., Palisi, T. M., Hope, D. A., and Thomas, K. A. (1990b) *Proc. Natl. Acad. Sci. U. S. A.* **87,** 2628–2632

Connolly, D. T., Olander, J. V., Heuvelman, D., Nelson, R., Monsell, R., Siegel, N., Haymore, B. L., Leimgruber, R., and Feder, J. (1989a) *J. Biol. Chem.* **264,** 20017–20024

Connolly, D. T., Heuvelman, D. M., Nelson, R., Olander, J. V., Eppley, B. L., Delfino, J. J., Siegel, N. R., Leimgruber, R. M., and Feder, J. (1989b) *J. Clin. Invest.* **84,** 1470–1478

Corden, J., Wasylyk, B., Buchwaldet, A., Sassone-Corsi, P., Kedinger, C., and Chambon, P. (1980) *Science* **209,** 1406–1414

Curran, T., and Franza, B. R., Jr. (1988) *Cell* **55,** 395–397

Derynck, R., Jarrett, J. A., Chen, E. Y., Eaton, D. H., Bell, J. R., Assoian, R. K., Roberts, A. B., Sporn, M. B., and Goeddel, D. V. (1985) *Nature* **316,** 701–705

Ferrara, N., and Henzel, W. J. (1989) *Biochem. Biophys. Res. Commun.* **161,** 851–858

Gidoni, D., Dynan, W. S., and Tjian, R. (1984) *Nature* **312,** 409–413

Gospodarowicz, D. (1990) *UCLA Symp. Mol. Cell. Biol.* **114,** 15–30

Gospodarowicz, D., Moran, J., and Braun, D. (1977) *J. Cell. Physiol.* **91,** 377–385

Gospodarowicz, D., Haaparanta, T., and Neufeld, G. (1988) *Eur. J. Cell Biol.* **46,** 144–151

Gospodarowicz, D., Abraham, J. A., and Schilling, J. (1989) *Proc. Natl. Acad. Sci. U. S. A.* **86,** 7311–7315

Imagawa, M., Chiu, R., and Karin, M. (1987) *Cell* **51,** 251–260

Johnson, P. F., and McKnight, S. L. (1989) *Annu. Rev. Biochem.* **58,** 799–839

Kadonaga, J. T., Jones, K. A., and Tjian, R. (1986) *Trends Biochem. Sci.* **11,** 20–23

Keck, P. J., Hauser, S. D., Krivi, G., Sanzo, K., Warren, T., Feder, J., and Connolly, D. T. (1989) *Science* **246,** 1309–1312

Laemmli, U. K. (1970) *Nature* **227,** 680–685

Lehrach, H., Diamond, D., Wozney, J. M., and Boedtker, H. (1977) *Biochemistry* **16,** 4743–4751

Leung, D. W., Cachianes, G., Kuang, W.-J., Goeddel, D. V., and Ferrara, N. (1989) *Science* **246,** 1306–1309

Levy, A. P., Tamargo, R., Brem, H., and Nathans, D. (1989) *Growth Factors* **2,** 9–19

Mitchell, P. J., and Tjian, R. (1989) *Science* **245,** 371–378

Plouët, J., Schilling, J., and Gospodarowicz, D. (1989) *EMBO J.* **8,** 3801–3806

Rao, C. D., Igarashi, H., Chiu, I.-M., Robbins, K. C., and Aaronson, S. A. (1986) *Proc. Natl. Acad. Sci. U. S. A.* **83,** 2392–2396

Saiki, R. K., Gelfand, D. H., Stoffel, S., Scharf, S. J., Higuchi, R., Horn, G. T., Mullis, K. B., and Erlich, H. A. (1988) *Science* **239,** 487–491

Sanger, F., Coulson, A. R., Barrell, B. G., Smith, A. J. H, and Roe, B. A. (1980) *J. Mol. Biol.* **143,** 161–178

Senger, D. R., Galli, S. J., Dvorak, A. M., Perruzzi, C. A., Harvey, V. S., and Dvorak, H. F. (1983) *Science* **219,** 983–985

Senger, D. R., Perruzzi, C. A., Feder, J., and Dvorak, H. F. (1986) *Cancer Res.* **46,** 5629–5632

Sternfeld, M. D., Hendrickson, J. E., Keeble, W. W., Rosenbaum, J. T., Robertson, J. E., Pittelkow, M. R., and Shipley, G. D. (1988) *J. Cell. Physiol.* **136,** 297–304

Tischer, E., Gospodarowicz, D., Mitchell, R., Silva, M., Schilling, J., Lau, K., Crisp, T., Fiddes, J. C., and Abraham, J. A. (1989) *Biochem. Biophys. Res. Commun.* **165,** 1198–1206

Tong, B. D., Auer, D. E., Jaye, M., Kaplow, J. M., Ricca, G., McConathy, E., Drohan, W., and Deuel, T. F. (1987) *Nature* **328,** 619–621

Vlodavsky, I., Folkman, J., Sullivan, R., Friedman, R., Ishai-Michaeli, R., Sasse, J., and Klagsbrun, M. (1987) *Proc. Natl. Acad. Sci. U. S. A.* **84,** 2292–2296

Yanisch-Perron, C., Vieira, J., and Messing, J. (1985) *Gene (Amst.)* **33,** 103–119

THE JOURNAL OF BIOLOGICAL CHEMISTRY
© 1997 by The American Society for Biochemistry and Molecular Biology, Inc.

Vol. 272, No. 11, Issue of March 14, pp. 7151–7158, 1997
Printed in U.S.A.

$VEGF_{145}$, a Secreted Vascular Endothelial Growth Factor Isoform That Binds to Extracellular Matrix*

(Received for publication, August 2, 1996, and in revised form, November 20, 1996)

Zoya Poltorak‡, Tzafra Cohen‡§, Revital Sivan‡¶, Yelena Kandelis¶, Gadi Spira¶, Israel Vlodavsky‖, Eli Keshet, and Gera Neufeld‡ ‡‡**

*From the ‡Department of Biology and the §Department of Food Engineering and Biotechnology and the ¶B. Rappaport Faculty of Medicine, Technion-Israel Institute of Technology, Haifa 32000, Israel, the ‖Department of Oncology, Hadassah University Hospital, Jerusalem 91120, Israel, and the **Department of Molecular Biology, The Hebrew University-Hadassah Medical School, Jerusalem 91010, Israel*

A vascular endothelial growth factor (VEGF) mRNA species containing exons 1–6 and 8 of the VEGF gene was found to be expressed as a major VEGF mRNA form in several cell lines derived from carcinomas of the female reproductive system. This mRNA is predicted to encode a VEGF form of 145 amino acids ($VEGF_{145}$). Recombinant $VEGF_{145}$ induced the proliferation of vascular endothelial cells and promoted angiogenesis *in vivo*. $VEGF_{145}$ was compared with previously characterized VEGF species with respect to interaction with heparin-like molecules, cellular distribution, VEGF receptor recognition, and extracellular matrix (ECM) binding ability. $VEGF_{145}$ shares with $VEGF_{165}$ the ability to bind to the KDR/*flk-1* receptor of endothelial cells. It also binds to heparin with an affinity similar to that of $VEGF_{165}$. However, $VEGF_{145}$ does not bind to two additional endothelial cell surface receptors that are recognized by $VEGF_{165}$ but not by $VEGF_{121}$. $VEGF_{145}$ is secreted from producing cells as are $VEGF_{121}$ and $VEGF_{165}$. However, $VEGF_{121}$ and $VEGF_{165}$ do not bind to the ECM produced by corneal endothelial cells, whereas $VEGF_{145}$ binds efficiently to this ECM. Basic fibroblast growth factor (bFGF)-depleted ECM containing bound $VEGF_{145}$ induces proliferation of endothelial cells, indicating that the bound $VEGF_{145}$ is active. The mechanism by which $VEGF_{145}$ binds to the ECM differs from that of bFGF. Digestion of the ECM by heparinase inhibited the binding of bFGF to the ECM and released prebound bFGF, whereas the binding of $VEGF_{145}$ was not affected by heparinase digestion. It therefore seems that $VEGF_{145}$ possesses a unique combination of biological properties distinct from those of previously characterized VEGF species.

The vascular endothelial growth factor (VEGF)[1] isoforms display a limited structural similarity to platelet-derived growth factor and are important regulators of angiogenesis and blood vessel permeability (1–3). The human VEGF isoforms are generated by alternative splicing from a single gene (4–6). The domain encoded by exons 1–5 contains information required for the recognition of the known VEGF receptors KDR/*flk-1* and *flt-1* (7) and is present in all VEGF isoforms. The amino acids encoded by exon 8 are also present in all the VEGF splice variants. The VEGF isoforms are distinguished by the presence or the absence of the peptides encoded by exons 6 and 7 of the VEGF gene. $VEGF_{121}$ is 121 amino acids long and lacks both exons. $VEGF_{165}$ contains the exon 7-encoded peptide, whereas $VEGF_{189}$ contains both exon 6- and exon 7-encoded peptides (6, 8, 9). $VEGF_{121}$ and $VEGF_{165}$ promote angiogenesis, cause permeabilization of blood vessels, and induce proliferation of vascular endothelial cells (10–14). $VEGF_{189}$ has not yet been purified, but studies with cells expressing $VEGF_{189}$ indicate that it may induce endothelial cell proliferation (8, 9). Low levels of a mRNA corresponding in size to a mRNA encoding a putative VEGF variant of 145 amino acids ($VEGF_{145}$) containing exon 6 but lacking exon 7 were detected previously in reverse PCR experiments, but the protein encoded by this mRNA has not yet been characterized (15, 16).

The different VEGF isoforms differ in their heparin binding ability. $VEGF_{121}$ does not bind to heparin, whereas $VEGF_{165}$ and $VEGF_{189}$ do (8, 17–19). The heparin binding affinity of $VEGF_{189}$ was reported to be higher than that of $VEGF_{165}$, suggesting that exon 6 contributes to the heparin binding ability of $VEGF_{189}$ (8). $VEGF_{165}$ and $VEGF_{121}$ are secreted efficiently from producing cells and do not bind efficiently to the ECM produced by CEN4 cells (8, 9). In contrast, $VEGF_{189}$ is retained on the cell surface and in the ECM, from which it can be released by prolonged incubation with heparin. (9). The peptide encoded by exon 7 also seems to affect the receptor recognition patterns of VEGF isoforms. $VEGF_{121}$ recognizes a single VEGF receptor in endothelial cells that was identified as the KDR/*flk-1* VEGF receptor (20, 21). $VEGF_{165}$ also binds to this receptor but recognizes two additional VEGF receptors of unknown structure that are found in endothelial cells and in several transformed cell types (21, 22).

We have observed that $VEGF_{145}$ is one of the main VEGF isoforms expressed by several cell lines derived from carcinomas of the female reproductive system. We have characterized $VEGF_{145}$ and have compared its biological properties with those of other VEGF forms. Recombinant $VEGF_{145}$ expressing the exon 6-derived peptide binds to heparin but behaves like $VEGF_{121}$ with regard to its receptor recognition ability. In contrast to $VEGF_{121}$ and $VEGF_{165}$, it binds to a basement membrane like ECM produced by corneal endothelial cells in a biologically active form. $VEGF_{145}$ therefore represents a VEGF form possessing distinct biological characteristics.

* This work was supported by a Joint Angiogenesis Research Center grant from the Israel Academy of Sciences (to G. N., I. V., and E. K.), a grant from the German-Israeli Binational Foundation, and a grant from the Israel Ministry of Health (to G. N.). The costs of publication of this article were defrayed in part by the payment of page charges. This article must therefore be hereby marked "*advertisement*" in accordance with 18 U.S.C. Section 1734 solely to indicate this fact.

‡‡ To whom correspondence should be addressed.

[1] The abbreviations used are: VEGF, vascular endothelial growth factor; BCE, bovine corneal endothelial; bFGF, basic fibroblast growth factor; ECM, extracellular matrix; HUVEC, human umbilical vein-derived endothelial cell; PCR, polymerase chain reaction; PAGE, polyacrylamide gel electrophoresis.

EXPERIMENTAL PROCEDURES

Materials—Human recombinant $VEGF_{165}$ and $VEGF_{121}$ were purified from Sf-9 insect cells, whereas recombinant human bFGF was produced in bacteria as described previously (19, 23, 24). A rabbit polyclonal antibody directed against $VEGF_{165}$ (23) and a mouse monoclonal IgM antibody (M-35) directed against full-length $VEGF_{165}$ were produced in our laboratory using standard techniques. Heparinases type I, II, and III were kindly donated by Dr. J. Zimermann (Ibex Technologies, Montreal, Canada). The bicystronic mammalian expression vector MIRB was kindly provided to us by Dr. Craig MacArthur (Washington University, St. Louis, MO) (25). Anti-VEGF monoclonal antibody clone 26503.11 and peroxidase- and alkaline phosphatase-conjugated anti-rabbit IgG antibodies were from Sigma. Disuccinimidyl suberate was from Pierce. Sodium alginate was from Fluka. Heparin-Sepharose was purchased from Pharmacia Biotech Inc. ^{125}I-Sodium was obtained from New England Nuclear. Anti-mouse IgM antibodies conjugated to alkaline phosphatase were from Southern Biotechnology Associates Inc. (Birmingham, AL). Tissue culture plasticware was from Nunc, and 96-well dishes for enzyme-linked immunosorbent assays were bought from Corning. Grace's medium was obtained from Life Technologies, Inc. All other tissue culture reagents were from Biological Industries Inc. (Kibbutz Beth Haemek, Israel).

Identification of $VEGF_{145}$ mRNA in Cancer Cells—Total mRNA was prepared from OC-238 human epithelial ovarian carcinoma cells (26). Complementary DNA was synthesized from 300 ng of total RNA using oligo(dT) as a primer and avian myeloblastosis virus reverse transcriptase. PCR amplification was carried out in the presence of a [^{32}P]dCTP tracer (2 μCi in a 100-μl reaction volume), 1 mM of each dNTP, 2.5 mM $MgCl_2$, and 2.5 units of *Taq* polymerase. 25 amplification cycles were used, each consisting of a 1-min incubation at 94 °C, a 2-min incubation at 65 °C, and a 3-min incubation at 72 °C. The VEGF-specific oligonucleotides used were GGAGAGATGAGCTTCCTACAG and TCACCGCCTTGGCTTGTCACA, corresponding to amino acids 92–98 and to the six carboxyl-terminal amino acids of VEGF, respectively. A pair of primers from the L19 ribosomal protein were included in the reactions as an internal control. Amplified fragments were resolved in a 6% nondenaturing polyacrylamide gel and were visualized by autoradiography. The band corresponding to the $VEGF_{145}$ mRNA (see Fig. 1*B*) was excised, reamplified, and sequenced.

A similar procedure using different primers was used to detect $VEGF_{145}$ mRNA in A431 and HeLa cells. The VEGF-specific primers used here were derived from the 5′ of the coding region (amino acids 13–20) and from the 3′ region encompassed by the last 6 amino acids of VEGF including the translation stop codon of the VEGF sequence.

Construction of $VEGF_{145}$ Encoding Expression Vectors—In order to produce recombinant $VEGF_{145}$, we prepared a $VEGF_{145}$ cDNA construct by deleting the oligonucleotides encoded by exon 7 out of the $VEGF_{189}$ cDNA. Primers used to amplify exons 1–6 of the VEGF cDNA were the external primer GCTTCCGGCTCGTATGTTGTGTGG, corresponding to a puc118 sequence, and the internal primer ACGCTCCAGGACTTATACCGGGA, corresponding to a sequence at the 3′ end of exon 6. Primers used to amplify the 3′ end of the VEGF cDNA were complementary to the puc118 sequence GGTAACGCCAGGGTTTTCCCAGTC and to the 3′ end of the exon 6 sequence (underlined) and to the start of exon 8 (CGGTATAAGTCCTGGAGCGTATGTGACAAGCCGAGGCGGTGA). Following amplification, the PCR products were precipitated, and the products were reamplified using only the puc118-derived external primers. The product was gel purified, subcloned into the PCR-II vector, and sequenced using the sequenase-II kit from U. S. Biochemical Corp. This cDNA was further used for protein expression studies.

Production and Purification of Recombinant $VEGF_{145}$—The $VEGF_{145}$ cDNA was subcloned into the *Bam*HI site of the MIRB expression vector (25). Following transfection into BHK-21 cells and selection with 0.6 mg/ml G418, $VEGF_{145}$-expressing cells were identified using anti-VEGF antibodies. The $VEGF_{145}$ cDNA was also subcloned into the transfer plasmid pVL-1393 (Invitrogen) downstream from the polyhedrin promoter to yield pVL-1393/v145. This plasmid and baculovirus wild type DNA were co-transfected into Sf9 cells using the calcium-phosphate co-precipitation method, and recombinant baculoviruses were isolated as described (23).

$VEGF_{145}$ was produced in Sf9 cells as described for $VEGF_{165}$ (23). The conditioned medium contained approximately 5 mg of $VEGF_{145}$/liter. The conditioned medium was concentrated by precipitation with 70% ammonium sulfate at 4 °C for 12 h. The precipitate was solubilized in 20 mM Tris, pH 7, and 0.1 M NaCl, dialyzed extensively against this buffer at 4 °C, and applied to a heparin-Sepharose column. The column was washed with the same buffer containing 0.3 M salt, followed by elution with the same buffer containing 0.8 M NaCl. A small residual amount also eluted at 2 M NaCl. The 0.8 M salt eluant was further purified by reverse phase high pressure liquid chromatography on an Applied Biosystems Brownlee C-8 column using a linear gradient of acetonitrile (20–80%) containing 0.1% trifluoroacetic acid. $VEGF_{145}$ was eluted at 48% acetonitrile. The trifluoroacetic acid in the eluant was neutralized using Tris base, and the acetonitrile was removed using a SpeedVac evaporator at room temperature.

Enzyme-linked Immunosorbent Assays—Increasing concentrations of VEGF in 50 μl of coating buffer (20 mM K_2HPO_4, 10 mM KH_2PO_4, 1 mM EDTA, 0.8% NaCl, pH 7.2) were adsorbed to 96-well dishes for 3 h at 25 °C. Free VEGF was aspirated, and the wells were blocked with coating buffer containing 1% bovine serum albumin for 1 h. The wells were extensively washed with wash buffer (10 mM Tris-HCl, pH 7.2, 150 mM NaCl, and 0.1% Tween 20), incubated with the anti-VEGF M-35 monoclonal antibody for 2 h at 25 °C, washed again, and incubated for 1 h with an alkaline phosphatase-conjugated secondary antibody. After final washing, the amount of bound antibody was determined using *para*-nitrophenylphosphate as substrate.

Cell Culture and Production of ECM-coated Dishes—Human umbilical vein-derived endothelial cells (HUVECs) were prepared from umbilical veins and cultured as described previously in M199 medium supplemented with 20% fetal calf serum, vitamins, 1 ng/ml bFGF, and antibiotics (21, 27). Proliferation assays using HUVECs were done as described previously (11). Bovine corneal endothelial (BCE) cells were isolated from steer eyes and cultured as described previously (28). ECM-coated dishes were prepared from cells grown in the presence or the absence of 30 mM chlorate as described previously (28, 29).

Binding of VEGFs to HUVECs and to ECM-coated Dishes—The binding and the cross-linking of ^{125}I-$VEGF_{165}$ to confluent layers of HUVECs grown in 5-cm dishes in the presence or the absence of various competitors was done essentially as described. $VEGF_{165}$ was purified from infected Sf9 cells and iodinated as described (19, 21, 23, 30).

Binding of VEGFs to ECM-coated 96- or 24-well dishes was performed at room temperature. The ECM-coated wells were washed with rinse buffer (10 mM Tris-HCl, pH 7.2, 150 mM NaCl, and 0.1% Tween 20). Nonspecific sites were blocked with binding buffer (20 mM K_2HPO_4, 10 mM KH_2PO_4, 1 mM EDTA, 0.8% NaCl, 1 mg/ml bovine serum albumin, pH 7.2) for 1 h at room temperature. The binding buffer was aspirated and iodinated, or unlabeled growth factors were incubated with the ECM-coated wells in binding buffer for 2 h at 24 °C. Free growth factors were removed by aspiration, and the ECM was washed twice with rinse buffer. In binding experiments, 0.2 N NaOH was added to dissociate bound growth factors, and aliquots were counted in a γ counter or neutralized using Tris base and analyzed by SDS-PAGE followed by autoradiography. Alternatively, the wells were further incubated with various anti-VEGF monoclonal antibodies in binding buffer for 2 h and washed. Bound antibody was detected with appropriate secondary antibodies coupled to alkaline-phosphatase, using *para*-nitrophenylphosphate as substrate. Our M-35 anti-VEGF monoclonal antibody and commercial anti-VEGF monoclonal antibodies produced identical results in these assays.

For biological activity experiments, 15,000 HUVECs were seeded on ECM containing various amounts of adsorbed VEGF in a final volume of 1 ml of growth medium. Cells were trypsinized and counted after 3 days in a coulter counter. All experiments were repeated at least twice with similar results.

RESULTS

$VEGF_{145}$ Is Expressed as a Major VEGF Splice Variant in Several Tumorigenic Cell Lines Originating in the Female Reproductive System—Reverse PCR analysis of mRNA from OC-238 human epithelial ovarian carcinoma cells (Fig. 1*B*), HeLa cells, and A431 cells (Fig. 1*C*) detected a VEGF mRNA containing a coding region smaller than that of $VEGF_{165}$ but larger than that of $VEGF_{121}$. The size of the coding region corresponded to the expected size of a mRNA encoding a VEGF form containing exons 1–6 and 8 and should lead to the production of a VEGF form containing 145 amino acids ($VEGF_{145}$) (15). In all these cell lines the $VEGF_{145}$ cDNA seemed to be expressed at levels comparable with those of $VEGF_{165}$. The $VEGF_{145}$ mRNA was not detected in several other transformed cell lines including C6 glioma cells and U937 cells. Sequence analysis of the PCR product from the OC-238 cells showed that this mRNA

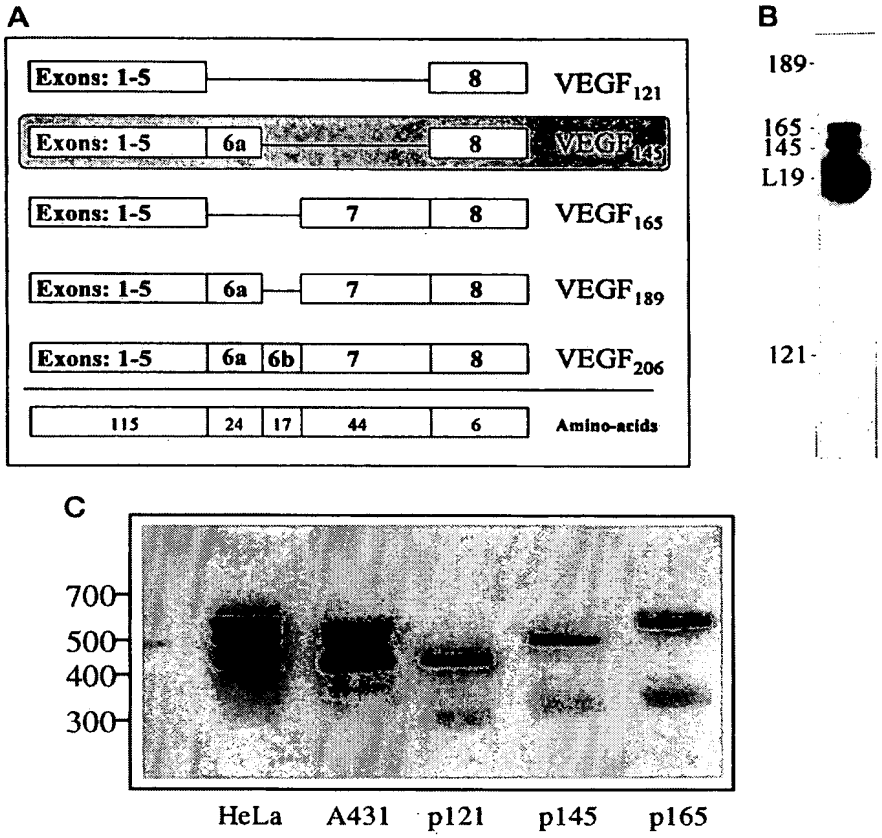

FIG. 1. *A*, the structure of the VEGF splice variants. The peptides encoded by the various exons of the human VEGF gene are shown in *boxes* but are not drawn to scale. The number of amino acids in each of the exon-encoded peptides is shown at the *bottom*. The exon structure of $VEGF_{145}$ is *shaded*. *B*, expression of $VEGF_{145}$ mRNA in OC-238 human epithelial ovarian carcinoma cells. Total RNA from OC-238 cells was translated into cDNA and amplified by PCR using radioactively labeled nucleotides. PCR products were separated on a polyacrylamide gel as described under "Experimental Procedures." Shown is an autoradiogram of the gel. The amplified species of VEGF and L19 cDNA are indicated. *C*, expression of $VEGF_{145}$ in A431 and HeLa cells. Total RNA from HeLa and A431 cells was translated into cDNA and amplified by PCR using radioactively labeled nucleotides as described under "Experimental Procedures." Plasmids containing the $VEGF_{121}$ cDNA, the $VEGF_{165}$ cDNA, and the $VEGF_{145}$ recombinant cDNA were included in separate PCR reactions using the primers described under "Experimental Procedures." Shown is an autoradiogram of the gel.

was indeed generated by alternative splicing and that it contains exons 6 and 8 but not exon 7 of the VEGF gene.

To study the properties of $VEGF_{145}$, we have expressed the $VEGF_{145}$ cDNA in Sf9 insect cells using the baculovirus expression system (23). Most of the $VEGF_{145}$ produced by the infected Sf9 cells was found in the conditioned medium as a homodimer of ~41 kDa, with small amounts of monomeric $VEGF_{145}$ (Fig. 2*B*). The $VEGF_{145}$ dimers dissociated into monomers upon reduction with dithiotreitol (Fig. 2*A*). $VEGF_{145}$ was partially purified by heparin-Sepharose affinity chromatography. $VEGF_{145}$ was eluted from heparin-Sepharose columns using a stepwise salt gradient. Most of the $VEGF_{145}$ eluted at 0.6–0.7 M NaCl, indicating that the heparin binding affinity of $VEGF_{145}$ is similar to that of $VEGF_{165}$ (data not shown) (17, 23). The recombinant $VEGF_{145}$ was biologically active and induced the proliferation of HUVECs. The ED_{50} of $VEGF_{145}$ was 30 ng/ml, whereas $VEGF_{165}$ was 6-fold more active than $VEGF_{145}$ in this assay (Fig. 3).

$VEGF_{145}$ Induces Angiogenesis in Vivo—To determine whether $VEGF_{145}$ can induce angiogenesis *in vivo*, the $VEGF_{145}$ cDNA was subcloned into the *Bam*HI site of the mammalian bicystronic expression vector MIRB (25). The MIRB/$VEGF_{145}$ plasmid was transfected into BHK-21 cells (31), and stable cell lines producing $VEGF_{145}$ were isolated. The $VEGF_{145}$ produced by the mammalian cells was biologically active and was secreted into the growth medium. A stable clone producing 0.1 μg of $VEGF_{145}$ per 10^6 cells was isolated. The $VEGF_{145}$ expressing cells were embedded in alginate beads, and the beads were implanted under the skin of BALB/c mice (32). The pellets containing the alginate beads were removed after 4 days and photographed. Clusters of alginate beads containing $VEGF_{145}$ expressing cells were dark red with blood, whereas beads containing cells transfected with vector alone had a much lower content of blood (Fig. 4). When examined under higher magnification, pellets containing $VEGF_{145}$ producing cells appeared much more vascularized than pellets containing control cells.

$VEGF_{145}$ Binds to the KDR/flk-1 Receptor but Not to the Two Smaller VEGF Receptors of HUVECs—^{125}I-$VEGF_{165}$ forms high molecular weight complexes with three types of VEGF receptors following cross-linking to HUVECs (Fig. 5, *lane 1*), whereas ^{125}I-$VEGF_{121}$ only binds to the larger of these receptors. The common receptor to which both $VEGF_{121}$ and $VEGF_{165}$ bind is the KDR/*flk-1* VEGF receptor (Fig. 5, *open arrow*) (21). In order to compare the receptor recognition pattern of $VEGF_{145}$ with those of $VEGF_{165}$, ^{125}I-$VEGF_{165}$ was bound to HUVECs in the presence of 1 μg/ml of heparin and increasing concentrations of $VEGF_{145}$. Bound ^{125}I-$VEGF_{165}$ was subsequently covalently cross-linked to the VEGF receptors. $VEGF_{145}$ inhibited the binding of ^{125}I-$VEGF_{165}$ to the KDR/*flk-1* receptor of the HUVECs (Fig. 5). This result was verified in a cell-free binding experiment in which $VEGF_{145}$ competed with ^{125}I-$VEGF_{165}$ for binding to a soluble fusion protein containing the extracellular domain of the *flk-1* receptor (data not shown) (33). In contrast, $VEGF_{145}$ did not effectively inhibit the binding of ^{125}I-$VEGF_{165}$ to the two smaller VEGF receptors of the HUVECs (Fig. 5, *filled arrow*), indicating that the affinity of $VEGF_{145}$ toward these two receptors is substantially lower than that of $VEGF_{165}$. This behavior resembles the behavior of $VEGF_{121}$ (21) and indicates that the presence of exon 6 is not sufficient to enable efficient binding of $VEGF_{145}$ to these two receptors, despite the heparin binding properties that exon 6 confers on $VEGF_{145}$.

$VEGF_{145}$ Binds to the ECM Produced by Corneal Endothelial

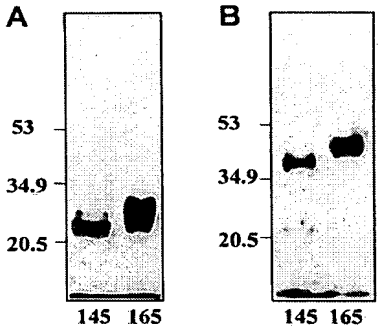

FIG. 2. **Production of VEGF$_{145}$ in Sf9 cells.** VEGF$_{145}$ and VEGF$_{165}$ were produced in Sf9 insect cells as described under "Experimental Procedures." Conditioned medium containing recombinant VEGF was collected, and 10-μl aliquots were either reduced using 0.1 M dithiothreitol (*A*) or not reduced (*B*). Proteins were separated by SDS-PAGE (12% gel) and transferred by electroblotting to nitrocellulose. Filters were blocked for 1 h at room temperature with buffer containing 10 mM Tris-HCl, pH 7, 0.15 M NaCl, and 0.1% Tween 20 (TBST) supplemented with 10% low fat milk. The filters were incubated for 2 h at room temperature with rabbit anti-VEGF polyclonal antibodies in TBST (23), washed three times with TBST, and incubated with anti-rabbit IgG peroxidase-conjugated antibodies for 1 h at room temperature. Bound antibody was visualized using the ECL detection system.

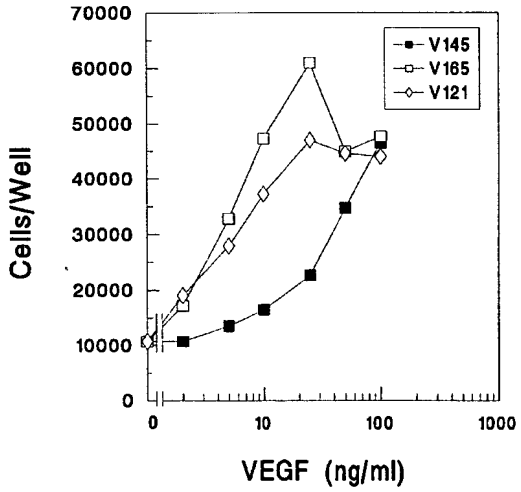

FIG. 3. **VEGF$_{145}$ stimulates the proliferation of endothelial cells.** HUVECs were seeded in 24-well dishes (20,000 cells/well), and increasing concentrations of VEGF$_{121}$ (◇), VEGF$_{145}$ (■), and VEGF$_{165}$ (□) were added every other day as described under "Experimental Procedures." Cells were counted in a Coulter counter after 4 days.

Cells—VEGF$_{189}$ binds efficiently to the ECM produced by CEN4 cells, whereas VEGF$_{165}$ binds to it very weakly (9). The fact that VEGF$_{189}$ binds heparin with high affinity led to the suggestion that the interaction of VEGF$_{189}$ with the ECM is mediated by heparan sulfate proteoglycans (8, 9). The heparin binding affinities of VEGF$_{145}$ and VEGF$_{165}$ are similar and substantially lower than the heparin binding affinity of VEGF$_{189}$ (8). We therefore expected VEGF$_{145}$ to bind poorly to ECM. Unexpectedly, experiments in which VEGF$_{145}$ was bound to an ECM produced by bovine corneal endothelial cells (28, 34) showed that VEGF$_{145}$ bound efficiently, whereas the binding of VEGF$_{165}$ was marginal (Fig. 6*A*). In these experiments the binding was monitored with anti-VEGF antibodies, but similar results were obtained when binding to the ECM was assayed directly using ^{125}I-VEGF$_{145}$ (30 ng/ml) or ^{125}I-VEGF$_{165}$ (50 ng/ml) (Fig. 6*B*, *first* and *third lanes*). The binding

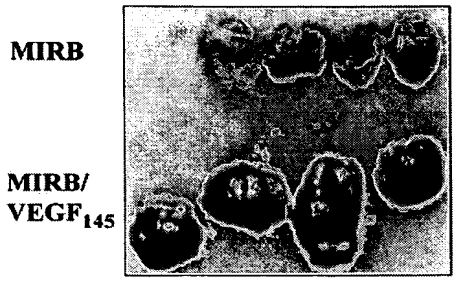

FIG. 4. **VEGF$_{145}$ stimulates angiogenesis *in vivo*.** The angiogenic activity of VEGF$_{145}$ was determined using the alginate assay (32). Stable clones of BHK-21 cells transfected with the MIRB expression vector (*MIRB*) or with the VEGF$_{145}$ expression vector MIRB/VEGF$_{145}$ were trypsinized and suspended in Dulbecco's modified Eagle's medium to a concentration of 2.7×10^7 cells/ml. Sodium alginate (1.2%, 0.66 ml) was mixed with 1.33 ml of cell suspension. Beads of 1-μl diameter were formed by contact with a solution of 80 mM $CaCl_2$. The beads were washed three times with saline. Each BALB/c mouse out of a group of four was injected subcutaneously with 400 μl of packed beads containing a given cell type. Clusters of beads were excised after 4 days and photographed. Blood-rich areas appear as dark areas in the photograph.

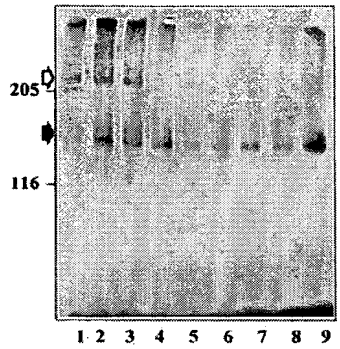

FIG. 5. **Effect of VEGF$_{145}$ on ^{125}I-VEGF$_{165}$ binding to endothelial cells.** ^{125}I-VEGF$_{165}$ (10 ng/ml) was bound to confluent HUVECs grown in 5-cm dishes for 2 h at 4 °C in the presence of 1 μg/ml heparin and the following concentrations of VEGF$_{145}$ (μg/ml): *lane 1*, 0; *lane 2*, 0.05, *lane 3*, 0.1; *lane 4*, 0.25; *lane 5*, 0.5; *lane 6*, 1; *lane 7*, 2; *lane 8*, 3. *Lane 9* received 2 μg/ml of VEGF$_{121}$. Bound ^{125}I-VEGF$_{165}$ was subsequently cross-linked to the cells using disuccinimidyl suberate, and cross-linked complexes were visualized by autoradiography.

of ^{125}I-VEGF$_{145}$ to the ECM was substantially but not completely inhibited by 10 μg/ml heparin (Fig. 6*B*, *second lane*). The ^{125}I-VEGF$_{145}$ used in these experiments contained some impurities (Fig. 6*C*), but the major iodinated protein that was recovered from the ECM had a mass corresponding to that of ^{125}I-VEGF$_{145}$ (Fig. 6*B*, *first lane*). To make sure that ^{125}I-VEGF$_{145}$ binds to the ECM and not to exposed plastic surfaces, the ECM was scraped off and washed by centrifugation, and the amount of adsorbed ^{125}I-VEGF$_{145}$ in the pellet was determined. The ECM contained ~70% of the adsorbed ^{125}I-VEGF$_{145}$. It therefore appears that the presence of the exon 6-derived peptide in VEGF$_{145}$ enables efficient binding to the ECM, whereas the exon 7 derived peptide of VEGF$_{165}$ does not suffice to confer this ability on VEGF$_{165}$.

VEGF$_{145}$ Binds to the ECM Using a Mechanism That Is Not Dependent on ECM-associated Heparan Sulfates—The interaction of bFGF with the ECM is mediated by the heparan sulfate moieties of ECM associated proteoglycans (35). It was of interest to determine if VEGF$_{145}$ uses a similar mechanism. When ^{125}I-VEGF$_{145}$ was bound to ECM-coated dishes in the presence of 10 μg/ml heparin, the binding was inhibited by ~60% (Fig. 7*A*). Under the same conditions the binding of ^{125}I-bFGF to the

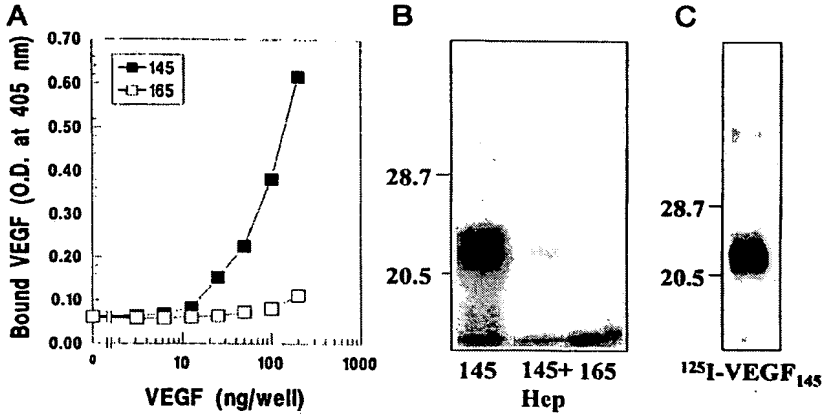

FIG. 6. **Binding of $VEGF_{145}$ and $VEGF_{165}$ to ECM-coated dishes.** *A*, ECM-coated 96-well dishes were incubated with increasing concentrations of $VEGF_{145}$ (■) or $VEGF_{165}$ (□). The amount of ECM-bound VEGF was quantified using the M-35 anti-VEGF monoclonal antibody as described under "Experimental Procedures." *B*, ^{125}I-$VEGF_{145}$ (*first* and *second lanes*, 30 ng/ml) or ^{125}I-$VEGF_{165}$ (*third lane*, 50 ng/ml) was bound to ECM-coated wells. Heparin (10 μg/ml) was added with the $VEGF_{145}$ in the *second lane*. The binding and the subsequent extraction of bound growth factors were done as described under "Experimental Procedures." Extracted growth factors were subjected to SDS-PAGE (12% gel) followed by autoradiography. *C*, the ^{125}I-$VEGF_{145}$ used in the experiment shown in *B* (0.2 ng) was chromatographed under reducing conditions on a 12% SDS-PAGE gel. Shown is an autoradiogram of the gel.

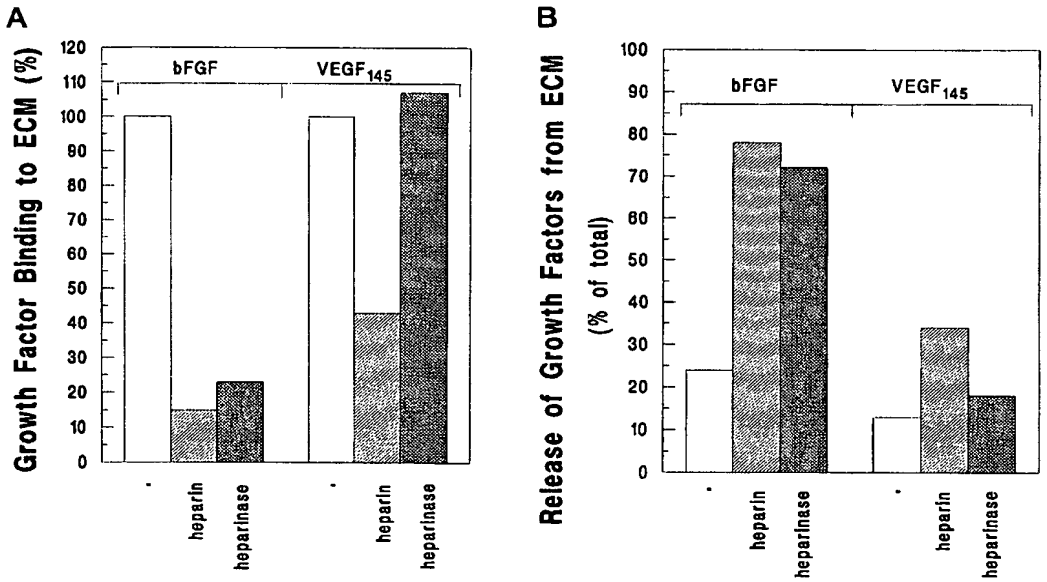

FIG. 7. **The effects of heparinase-II and heparin on the binding of ^{125}I-$VEGF_{145}$ and ^{125}I-bFGF to ECM-coated wells.** *A*, effect of heparin and heparinase on growth factor binding. ECM-coated wells were incubated with or without 0.1 unit/ml heparinase-II in binding buffer for 2 h at 37 °C. Subsequently, ^{125}I-$VEGF_{145}$ (40 ng/ml) or ^{125}I-bFGF (114 ng/ml) was added to the wells in the presence or the absence of 10 μg/ml heparin. Following incubation for 3 h at 25 °C, the wells were washed, and ECM-associated iodinated growth factors were dissociated by digestion with trypsin for 15 min at 37 °C. The amount of bound growth factor was determined using a γ counter (100% binding was 15,000 and 25,000 cpm/well for ^{125}I-$VEGF_{145}$ and ^{125}I-bFGF, respectively). *B*, effect of heparin and heparinase-II on the release of bound growth factors from the ECM. ^{125}I-$VEGF_{145}$ or ^{125}I-bFGF were bound to ECM-coated wells as described above. The wells were washed and reincubated in binding buffer alone, with 10 μg/ml heparin, or with 0.1 units/ml heparinase-II in a final volume of 50 μl. Following 12 h of incubation at 25 °C, the integrity of the ECM was verified by microscopy, and 45-μl aliquots were taken for counting in a γ counter. NaOH was then added to the wells, and the amount of ECM-associated growth factors was determined. The experiment was carried out in parallel to the experiment described in *A* above. The experiments in *A* and *B* were carried out in duplicate, and variation did not exceed 10%. Shown are the mean values. The experiments were repeated four times with similar results.

ECM was inhibited by 80% (Fig. 7*A*). The binding of ^{125}I-$VEGF_{145}$ to the ECM was also inhibited by 80% in the presence of 0.8 M salt, indicating that the interaction is probably not hydrophobic (data not shown). These results are compatible with the expected behavior of proteins that bind to the ECM via heparin-like molecules. However, ^{125}I-$VEGF_{145}$ also bound efficiently to an ECM that was digested with heparinase-II (36). In contrast, there was almost no binding of ^{125}I-bFGF to heparinase-II-digested ECM (Fig. 7*A*) (37, 38).

In order to further investigate the mode of interaction of $VEGF_{145}$ with the ECM, we measured the heparin- or heparinase-II-induced release of prebound $VEGF_{145}$ or bFGF from the ECM. When the ECM-coated wells were incubated for 2 h at 37 °C with buffer, only 20% of the bound ^{125}I-bFGF and 13% of

the bound ^{125}I-VEGF$_{145}$ dissociated from the ECM (Fig. 7*B*). This background release may be attributed in part to a proteolytic activity residing in the ECM (8, 39). When 10 μg/ml heparin were included in the buffer, only 33% of ^{125}I-VEGF$_{145}$ was released from the matrix, as compared with the release of 78% of the prebound ^{125}I-bFGF. An even sharper difference was observed when heparinase-II was added to the buffer. The enzyme released 72% of the bound ^{125}I-bFGF, but only 17% of the bound ^{125}I-VEGF$_{145}$ was released (Fig. 7*B*). Similar results were obtained when the experiment was performed with unlabeled VEGF$_{145}$, using a commercial monoclonal anti-VEGF antibody to detect VEGF associated with the ECM (data not shown).

To determine the efficiency of the heparinase-II digestion, the ECM was metabolically labeled with [^{35}S]sulfate and subsequently digested with heparinase-II. The digestion released 80–85% of the labeled sulfate residues (data not shown). To determine whether VEGF$_{145}$ can bind to ECM depleted of all types of sulfated glycosaminoglycans, BCE cells were grown in the presence of 30 mM chlorate, an inhibitor of glycosaminoglycan sulfation (29). These ECMs were further digested with a mixture of heparinases I, II, and III (36, 40). Neither of these treatments significantly inhibited the binding of VEGF$_{145}$ to the ECM, despite a >95% decrease in the content of ECM-associated sulfate moieties (data not shown).

Because endothelial cells do not proliferate when they are seeded on ECM produced in the presence of chlorate (29), we examined whether VEGF$_{145}$ bound to such ECM retains its biological activity. Wells coated with ECM produced in the presence of chlorate were incubated with increasing concentrations of either VEGF$_{145}$ or VEGF$_{165}$. The wells were subsequently washed extensively and HUVECs were seeded in the wells. ECM incubated with VEGF$_{145}$ induced proliferation of vascular endothelial cells, whereas ECM incubated with VEGF$_{165}$ did not (Fig. 8). We therefore conclude that the ECM-associated VEGF$_{145}$ is biologically active.

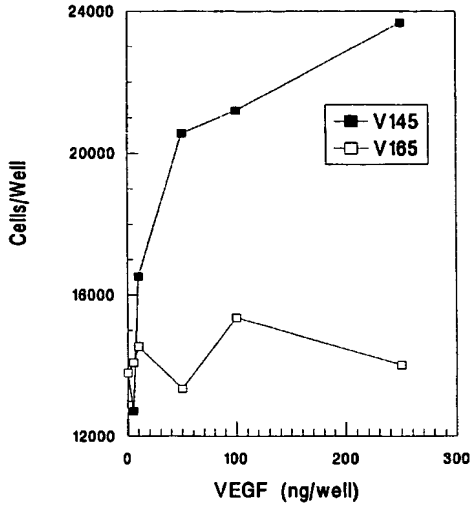

FIG. 8. **VEGF$_{145}$ bound to the ECM produced by BCE cells promotes proliferation of endothelial cells.** Wells of 24-well dishes were coated with an ECM produced by BCE cells cultured in the presence of 30 mM chlorate as described (29). The ECM-coated wells were incubated with increasing concentrations of VEGF$_{145}$ (■) or VEGF$_{165}$ (□) as indicated and washed extensively as described. HUVECs (15,000 cells/well) were seeded in the ECM-coated wells in growth medium lacking growth factors. Cells were trypsinzed and counted after 3 days. The numbers represent the average number of cells in duplicate wells. The experiment was repeated twice with similar results. Variation within duplicates did not exceed 10%.

DISCUSSION

Alternative splicing represents an important mechanism for the generation of diversity in growth factors and in their receptors. The alternative splice forms generated from the VEGF gene share angiogenic properties and are active as mitogens for endothelial cells. The VEGF$_{145}$ mRNA has been previously detected as a rare VEGF mRNA species in placenta (15, 16). We have found expression of the VEGF$_{145}$ mRNA in several tumorigenic cell types originating from the female reproductive system at levels comparable with the expression levels of VEGF$_{165}$. Several transformed cell lines from other sources did not express this mRNA, indicating that the expression of VEGF$_{145}$ may be more restricted compared with other VEGF forms (6). However, it remains to be seen whether production of VEGF$_{145}$ is restricted to the female reproductive system.

To study the properties of VEGF$_{145}$, we have produced recombinant VEGF$_{145}$ in mammalian and in insect cells. VEGF$_{145}$ was found to induce endothelial cell proliferation and *in vivo* angiogenesis, in agreement with previous studies that have indicated that these functions are not dependent on the presence of either exon 6 or exon 7 (10) and seem to be associated with the ability to bind to the KDR/*flk-1* VEGF receptor (41, 42). However, VEGF$_{145}$ seemed to be somewhat less active than VEGF$_{165}$, and it is possible therefore that the presence of exon 6 in VEGF$_{145}$ can subtly alter the conformation of the protein at the KDR/*flk-1* binding site (7). The VEGF$_{145}$ protein was secreted into the growth medium of producing cells. VEGF$_{121}$, VEGF$_{145}$, and VEGF$_{165}$ are secreted into the medium by producing cells, whereas VEGF$_{189}$ and VEGF$_{206}$ are sequestered by cell surface heparan sulfates (8). It therefore seems that the simultaneous presence of both exon 6 and exon 7 is required for efficient binding of VEGF to cell surfaces, whereas the presence of each of these exons on its own does not confer this property on VEGF.

Unlike VEGF$_{121}$, VEGF$_{145}$ was able to bind to heparin-Sepharose columns, indicating that the exon 6 encoded peptide acts as an independent heparin binding domain. The affinity of VEGF$_{145}$ for heparin was similar to that of VEGF$_{165}$, even though the structures of the heparin binding domains of the two isoforms differ. All the VEGF isoforms tested to date bind to the KDR/*flk-1* receptor of endothelial cells (21), and VEGF$_{145}$ was no exception. However, unlike VEGF$_{165}$, VEGF$_{121}$ and VEGF$_{145}$ do not bind efficiently to two additional VEGF receptors on HUVECs (21). The fact that VEGF$_{121}$ and VEGF$_{145}$ are both mitogenic and angiogenic indicates that these two receptors do not play a central role in the angiogenic and mitogenic response of endothelial cells. The biological function and the molecular structure of these two additional receptors is unknown. They appear to be novel VEGF receptors because they are not recognized by VEGF$_{121}$, whereas both KDR/*flk-1* and *flt-1* are recognized by VEGF$_{121}$.[2] In addition these two receptors are not immunoprecipitated by antibodies directed against the intracellular domains of the known VEGF receptors (21), and they can be detected in tumor cells that do not express detectable levels of KDR/*flk-1* or *flt-1* mRNA (22). Our results suggests that specific exon 7 sequences that are not present in the exon 6-derived peptide are required for the interaction of VEGF$_{165}$ with these two receptors. The heparin binding ability conferred on VEGF$_{165}$ by the exon 7 peptide may not play a central role in the recognition of these receptors by VEGF$_{165}$ because VEGF$_{145}$ and VEGF$_{165}$ bind with similar affinities to heparin yet differ in their ability to recognize these two receptors.

VEGF$_{189}$ is not found in the conditioned medium of produc-

[2] G. Neufeld, unpublished results.

ing cells and is sequestered on cell surface heparan sulfates and in the ECM. In view of the strong interaction of $VEGF_{189}$ with heparin, it was suggested that $VEGF_{189}$ binds tightly to cell surface and ECM localized heparan sulfates, allowing the sequestration of $VEGF_{189}$ in the ECM and on cell surfaces. This was supported by experiments that showed that heparin can dissociate bound $VEGF_{189}$ from the ECM, although long incubation times and high heparin concentrations were required (9). In contrast, $VEGF_{165}$ interacts weakly at best with cell surface heparan sulfates and with the ECM and is released into the medium of producing cells (8, 9). We expected $VEGF_{145}$ to bind weakly to cell surfaces and to the ECM because $VEGF_{165}$ and $VEGF_{145}$ appear to bind to heparin with similar affinities. Indeed, we have found that $VEGF_{145}$ is secreted as expected into the medium of $VEGF_{145}$ producing cells. However, $VEGF_{145}$ bound to the ECM produced by corneal endothelial cells much better than either $VEGF_{165}$ or $VEGF_{121}$. The lowest $VEGF_{145}$ concentration at which binding to the ECM was observed was about an order of magnitude lower than the concentration at which binding of $VEGF_{165}$ to the ECM was detected. In addition we have observed that $VEGF_{145}$ that is bound to ECM is able to promote proliferation of endothelial cells. These observations prompted us to compare the ECM binding behavior of $VEGF_{145}$ with that of bFGF, a growth factor that binds specifically to ECM-associated heparan sulfate moieties (38). Unexpectedly, our observations suggested that $VEGF_{145}$ and bFGF do not bind to common binding sites on the BCE cell-derived ECM. Digestion of the ECM with heparinases releases bound bFGF but does not release bound $VEGF_{145}$. It is possible that $VEGF_{145}$ binds to a heparan sulfate subpopulation that is not recognized by bFGF or by the heparinases used in the present study. However, $VEGF_{145}$ was also able to bind efficiently to an ECM produced in the presence of chlorate, an inhibitor of glycosaminoglycan sulfation (43) and to ECM digested with a mixture of three different heparinases resulting in a greater than 95% depletion of ECM-associated sulfate groups. These experiments therefore indicate that $VEGF_{145}$ can bind to ECM components distinct from the heparan sulfate side chains of proteoglycans. A similar observation was reported for transforming growth factor-β1, a heparin binding protein (44) that binds to the core protein of the ECM-associated chondroitin sulfate/dermatan sulfate proteoglycan decorin (45) rather than to ECM-associated heparan sulfate moieties.

All the splice variants induce angiogenesis *in vivo*, so why are five VEGF variants produced? Angiogenesis is often initiated under adverse conditions, such as the conditions encountered during wound healing. Many cell types produce several VEGF forms simultaneously (6, 46), and it is possible that each form offers advantages in different situations. The simultaneous production of several different VEGF forms may therefore ensure a balanced angiogenic response under diverse circumstances. When the properties of the VEGF variants are examined, it is apparent that the differences in their heparin binding abilities may affect their diffusion from a VEGF producing source to target blood vessels. $VEGF_{121}$ does not bind to either heparan sulfates or to the ECM and should therefore diffuse more readily than the heparin and ECM binding VEGF forms. The ECM may serve as a storage depot for the VEGF forms that bind efficiently to the ECM, and these forms may dissociate slowly from the ECM providing prolonged angiogenic stimulation or be released from the ECM as a result of the activity of proteases (8). The balance may tip toward the production of preferred VEGF isoforms under certain conditions (46). Production of $VEGF_{145}$ may be such a case because the variety of cell types that produce $VEGF_{145}$ appears to be limited compared with the range of cell types producing $VEGF_{121}$ or $VEGF_{165}$. However, the mechanism that determines what VEGF forms should be produced by a given cell type remains to be elucidated.

Acknowledgments—We thank Yael Shiffenbauer and Dr. Michal Neeman for help in reverse PCR experiments. We thank Dr. Dina Ron and Dr. Dan Cassel for critically reading this manuscript and for helpful discussions.

REFERENCES

1. Tischer, E., Gospodarowicz, D., Mitchell, R., Silva, M., Schilling, J., Lau, K., Crisp, T., Fiddes, J. C., and Abraham, J. A. (1989) *Biochem. Biophys. Res. Commun.* **165,** 1198–1206
2. Leung, D. W., Cachianes, G., Kuang, W. J., Goeddel, D. V., and Ferrara, N. (1989) *Science* **246,** 1306–1309
3. Keck, P. J., Hauser, S. D., Krivi, G., Sanzo, K., Warren, T., Feder, J., and Connolly, D. T. (1989) *Science* **246,** 1309–1312
4. Tischer, E., Mitchell, R., Hartman, T., Silva, M., Gospodarowicz, D., Fiddes, J. C., and Abraham, J. A. (1991) *J. Biol. Chem.* **266,** 11947–11954
5. Houck, K. A., Ferrara, N., Winer, J., Cachianes, G., Li, B., and Leung, D. W. (1991) *Mol. Endocrinol.* **5,** 1806–1814
6. Neufeld, G., Cohen, T., Gitay-Goren, H., Poltorak, Z., Tessler, S., Gengrinovitch, S., and Levi, B. (1996) *Cancer Metastasis Rev.* **15,** 153–158
7. Keyt, B. A., Nguyen, H. V., Berleau, L. T., Duarte, C. M., Park, J., Chen, H., and Ferrara, N. (1996) *J. Biol. Chem.* **271,** 5638–5646
8. Houck, K. A., Leung, D. W., Rowland, A. M., Winer, J., and Ferrara, N. (1992) *J. Biol. Chem.* **267,** 26031–26037
9. Park, J. E., Keller, G. A., and Ferrara, N. (1993) *Mol. Biol. Cell* **4,** 1317–1326
10. Kondo, S., Matsumoto, T., Yokoyama, Y., Ohmori, I., and Suzuki, H. (1995) *Biochim. Biophys. Acta* **1243,** 195–202
11. Gengrinovitch, S., Greenberg, S. M., Cohen, T., Gitay-Goren, H., Rockwell, P., Maione, T. E., Levi, B.-Z., and Neufeld, G. (1995) *J. Biol. Chem.* **270,** 15059–15065
12. Ferrara, N., Winer, J., Burton, T., Rowland, A., Siegel, M., Phillips, H. S., Terrell, T., Keller, G. A., and Levinson, A. D. (1993) *J. Clin. Invest.* **91,** 160–170
13. Kim, K. J., Li, B., Winer, J., Armanini, M., Gillett, N., Phillips, H. S., and Ferrara, N. (1993) *Nature* **362,** 841–844
14. Millauer, B., Shawver, L. K., Plate, K. H., Risau, W., and Ullrich, A. (1994) *Nature* **367,** 576–579
15. Charnock-Jones, S. D., Sharkey, A. M., Rajput-Williams, J., Burch, D., Schofield, J. P., Fountain, S. A., Boocock, C., and Smith, S. K. (1993) *Biol. Reprod.* **48,** 1120–1128
16. Cheung, C. Y., Singh, M., Ebaugh, M. J., and Brace, R. A. (1995) *Am. J. Obstet. Gynecol.* **173,** 753–759
17. Gospodarowicz, D., Abraham, J. A., and Schilling, J. (1989) *Proc. Natl. Acad. Sci. U. S. A.* **86,** 7311–7315
18. Ferrara, N., and Henzel, W. J. (1989) *Biochem. Biophys. Res. Commun.* **161,** 851–858
19. Cohen, T., Gitay-Goren, H., Sharon, R., Shibuya, M., Halaban, R., Levi, B.-Z., and Neufeld, G. (1995) *J. Biol. Chem.* **270,** 11322–11326
20. Terman, B. I., Dougher-Vermazen, M., Carrion, M. E., Dimitrov, D., Armellino, D. C., Gospodarowicz, D., and Böhlen, P. (1992) *Biochem. Biophys. Res. Commun.* **187,** 1579–1586
21. Gitay-Goren, H., Cohen, T., Tessler, S., Soker, S., Gengrinovitch, S., Rockwell, P., Klagsbrun, M., Levi, B.-Z., and Neufeld, G. (1996) *J. Biol. Chem.* **271,** 5519–5523
22. Soker, S., Fidder, H., Neufeld, G., and Klagsbrun, M. (1996) *J. Biol. Chem.* **271,** 5761–5767
23. Cohen, T., Gitay-Goren, H., Neufeld, G., and Levi, B. (1992) *Growth Factors.* **7,** 131–138
24. Tessler, S., and Neufeld, G. (1990) *J. Cell Physiol.* **145,** 310–317
25. MacArthur, C. A., Lawshe, A., Shankar, D. B., Heikinheimo, M., and Shackleford, G. M. (1995) *Cell Growth & Differ.* **6,** 817–825
26. Maymon, R., Maymon, B. B., Holzinger, M., Tartakovsky, B., and Leibovici, J. (1994) *Gynecol. Oncol.* **55,** 265–270
27. Neufeld, G., and Gospodarowicz, D. (1988) *J. Cell Physiol.* **136,** 537–542
28. Neufeld, G., and Gospodarowicz, D. (1987) *J. Cell Physiol.* **132,** 287–294
29. Miao, H.-Q., Ishai-Michaeli, R., Atzmon, R., Peretz, T., and Vlodavsky, I. (1996) *J Biol Chem* **271,** 4879–4886
30. Vaisman, N., Gospodarowicz, D., and Neufeld, G. (1990) *J. Biol. Chem.* **265,** 19461–19466
31. Neufeld, G., Mitchell, R., Ponte, P., and Gospodarowicz, D. (1988) *J. Cell Biol.* **106,** 1385–1394
32. Plunkett, M. L., and Hailey, J. A. (1990) *Lab. Invest.* **62,** 510–517
33. Tessler, S., Rockwell, P., Hicklin, D., Cohen, T., Levi, B.-Z., Hicklin, D., Witte, L., Lemischka, I. R., and Neufeld, G. (1994) *J. Biol. Chem.* **269,** 12456–12461
34. Vlodavsky, I., Folkman, J., Sullivan, R., Fridman, R., Ishai Michaeli, R., Sasse, J., and Klagsbrun, M. (1987) *Proc. Natl. Acad. Sci. U. S. A.* **84,** 2292–2296
35. Vlodavsky, I., Bashkin, P., Ishai Michaeli, R., Chajek Shaul, T., Bar Shavit, R., Haimovitz Friedman, A., Klagsbrun, M., and Fuks, Z. (1991) *Ann. N. Y. Acad. Sci.* **638,** 207–220
36. Desai, U. R., Wang, H. M., and Linhardt, R. J. (1993) *Arch. Biochem. Biophys.* **306,** 461–468
37. Bashkin, P., Neufeld, G., Gitay-Goren, H., and Vlodavsky, I. (1992) *J. Cell. Physiol.* **151,** 126–137
38. Bashkin, P., Doctrow, S., Klagsbrun, M., Svahn, C. M., Folkman, J., and Vlodavsky, I. (1989) *Biochemistry* **28,** 1737–1743
39. Korner, G., Bjornsson, T. D., and Vlodavsky, I. (1993) *J. Cell Physiol.* **154,**

456–465
40. Lohse, D. L., and Linhardt, R. J. (1992) *J. Biol. Chem.* **267,** 24347–24355
41. Waltenberger, J., Claesson-Welsh, L., Siegbahn, A., Shibuya, M., and Heldin, C.-H. (1994) *J. Biol. Chem.* **269,** 26988–26995
42. Seetharam, L., Gotoh, N., Maru, Y., Neufeld, G., Yamaguchi, S., and Shibuya, M. (1995) *Oncogene* **10,** 135–147
43. Hoogewerf, A. J., Cisar, L. A., Evans, D. C., and Bensadoun, A. (1991) *J. Biol. Chem.* **266,** 16564–16571
44. McCaffrey, T. A., Falcone, D. J., Vicente, D., Du, B. H., Consigli, S., and Borth, W. (1994) *J. Cell Physiol.* **159,** 51–59
45. Hildebrand, A., Romaris, M., Rasmussen, L. M., Heinegard, D., Twardzik, D. R., Border, W. A., and Ruoslahti, E. (1994) *Biochem. J.* **302,** 527–534
46. Bacic, M., Edwards, N. A., and Merrill, M. J. (1995) *Growth Factors* **12,** 11–15

THE JOURNAL OF BIOLOGICAL CHEMISTRY
© 1990 by The American Society for Biochemistry and Molecular Biology, Inc.

Vol. 265, No. 32, Issue of November 15, pp. 19461-19466, 1990
Printed in U.S.A.

Characterization of the Receptors for Vascular Endothelial Growth Factor*

(Received for publication, July 6, 1990)

Nora Vaisman‡, Denis Gospodarowicz§, and Gera Neufeld‡¶

From the ‡Department of Biology, Technion, Israel Institute of Technology, Technion City, Haifa, 32000, Israel and the §Cancer Research Institute, University of California Medical Center, San Francisco, California 94143

Vascular endothelial growth factor (vEGF) is a recently discovered mitogen for endothelial cells. It is also a potent angiogenic factor. We have characterized the vEGF receptors of endothelial cells using both binding and cross-linking techniques. Scatchard analysis of equilibrium binding experiments revealed two types of high-affinity binding sites on the cell surfaces of bovine endothelial cells. One of the sites has a dissociation constant of 10^{-12} M and is present at a density of 3×10^3 receptors/cell. The other has a dissociation constant of 10^{-11} M, with 4×10^4 receptors/cell.

A high molecular weight complex containing ^{125}I-vEGF is formed when ^{125}I-vEGF is cross-linked to bovine endothelial cells. This complex has an apparent molecular mass of 225 kDa. Two other faintly labeled complexes with apparent molecular masses of 170 and 195 kDa also are detected. Reduction in the presence of dithiothreitol causes a substantial increase in the labeling intensity of the 170- and 195-kDa complexes, suggesting that these complexes are derived from the 225-kDa complex by reduction of disulfide bonds.

The labeling of the vEGF receptors was inhibited by an excess of unlabeled vEGF but not by high concentrations of several other growth factors. Suramin and protamine, as well as several species of lectins, inhibited the binding. The expression of functional vEGF receptors was inhibited when the cells were preincubated with tunicamycin, indicating that glycosylation of the receptor is important for the expression of functional vEGF receptors. Pretreatment with swainsonine on the other hand, did not prevent formation of functional receptors. However, the mass of the 225-kDa complex is decreased by 20 kDa when ^{125}I-vEGF is cross-linked to swainsonine-treated endothelial cells.

Angiogenesis is a multistep phenomenon that involves capillary endothelial cell proliferation, migration, and tissue infiltration (1). It plays a central role in a variety of physiological and pathological processes such as embryonic development, wound healing, atherosclerosis, and tumor growth (1–3). Several factors that induce angiogenesis have been isolated and characterized recently. Some of these factors, like epidermal growth factor (4), and tumor necrosis factor (5), are probably not directly mitogenic for endothelial cells and might induce angiogenesis by an indirect mechanism. Others, like acidic fibroblast growth factor (FGF)[1] (3), basic fibroblast growth factor (bFGF) (3), or platelet-derived endothelial cell growth factor (6), directly induce proliferation of endothelial cells, and might therefore exercise direct control over angiogenesis.

Recently, a novel mitogen for endothelial cells was isolated from the conditioned medium of mouse-derived AtT-20 cells (7). The factor was named vascular endothelial growth factor (vEGF). It is a potent angiogenic factor and has a structure similar to that of another recently discovered angiogenic factor produced by bovine pituitary-derived folliculo stellate cells (8–10). When the gene coding for that factor was cloned, it was found to be homologous to the independently discovered vascular permeability factor, so named because it induces leakage from blood vessels when injected intradermally (11). All of these vEGF forms display a mitogenic activity which seems to be restricted to endothelial cells (7–12).

In a recent study, it was reported that vascular permeability factor interacts with a single class of receptors present on the cell surface of several types of endothelial cells. The receptor was reported to have an apparent molecular mass greater than 330 kDa and did not contain disulfide-linked subunits (12).

We have conducted binding and cross-linking experiments using vEGF isolated from the conditioned medium of AtT-20 mouse-derived cells (7). We report that cell extracts prepared under nonreducing conditions from bovine endothelial cells to which ^{125}I-vEGF was chemically cross-linked contain a major ^{125}I-vEGF-receptor complex that has an apparent molecular mass of 225 kDa. The receptor contained in this complex is apparently made up of disulfide-linked subunits and appears to be a glycoprotein.

EXPERIMENTAL PROCEDURES

Materials—Disuccinimidyl suberate (DSS) was purchased from Pierce Chemical Co. Heparin-Sepharose was obtained from Pharmacia LKB Biotechnology Inc. ^{125}I was obtained from the Nuclear Research Center, Negev, Israel. [^{3}H]Thymidine and [^{35}S]methionine were from Du Pont-New England Nuclear. Human recombinant bFGF was kindly provided by Dr. Abraham from California Biotechnology Inc. Leupeptin and aprotinin were purchased from Boehringer Mannheim. Porcine platelet-derived growth factor was from R & D Systems. EGF was isolated and purified from mouse submaxillary glands as described previously (13). Suramin was purchased from Mobay Chemical Co. Tissue culture media and reagents were from

* This study was supported by Grant 87-00215 from the USA-Israel Binational Science Foundation; by grants from the Israel Cancer Research Fund, Israel Cancer Society, and the Israel Academy of Sciences and Humanities (to G. N.); and by a grant from the National Institutes of Health (to D. G.). The costs of publication of this article were defrayed in part by the payment of page charges. This article must therefore be hereby marked "*advertisement*" in accordance with 18 U.S.C. Section 1734 solely to indicate this fact.

¶ To whom correspondence should be addressed.

[1] The abbreviations used are: FGF, fibroblast growth factor; ABAE, aortic arch-derived bovine endothelial cells; bFGF, basic fibroblast growth factor; BSA, bovine serum albumin; DSS, disuccinimidyl suberate; EGF, epidermal growth factor; HEPES, *N*-2-hydroxyethylpiperazine-*N'*-2-ethanesulfonic acid; PBS, Dulbecco's phosphate-buffered saline; SDS-PAGE, sodium dodecyl sulfate-polyacrylamide gel electrophoresis; vEGF, vascular endothelial growth factor.

EXHIBIT E

Biological Industries, Kibbutz Beth Haemek, Israel. Tissue culture plasticware was obtained from Nunc. All other chemicals were of analytical grade and were purchased from Sigma. Low molecular weight protein standards were obtained from Sigma and included BSA (66 kDa), egg albumin (45 kDa), glyceraldehyde-3-phosphate dehydrogenase (36 kDa), carbonic anhydrase (29 kDa), trypsinogen (24 kDa), and soybean trypsin inhibitor (20.1 kDa). High molecular mass protein markers were obtained from Bio-Rad and included myosin (200 kDa), β-galactosidase (116 kDa), phosphorylase *b* (97 kDa), BSA (66 kDa), and ovalbumin (42.6 kDa).

Cell Culture—Bovine aortic arch-derived endothelial cells (ABAE cells), bovine adrenal cortex-derived capillary endothelial cells (ACE cells), and baby hamster kidney-derived clone 21 cells (BHK-21 cells) were isolated, characterized, and cultured as previously described (14, 15). Mitogenic assays utilizing these cells were done as described previously (7). Balb/c 3T3 clone A31 cells were kindly provided by Dr. Vlodavsky (Sharet Institute, Jerusalem) and were cultured in Dulbecco's modified Eagle's medium supplemented with 10% fetal calf serum and antibiotics. AtT-20 cells were cultured as described previously (7).

Iodination of vEGF—vEGF was isolated from the conditioned medium of AtT-20 cells and purified to homogeneity as previously described (7). Pure vEGF (1 μg) in a solution containing 28% acetonitrile and 0.1% trifluoroacetic acid was brought to pH 7 by the addition of 1 M K_2HPO_4. It was then added to a reaction buffer containing 20 mM sodium phosphate buffer (pH 7.2) and 0.4 mCi of $Na^{125}I$. The final volume was 120 μl. To this mixture were added 8 μg of freshly dissolved chloramine T (16), and the reaction was allowed to proceed for 45 s at room temperature. The iodination was quenched by the addition of 50 μl of sodium metabisulfite (2 mg/ml) and 50 μl of 10 mM KI. The ^{125}I-vEGF-containing solution was then adsorbed to a small heparin-Sepharose column (0.1 ml bed volume). The column was washed with 3 ml of a buffer containing 20 mM sodium phosphate (pH 7.2) and 0.1 M NaCl. ^{125}I-vEGF was then eluted with the same buffer containing 0.8 M NaCl. To the peak fraction containing ^{125}I-vEGF (600 μl) were added 60 μl of 1% gelatin. The iodinated material was aliquoted and immediately frozen at −20 °C. The recovery from the column was typically 35% of the loaded ^{125}I-vEGF. The specific activity of the ^{125}I-vEGF varied between 8×10^4 and 1.5×10^5 cpm/ng of ^{125}I-vEGF. The iodinated ^{125}I-vEGF was biologically active. The concentration of ^{125}I-vEGF was determined by comparing the mitogenic activity of ^{125}I-vEGF with the mitogenic activity of known vEGF concentrations as described previously (7).

Cross-linking Experiments—Endothelial cells were grown to confluence in 5-cm tissue culture dishes (3×10^6 cells/dish) in the presence of bFGF (1 ng/ml), which was added to the cells every other day. Additions of bFGF were discontinued 2 days before cross-linking. The cells were transferred to 4 °C, and each dish was washed with 10 ml of cold PBS. Binding buffer (1.2 ml Dulbecco's modified Eagle's medium, 20 mM HEPES, pH 7.2, 0.1% gelatin), ^{125}I-vEGF, and other substances were then added to the desired concentrations. Dishes were incubated with gentle shaking for 2 h at 4 °C. At the end of the incubation, bound ^{125}I-vEGF was cross-linked to the cells with DSS using the method previously described for the cross-linking of ^{125}I-bFGF to cells (17, 18). All the buffers used after the cross-linking reaction contained the following protease inhibitors: phenylmethylsulfonyl fluoride (1 mM), leupeptin (1 μg/ml), aprotinin (1.5 μg/ml), and EDTA (1 mM). After the cross-linking step, the cells were scraped off and solubilized in 50 μl of cold lysis buffer (10 mM Tris-HCl, pH 7, 1% Nonidet P-40, and protease inhibitors), as described for the cross-linking of ^{125}I-bFGF to cells (17, 18). To the supernatant left after a 3-min centrifugation at 12,000 × *g*, was added an equal volume of SDS sample buffer containing 125 mM Tris-HCl, pH-6.8, 4% SDS, and 20% glycerol. Samples were boiled for 3 min and analyzed by SDS-PAGE using 6% polyacrylamide gels. Equal amounts of protein were loaded in each lane. Protein was determined by the method of Peterson (19). Gels were subsequently stained with Coomassie Brilliant Blue, dried, and subjected to autoradiography at −70 °C using Kodak X-Omat AR film. Densitometric analysis of autoradiograms was done using a Cliniscan-2 densitometer. All the experiments were performed at least twice with similar results, and the autoradiograms shown display representative experiments.

Binding Experiments—Endothelial cells were grown to confluence in 16-mm wells (5.5×10^5 cells/well). The cells were washed twice with cold PBS, and 200 μl of binding buffer were added. Binding of ^{125}I-vEGF to cells was carried out for 2 h at 4 °C using the same procedure previously described for the binding of ^{125}I-bFGF to BHK-21 cells (17). At the end of the incubation, cells were washed three times with ice-cold PBS containing 1 mg/ml BSA. They were then incubated at room temperature for 30 min with vigorous shaking in 0.5 ml of a solution containing 1% Triton X-100 and 1 mg/ml BSA. A volume of 0.4 ml was then taken for counting in a γ counter. Nonspecific binding was typically 20–25% when 1.6 ng/ml ^{125}I-vEGF was bound to ABAE cells in the presence of 100 ng/ml of unlabeled vEGF. All the experiments were carried out in duplicate and were repeated at least twice. The variation between duplicate determinations in an experiment was less than 10%. Scatchard analysis of binding results was performed with the aid of the LIGAND program (20, 21).

[^3H]Thymidine and [^{35}S]Methionine Incorporation Assays—[^3H]Thymidine incorporation into quiescent Balb/c 3T3 clone A31 fibroblasts was performed essentially as described previously (22). [^{35}S]Methionine incorporation into ABAE cells was done as described previously (23).

RESULTS

Analysis of vEGF Binding—Mouse-derived vEGF was isolated from the conditioned medium of AtT-20 cells and iodinated using the chloramine-T method (7). The iodinated vEGF migrates as a single band of 45 kDa, corresponding to the molecular mass of the vEGF dimer (7). Reduction with dithiothreitol causes the dissociation of the dimer into 23-kDa polypeptides (Fig. 1). The iodinated vEGF induced the proliferation of ABAE cells at a concentration range that was similar to that of unlabeled vEGF (not shown).

When ^{125}I-vEGF (8 ng/ml) is bound to ABAE cells at 4 °C, the binding reaches a maximum after 1 h of incubation (not shown). The binding was highly specific since it was inhibited by unlabeled vEGF (at 100 ng/ml) but not by 0.5 μg/ml of platelet-derived growth factor, bFGF, or EGF (not shown). Two types of high affinity binding sites could be distinguished when increasing concentrations of ^{125}I-vEGF ranging from 0.1 to 40 ng/ml were bound to ABAE cells. One class of binding sites has a dissociation constant of about 1 pM, with 3×10^3 receptors/cell. The other class has a dissociation constant of about 10 pM, with 4×10^4 receptors/cell. The experiment was repeated three times, and the values given here represent an average of the results. A representative experiment is shown in Fig. 2.

Identification of Putative vEGF Receptor Species in Endothelial Cells—ABAE cells were incubated at 4 °C with decreasing concentrations of ^{125}I-vEGF ranging from 20 to 0.1 ng/ml. At the end of the incubation, bound ^{125}I-vEGF was cross-linked to the cells using DSS. The cells were extracted, and the extracts were subjected to SDS-PAGE under reducing conditions. Three ^{125}I-vEGF-labeled complexes of high molecular mass are detected in these extracts (Fig. 3). The heaviest

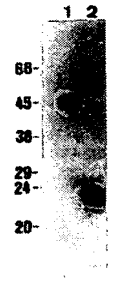

FIG. 1. **Homogeneity of ^{125}I-vEGF.** AtT-20-derived vEGF was iodinated as described under "Materials and Methods." ^{125}I-vEGF (10,000 cpm) in PBS containing 0.1% gelatin was diluted by addition of an equal volume of sample buffer. A second ^{125}I-vEGF-containing sample was incubated similarly, but the sample buffer also contained 0.1 M dithiothreitol (*lane 2*). Samples were boiled and subjected to SDS-PAGE chromatography on a 12% gel. Shown is an autoradiogram (24 h) from the fixed and dried gel.

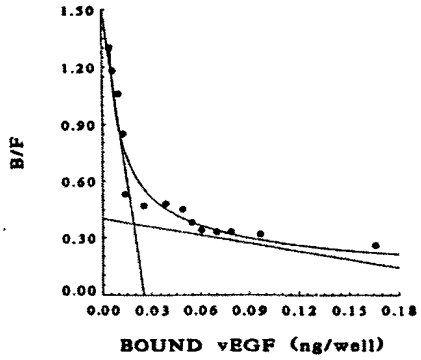

FIG. 2. **^{125}I-vEGF binding to ABAE cells.** ^{125}I-vEGF concentrations ranging from 55 pg/ml to 40 ng/ml were incubated for 2 h at 4 °C with confluent ABAE cells. At the end of the binding reaction, the cells were washed and solubilized, and the amount of bound ^{125}I-vEGF was determined, as described under "Materials and Methods". Binding results were analyzed by the method of Scatchard (20), with the aid of the LIGAND program (21). The dissociation constants and receptor numbers were calculated using a value of 45 kDa for the mass of the vEGF dimer.

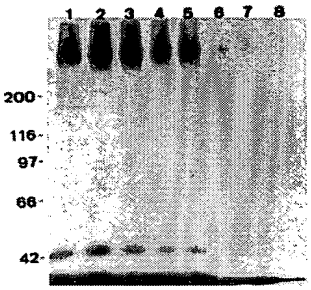

FIG. 3. **Cross-linking of decreasing ^{125}I-vEGF concentrations to ABAE cells.** Decreasing concentrations of ^{125}I-vEGF were bound and cross-linked to confluent ABAE cells. The cells were subsequently lysed, and extracts were subjected to SDS-PAGE on 6% polyacrylamide gels as described, except that the SDS sample buffer also contained 10% 2-mercaptoethanol. Shown is an autoradiogram prepared from a fixed and dried gel which was exposed for 2 weeks at −70 °C. The ^{125}I-vEGF concentrations used were (ng/ml): *lane 1*, 18; *lane 2*, 9; *lane 3*, 5; *lane 4*, 3; *lane 5*, 1.5; *lane 6*, 0.5; *lane 7*, 0.25; *lane 8*, 0.1.

complex has an apparent mass of 225 kDa and was strongly labeled. The two other complexes were labeled less intensely and had apparent molecular masses of 195 and 170 kDa, respectively (Fig. 3). The labeling intensity of the three complexes decreases sharply as the ^{125}I-vEGF concentration decreases from 1.5 to 0.5 ng/ml (33×10^{-12} to 11×10^{-12} M) (Fig. 3, *lanes 5* and *6*). None of these complexes is formed in the absence of DSS (see Fig. 8, *lane 2*), or when reduced ^{125}I-vEGF is used for cross-linking (not shown).

The labeling of the 195- and 170-kDa complexes is almost totally inhibited when the cell extracts are subjected to SDS-PAGE under nonreducing conditions (Fig. 4, *lane 2*). Proteolysis is apparently not involved in the generation of the 170- and 195-kDa complexes, since exposure to the reducing agent took place during the boiling of the samples, which was performed immediately before SDS-PAGE analysis. Prior to this stage, both reduced and nonreduced samples were treated equally. In addition, protease inhibitors and oxidized glutathione were included at all stages prior to SDS-PAGE.

The experiments described in this section therefore indicate that the 170- and 195-kDa complexes are derived from the 225-kDa complex by reduction of disulfide bonds. We will

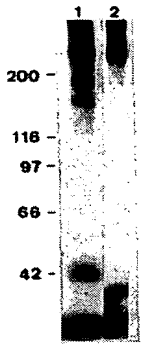

FIG. 4. **Reduction of ^{125}I-vEGF/receptor complexes.** ^{125}I-vEGF (15 ng/ml) was cross-linked to confluent ABAE cells. The cells were subsequently lysed as described, except that the lysis buffer also contained 1 mM oxidized glutathione. The extracts were centrifuged, and an equal volume of SDS sample buffer was added. The sample buffers added to one extract contain 0.1 M dithiothreitol (*lane 1*), while the sample buffer added to the other extract did not contain dithiothreitol (*lane 2*). The samples were immediately boiled for 3 min and subjected to SDS-PAGE chromatography on 6% polyacrylamide gels. Shown is an autoradiogram obtained after a 2-week exposure of the fixed and dried gel.

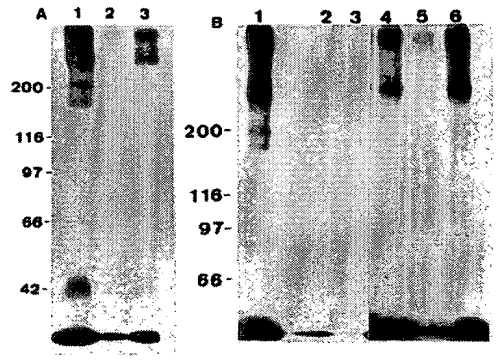

FIG. 5. **Binding of ^{125}I-vEGF is inhibited by protamine, suramin, and unlabeled vEGF.** *A*, ^{125}I-vEGF (15 ng/ml in *lanes 1* and *2*, 5 ng/ml in *lane 3*) was bound and subsequently cross-linked to confluent adrenal cortex-derived capillary endothelial cells. Unlabeled vEGF (150 ng/ml) was also added to the binding buffer of one of the cultures (*lane 2*). The cells were subsequently lysed, and the extract was subjected to SDS-PAGE chromatography on a 6% polyacrylamide gel as described. Shown is an autoradiogram obtained after a 2-week exposure of the fixed and dried gel. *B*, confluent ABAE cells were incubated for 12 h at 37 °C with suramin (*lane 4*, 0.2 mM; *lane 5*, 1 mM) or without it (*lanes 1–3* and *lane 6*). Cells were then washed twice with 10 ml of ice-cold PBS and once with 10 ml of ice-cold binding buffer, prior to the addition of 1.2 ml of binding buffer. ^{125}I-vEGF (15 ng/ml) was then added to all of the cultures. Some of the cultures received, in addition to ^{125}I-vEGF, protamine (*lane 2*, 9 μg/ml), or suramin (*lane 3*, 1 mM). Binding and subsequent cross-linking were carried out as described. The cells were then lysed, and cell extracts were subjected to SDS-PAGE chromatography on a 5% gel as described in the Fig. 3 legend. Shown is an autoradiogram obtained after a 2-week exposure of the fixed and dried gel.

therefore refer from now on to the 225-kDa complex as the one containing the vEGF receptor. Assuming that the complex consists of one receptor and one ^{125}I-vEGF molecule, it follows that the apparent molecular mass of the vEGF receptor is in the range of 180 kDa.

Specificity of vEGF Labeling—The labeling of the 225-kDa complex is completely inhibited when the cross-linking is done in the presence of 150 ng/ml of unlabeled vEGF (Fig. 5*A*, *lane 2*). To determine the specificity of the interaction between the 180-kDa putative receptor and vEGF, ^{125}I-vEGF

(8 ng/ml) was cross-linked to ABAE cells in the presence of different growth factors (500 ng/ml each). These growth factors included human recombinant bFGF, bovine-derived acidic fibroblast growth factor, porcine platelet-derived growth factor, mouse-derived EGF, and insulin. None of these competitors inhibits the labeling of the receptor.

Since various reports indicate that protamine and suramin can inhibit the binding of several growth factors to their respective receptors (24–26), we tested the effects of these substances upon the labeling of the vEGF receptors in cross-linking experiments. Both protamine (Fig. 5*B*, *lane 2*) and suramin (Fig. 5*B*, *lane 3*) inhibit the cross-linking of ^{125}I-vEGF to the vEGF receptor. Heparin, on the other hand, does not affect the labeling of the receptor at concentrations up to 50 μg/ml (not shown). This result is of interest because vEGF is known to bind quite tightly to heparin (7). It is therefore likely that the heparin binding domain and the receptor binding domains of vEGF are separate. When ABAE cells were preincubated with 1 mM suramin for 24 h before the binding of ^{125}I-vEGF, it was found that the labeling of the receptors was almost completely inhibited in spite of extensive washes before the initiation of the binding reaction. (Fig. 5*B*, *lane 5*). The inhibition was probably not associated with major cell damage since suramin-treated cells responded normally to bFGF (not shown).

The vEGF Receptor Appears to Be a Glycoprotein—Since many growth factor receptors are glycoproteins (22, 23, 27), we decided to test the effects of the glycosylation inhibitors tunicamycin and swainsonine (28, 29) on the labeling of the vEGF receptors. An incubation of ABAE cells with 0.8 μg/ml tunicamycin for 12 h caused complete inhibition of receptor labeling by ^{125}I-vEGF (Fig. 6, *lane 4*). The tunicamycin-induced inhibition of the labeling was not caused by a general inhibition of protein synthesis, since a tunicamycin concentration of 0.8 μg/ml caused only a 25% inhibition of protein synthesis as determined by [^{35}S]methionine incorporation. This experiment indicates therefore that *N*-linked sugar moieties are probably important for the expression of functional vEGF receptors. A 24-h preincubation with 2 μg/ml swainsonine, on the other hand, did not affect the labeling reaction. However, the apparent mass of the ^{125}I-vEGF-receptor complex that is formed when ^{125}I-vEGF is cross-linked to swainsonine-treated cells is 205 kDa instead of 225 kDa (not shown).

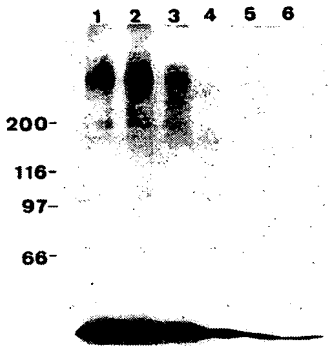

FIG. 6. **Effect of tunicamycin on ^{125}I-vEGF binding.** Confluent ABAE cells were incubated with the following concentrations of tunicamycin for 12 h at 37 °C (μg/ml): *lane 1*, 0; *lane 2*, 0.2; *lane 3*, 0.5; *lane 4*, 0.8; *lane 5*, 1; *lane 6*, 2. The cells were washed twice with 10 ml of ice-cold PBS at the end of the incubation. ^{125}I-vEGF (3 ng/ml) was then bound and cross-linked to the cells. Cell extracts were subsequently prepared and subjected to SDS-PAGE as described in the Fig. 3 legend. Shown is an autoradiogram obtained after a 3-week exposure of the fixed and dried gel.

To verify further the presence of sugar moieties on the receptor, we tested the effects of various lectins on the binding of ^{125}I-vEGF to the receptor. Wheat germ agglutinin, phytohemagglutinin, soybean agglutinin, and peanut agglutinin inhibited the labeling, while concanavalin A had no effect (Fig. 7). This result also indicates that receptor-associated sugar moieties are important for vEGF binding.

Cross-linking of ^{125}I-vEGF to Balb/c 3T3 Cells—Previous studies have indicated that vEGF is a highly specific mitogen for endothelial cells (7). We have tested several types of nonendothelial cells for the presence of vEGF receptors. Most cell types tested, including BHK-21 cells, Balb/MK cells, bovine granulosa cells, C2 myoblasts, and Ewing sarcoma-derived cells, did not display any vEGF binding ability. Sur-

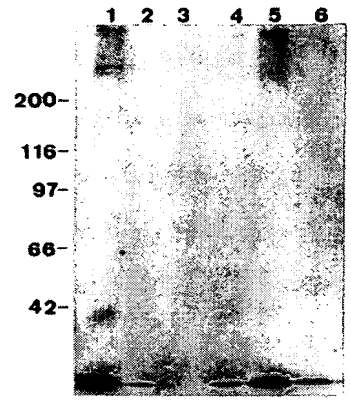

FIG. 7. **Effects of lectins on the cross-linking of ^{125}I-vEGF to endothelial cells.** Confluent ABAE cells were incubated with 10 ng/ml ^{125}I-vEGF for 2 h at 4 °C (*all lanes*). Some cultures also received 50 μg/ml of the following lectins: wheat germ agglutinin (*lane 2*), phytohemagglutinin (*lane 3*), soybean agglutinin (*lane 4*), concanavalin A (*lane 5*), and peanut agglutinin (*lane 6*). At the end of the incubation, bound ^{125}I-vEGF was cross-linked to the cells. Cell extracts were prepared and subsequently subjected to SDS-PAGE as described in the Fig. 3 legend. Shown is an autoradiogram obtained after a 3-week exposure of the fixed and dried gel.

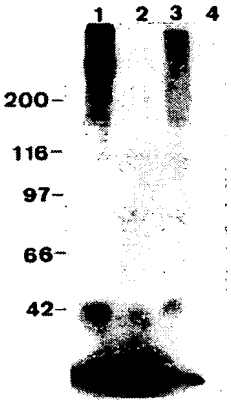

FIG. 8. **Balb/c 3T3 clone A31 cells contain vEGF receptors.** Confluent ABAE cells (*lanes 1* and *2*) or confluent Balb/c 3T3 clone A31 cells (*lanes 3* and *4*) (1.5×10^6 cells/5-cm dish) were washed and incubated with 5 ng/ml ^{125}I-vEGF (*all lanes*) for 2 h at 4 °C as described. Unlabeled vEGF (100 ng/ml) was also added to the binding buffer of one of the cultures (*lane 4*). At the end of the incubation, bound ^{125}I-vEGF was cross-linked to the cells using DSS as described. However, DSS was not added to one of the cultures (*lane 2*). The cells were subsequently extracted, and the extracts were subjected to SDS-PAGE chromatography as described in the Fig. 3 legend. Shown in an autoradiogram obtained after a 3-week exposure of the fixed and dried gel.

prisingly, when ^{125}I-vEGF is cross-linked to Balb/c 3T3 cells, two weak bands with apparent masses of 185 and 155 kDa, respectively, are labeled (Fig. 8, *lane 3*). The labeling of these bands was inhibited when the binding was done in the presence of 100 ng/ml vEGF (Fig. 8, *lane 4*). This observation is supported by experiments which show that 1 ng/ml vEGF causes a small, but consistent, increase (1.6-fold) in [^{3}H] thymidine incorporation with respect to unstimulated controls. In the same assays, bFGF (1 ng/ml) increased the incorporation of [^{3}H]thymidine by more than 10-fold.

DISCUSSION

The characterization of receptors which mediate the signals of angiogenic growth factors, such as vEGF, is of importance because of the potential involvement of these factors in pathological processes such as tumor angiogenesis. To study the vEGF receptor, we have iodinated vEGF to a high specific activity. The iodinated vEGF retained its mitogenic activity and appears to be homogeneous. Binding experiments in which endothelial cells were incubated with increasing concentrations of ^{125}I-vEGF reveal two classes of high affinity vEGF receptors. The first receptor type is present on ABAE cells at a density of 40,000 receptors/cell. This receptor type binds ^{125}I-vEGF with a dissociation constant of about 10 pM. The other receptor type has a density of about 3,000 receptors/cell and binds ^{125}I-vEGF with a dissociation constant of about 1 pM. The receptors are probably located on the cell surface since the binding experiments were done at 4 °C, a temperature at which internalization is inhibited. These results are in rough agreement with the results of another study published during the preparation of this article (30).

The binding of ^{125}I-vEGF to these receptors is highly specific. It can be inhibited by an excess of unlabeled vEGF but not by an excess of other types of growth factors. There is a good correlation between the binding ability of ^{125}I-vEGF and its bioactivity. Reduced preparations of ^{125}I-vEGF which have lost their bioactivity (7) also lose their ability to bind to the vEGF receptors. In addition, several cell types which do not respond to vEGF by proliferation also lack vEGF receptors.

The existence of high affinity vEGF receptors on the cell surface is also supported by the results of cross-linking experiments. Binding and subsequent cross-linking of ^{125}I-vEGF to endothelial cells results in the formation of labeled high molecular weight complexes containing ^{125}I-vEGF. These complexes are not formed in the absence of the cross-linking agent, or when reduced ^{125}I-vEGF is used. The labeling of these complexes is inhibited when an excess of unlabeled vEGF is present during the binding reaction. A range of other growth factors, including platelet-derived growth factor, EGF, and bFGF, do not inhibit the labeling of the complexes, a result which agrees well with the results of the binding experiments mentioned above. On the other hand, substances like suramin, which inhibits the binding of several growth factors to their receptors (26), or protamine, a protein possessing antiangiogenic properties (31), inhibit the labeling.

We also tested heparin, a glycosaminoglycan to which vEGF binds with high affinity (7), for its ability to inhibit the labeling of ^{125}I-vEGF/receptor complexes. Heparin concentrations as high as 50 μg/ml did not inhibit the labeling, indicating that the receptor binding domain of vEGF is distinct from the heparin binding domain. This behavior is also exhibited by bFGF, another angiogenic growth factor that binds to heparin with high affinity (32).

Cell extracts prepared from endothelial cells to which ^{125}I-vEGF was bound and subsequently cross-linked contain three high molecular weight complexes when analyzed by SDS-PAGE chromatography under reducing conditions. The heaviest ^{125}I-vEGF-containing complex has a molecular mass of 225 kDa, while the other two have molecular masses of 170 and 195 kDa, respectively. This result differs with respect to the results of a study in which ^{125}I-VPF was cross-linked to endothelial cells. In that study, only one complex with a mass greater then 330 kDa was seen under either reducing or nonreducing conditions (12). This difference might result from the use of different ligands, or because of technical reasons.

The labeling of the 170- and 195-kDa complexes was almost totally inhibited when the cell extracts were subjected to nonreducing SDS-PAGE chromatography. It therefore seems that the 170- and 195-kDa complexes are derived from the 225-kDa complex by reduction of disulfide bonds.

Proteolytic cleavage of the 225-kDa complex was probably not involved in the generation of the 170- and 195-kDa complexes, because the experiment was done in the presence of several types of protease inhibitors. Thiol proteases were probably not involved because reduction was performed during the boiling of the cell extracts in the SDS sample buffer. It therefore seems that the intact vEGF receptor is contained in the 225-kDa labeled complex and that the apparent molecular mass of the receptor is about 180 kDa, assuming that one vEGF molecule interacts with one receptor molecule.

^{125}I-vEGF itself is made up of two disulfide-linked monomers which can be dissociated by reduction. The masses of the 170- and 195-kDa complexes differ by the mass of approximately one vEGF monomer. It is therefore possible that the 170- and 195-kDa complexes differ only in their content of ^{125}I-vEGF monomers. Thus the 170-kDa complex might contain only one ^{125}I-vEGF monomer, while the 195-kDa complex might contain two ^{125}I-vEGF monomers which are equivalent to one intact ^{125}I-vEGF molecule. Accordingly, if these assumptions are correct, it follows that the vEGF receptor is made up of two subunits. The heavy subunit which contains the vEGF binding site has an apparent molecular mass of about 150 kDa, while the light subunit has a mass of about 30 kDa. Alternatively, it is possible that there are two types of vEGF receptors with approximately equal molecular masses. While this theory is less attractive, it nevertheless fits with the results of the binding studies which reveal two types of vEGF receptors.

The results of the binding studies, however, do not necessarily contradict the single receptor model. A single vEGF receptor type might exist in two states displaying different affinities for ^{125}I-vEGF, as was shown for the EGF receptor (33).

The vEGF receptor appears to be a glycoprotein. The mass of the 225-kDa ^{125}I-vEGF/receptor complex is decreased by 20 kDa when ABAE cells are treated with the glycosylation inhibitor swainsonine prior to the cross-linking reaction. Tunicamycin inhibits *N*-linked glycosylation at a stage which precedes the stage that is affected by swainsonine (29). Treatment of ABAE cells with tunicamycin leads to a loss of functional vEGF receptors. The loss of the receptors is not caused by a general inhibition of protein synthesis by tunicamycin. This indicates not only that functional vEGF receptors contain sugar moieties but also that these sugar moieties are required for the interaction between vEGF and its receptor. Support for the identification of the receptor as a glycoprotein is also obtained from experiments which show that several types of lectins, including wheat germ agglutinin, phytohemagglutinin, soybean agglutinin, and peanut agglutinin, but not concanavalin A, inhibit the binding of ^{125}I-vEGF to vEGF receptors. However, this inhibition might also

result from an interaction between ^{125}I-vEGF and some of these lectins, as the sequence of the vEGF gene is known to contain a potential glycosylation site (10).

It was previously reported that vEGF and vascular permeability factor are highly specific mitogens for endothelial cells (7, 11). We were not able to find vEGF receptors in several types of nonendothelial cells, which do not proliferate in response to vEGF. Mouse-derived Balb/c 3T3 clone A31 cells were an exception, since they seem to contain small amounts of vEGF receptors. This is supported by [^{3}H]thymidine incorporation assays which show that this cell type responds to vEGF, although the mitogenic stimulation observed is small.

In conclusion, our experiments indicate that vEGF binds to a receptor that is present on the cell surfaces of endothelial cells. This receptor has an apparent mass of 180 kDa, contains disulfide-linked subunits, and is a glycoprotein.

Acknowledgments—We thank Drs. D. Cassel, B. Horowitz, and H. Gitay-Goren for critically reading this study.

REFERENCES

1. Folkman, J. (1986) *Cancer Res.* **46,** 467–473
2. Folkman, J. (1990) *J. Natl. Cancer Inst.* **82,** 4–7
3. Gospodarowicz, D., Ferrara, N., Schweigerer, L., and Neufeld, G. (1987) *Endocr. Rev.* **8,** 95–114
4. Schreiber, A. B., Winkler, M. E., and Derynck, R. (1986) *Science* **232,** 1250–1253
5. Frater-Schroder, M., Risau, W., Hallmann, R., Gautschi, P., and Bohlen, P. (1987) *Proc. Natl. Acad. Sci. U. S. A.* **84,** 5277–5281
6. Ishikawa, F., Miyazono, K., Hellman, U., Drexler, H., Wernstedt, C., Hagiwara, K., Usuki, K., Takaku, F., Risau, W., and Heldin, C. H. (1989) *Nature* **338,** 557–562
7. Plouet, J., Schilling, J., and Gospodarowicz, D. (1989) *EMBO J.* **8,** 3801–3806
8. Gospodarowicz, D., Abraham, J. A., and Schilling, J. (1989) *Proc. Natl. Acad. Sci. U. S. A.* **86,** 7311–7315
9. Leung, D. W., Cachianes, G., Kuang, W. J., Goeddel, D. V., and Ferrara, N. (1989) *Science* **234,** 1306–1309
10. Tischer, E., Gospodarowicz, D., Mitchell, M., Silva, M., Schilling, J., Lau, K., Crisp, T., Fiddes, J. C., and Abraham, J. (1989) *Biochem. Biophys. Res. Commun.* **161,** 851–858
11. Keck, P. J., Hauser, S. D., Krivi, W., Sanzo, K., Warren, J., and Connolly, D. T. (1989) *Science* **246,** 1309–1312
12. Connolly, D. T., Heuvelman, D. M., Nelson, R., Olander, J. V., Eppley, B. L., Delfino, J. J., Siegel, N. R., Leimgruber, R. M., and Feder, J. (1989) *J. Clin. Invest.* **84,** 1470–1478
13. Savage, C. R., Jr., and Cohen, S. (1972) *J. Biol. Chem.* **247,** 7609–7611
14. Gospodarowicz, D., Massoglia, S., Cheng, J., and Fujii, D. K. (1986) *J. Cell. Physiol.* **127,** 121–136
15. Neufeld, G., Massoglia, S., and Gospodarowicz, D. (1986) *Regul. Pept.* **13,** 293–305
16. McConahey, P. J., and Dixon, F. J. (1980) *Methods Enzymol.* **70,** 210–213
17. Neufeld, G., and Gospodarowicz, D. (1985) *J. Biol. Chem.* **260,** 13860–13868
18. Neufeld, G., and Gospodarowicz, D. (1986) *J. Biol. Chem.* **261,** 5631–5637
19. Peterson, G. L. (1977) *Anal. Biochem.* **83,** 346–356
20. Scatchard, G. (1949) *Ann. N. Y. Acad. Sci.* **51,** 660–672
21. Munson, P. J., and Rodbard, D. (1980). *Anal. Biochem.* **107,** 220–239
22. Feige, J.-J., and Baird, A. (1988) *J. Biol. Chem.* **263,** 14023–14029
23. Soderquist, A. M., and Carpenter, G. (1984) *J. Biol. Chem.* **259,** 12586–12594
24. Neufeld, G., and Gospodarowicz, D. (1987) *J. Cell. Physiol.* **132,** 287–294
25. Huang, J. S., Huang, S. S., Kennedy, B., and Duel, T. F. (1982) *J. Biol. Chem.* **257,** 8130–8136
26. Garret, J. S., Coughlin, S. R., Niman, H. L., Tremble, P. M., Giels, G. M., and Williams, L. T. (1984) *Proc. Natl. Acad. Sci. U. S. A.* **81,** 7466–7470
27. Daniel, T. O., Milfay, D. F., Escobedo, J., and Williams, L. T. (1987) *J. Biol. Chem.* **262,** 9778–9784
28. Schwartz, R. T., and Datema, R. (1982) *Methods Enzymol.* **83,** 432–443
29. Tulsiani, D. R. P., Harris, T. M., and Touster, O. (1982) *J. Biol. Chem.* **257,** 7936–7939
30. Plouet, J., and Moukadiri, H. (1990) *Biochimie* **72,** 51–55
31. Taylor, S., and Folkman, J. (1982) *Nature* **297,** 307–312
32. Neufeld, G., and Gospodarowicz, D. (1988) *J. Cell. Physiol.* **136,** 537–542
33. Ullrich, A., and Schlessinger, J. (1990) *Cell* **61,** 203–212

FEBS Letters 355 (1994) 287–289

FEBS 14837

Singlet molecular oxygen production in the reaction of peroxynitrite with hydrogen peroxide

Paolo Di Mascio[a,*], Etelvino J.H. Bechara[a], Marisa H.G. Medeiros[a], Karlis Briviba[b], Helmut Sies[b]

[a]*Instituto de Química, Departamento de Bioquímica, Universidade de São Paulo, CP 20780, CEP 01498–970, São Paulo, Brazil*
[b]*Institut für Physiologische Chemie I, Heinrich-Heine-Universität Düsseldorf, PO Box 101007, D-40001 Düsseldorf, Germany*

Received 21 October 1994

Abstract Peroxynitrite and hydrogen peroxide are mediators of cytotoxicity. This study shows that the peroxynitrite anion reacts with hydrogen peroxide to release oxygen accompanied by emission of chemiluminescence (CL). Direct characterization of this light emission attributes it to the transition of singlet molecular oxygen to the triplet ground state. Chemiluminescence was monitored: (i) by dimol light emission in the red spectral region (>610 nm) using a red-sensitive photomultiplier; and (ii) by monomol light emission in the infrared (1270 nm) with a liquid nitrogen-cooled germanium diode. These properties of photoemission and the enhancing effect of deuterium oxide on CL intensity as well as the quenching effect of sodium azide are diagnostic of molecular oxygen in the excited singlet state. For comparison, singlet molecular oxygen arising from the thermolysis of the water-soluble endoperoxide of 3,3'-(1,4-naphthylidene)dipropionate or from the hypochlorite/H_2O_2 system was also monitored. These novel observations identify a potential singlet oxygen-dependent mechanism contributing to cytotoxicity mediated by peroxynitrite and hydrogen peroxide.

Key words: Singlet molecular oxygen; Peroxynitrite; Nitric oxide; Hydrogen peroxide; Chemiluminescence; Near-infrared emission

1. Introduction

Peroxynitrite ($ONOO^-$) is a biologically active species produced by the reaction of the superoxide anion radical ($O_2^{\cdot-}$) with nitric oxide ($NO^\cdot$) [1–3]. Nitric oxide, identified as the endothelium-derived relaxing factor [4], is formed by conversion of L-arginine to L-citrulline by an $NO^\cdot$ synthase. Endothelial cells, macrophages, neutrophils and neuronal cells have been shown to produce $NO^\cdot$ and $ONOO^-$ [5]. It has been suggested that decomposition of $ONOO^-$ generates the hydroxyl radical, a strong oxidant [6,7]. Recently, Noronha-Dutra et al. [8] reported that $NO^\cdot$ reacts with H_2O_2 accompanied by light emission in the visible spectral region with the features of singlet dioxygen, O_2 ($^1\Delta_g$), an excited state of molecular oxygen.

We studied here the oxygen-generating reaction of $ONOO^-$ with H_2O_2, using chemiluminescence (CL) measurement of the dimol (reaction 1) and monomol (reaction 2) light emission in the visible and infrared spectral regions, respectively, to provide evidence for the formation of O_2 ($^1\Delta_g$) in this system.

$$O_2\,(^1\Delta_g) + O_2\,(^1\Delta_g) \rightarrow 2\,O_2\,(^3\Sigma_g^-) + h\nu\ (634\text{ and }703\text{ nm}) \quad (1)$$

$$O_2\,(^1\Delta_g) \rightarrow O_2\,(^3\Sigma_g^-) + h\nu\ (1270\text{ nm}) \quad (2)$$

We suggest that, in analogy to the reaction of peroxybenzoate with H_2O_2 [9], $ONOO^-$ reacts with H_2O_2 to produce dioxygen, and that the oxygen released is present, at least in part, in the excited singlet state.

2. Materials and methods

Peroxynitrite was synthesized in a quenched flow reactor assembled according to Radi et al. [10]. In brief, separate solutions of 0.6 M $NaNO_2$ and 0.6 M HCl plus 0.7 M H_2O_2 were pumped with a peristaltic pump at 13 ml/min into a 4 mm Y-shaped glass tube. The acid-catalyzed reaction of nitrous acid with H_2O_2 forms peroxynitrous acid, which was deprotonated by pumping 3 M NaOH at the same flow rate into a T junction positioned at 2.5 cm downstream. Excess H_2O_2 was removed by passage over granular MnO_2. The solution was then filtered twice and frozen at −20°C for 5 days. Peroxynitrite forms a dark yellow top layer due to freeze fractionation, which was stored for further experiments. This solution contained 100–150 mM $ONOO^-$ as determined by absorbance at 302 nm ($\varepsilon_{302} = 1{,}670\ M^{-1}\cdot cm^{-1}$) [11].

Low-level CL was measured with a single-photon counting system, described elsewhere [12], equipped with a red-sensitive photomultiplier, cooled to −25°C by a thermoelectric cooler. Selective light emission at wavelengths >610 nm was obtained by a cut-off filter placed between the cuvette and the photomultiplier tube. Infrared emission of O_2 ($^1\Delta_g$) was measured with a liquid nitrogen-cooled germanium photodiode detector, sensitive in the spectral region from 800 nm to 1800 nm with a detector area of 0.25 cm^2 and a sapphire window, as described elsewhere [13].

All sample solutions were in a thermostated glass cuvette of (35 mm × 6 mm × 55 mm), CL was monitored after the injection (time = 0) of a solution of $ONOO^-$ (Fig. 1) to H_2O_2 in 0.5 M sodium phosphate buffer, pH 7.4, the final pH was 8. In the experiments shown in Fig. 2, peroxynitrite and H_2O_2 were present and the reaction started by the addition of acetic acid (time = 0), the final pH was 6. The intensity of the CL was pH-dependent, with a maximum Ge-diode signal at pH 8–9. When the reaction was performed at pH 1–2 or 13–14 no signal was observed. For comparison, O_2 ($^1\Delta_g$) generated chemically was observed upon thermal decomposition of the endoperoxide of the water-soluble disodium salt of 3,3'-(1,4-naphthylidene)dipropionate ($NDPO_2$) into the parent compound and molecular oxygen or in the hypochlorite/H_2O_2 system. The decomposition of $NDPO_2$ is temperature-dependent and slow. In contrast, the O_2 ($^1\Delta_g$) yield in the hypochlorite/H_2O_2 system is almost quantitative but very fast compared with the thermodecomposition of $NDPO_2$ [14].

Saturated $NO^\cdot$ solutions in H_2O were prepared by bubbling for 2 h with N_2, then 30 min with helium and 10 min with $NO^\cdot$ gas. The solutions were kept on ice and used immediately. Solutions of $NO^\cdot$ or SIN-1 (16 mM final concentration in ethanol) were injected directly into the sample containing 15 mM H_2O_2 while CL was being measured. Oxygen evolution was measured with a Clark-type electrode at room temperature.

Nitric oxide was purchased from Linde (Düsseldorf, Germany), SIN-1 was a kind gift of Cassella-Riedel Co. (Frankfurt, Germany), other chemicals were obtained from Sigma (Deisenhofen, Germany). The experiments were repeated several times.

*Corresponding author. Fax: (55) (11) 815-5579.
E-mail: pdmascio@quim.iq.usp.br

SSDI 0014-5793(94)01224-5

EXHIBIT F

3. Results and discussion

The mixture of $ONOO^-$ and H_2O_2 produces a fast increase in light emission at wavelengths identified for the chemiluminescence of O_2 ($^1\Delta_g$) (see reactions 1 and 2). As shown in Fig. 1A, trace 3, $ONOO^-$ injected into a nitrogen-purged solution of H_2O_2 in phosphate buffer produced CL in the red region (>610 nm). For comparison, O_2 ($^1\Delta_g$) was also generated by the reaction of hypochlorite/H_2O_2 (Fig. 1A, trace 2) and by the thermodissociation of $NDPO_2$ (Fig. 1A, trace 1).

The monomol light emission in the peroxynitrite/H_2O_2 reaction at 1270 nm is shown in Fig. 1B, trace 3. Likewise, the O_2 ($^1\Delta_g$) production from hypochlorite/H_2O_2 and from $NDPO_2$ are shown in traces 2 and 1, respectively. A calibration of the rate of O_2 ($^1\Delta_g$) production is performed on the basis of the rate of generation of NDP: in the experiment of trace 1 in Fig. 1B,

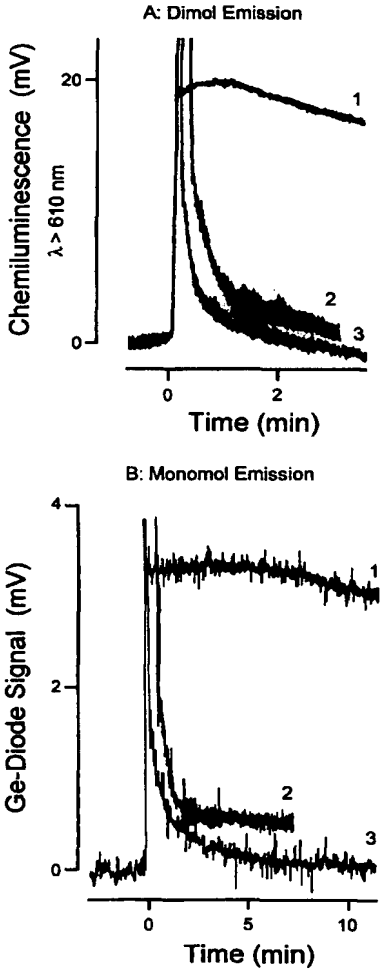

Fig. 1. Dimol (A) and monomol (B) light emission of O_2 ($^1\Delta_g$) generated by: (1) the thermodissociation of $NDPO_2$, (2) the hypochlorite/H_2O_2, and (3) the peroxynitrite/H_2O_2 systems. (1) $NDPO_2$ was 5 mM, (2) 10 mM hypochlorite was injected to 20 mM H_2O_2 and (3) $ONOO^-$ (5 mM) was injected into a 4 ml of 20 mM H_2O_2. Conditions: 0.5 M sodium phosphate buffer (final pH, 8), temperature was 37°C.

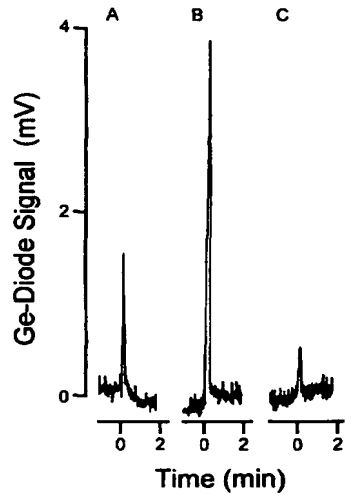

Fig. 2. Effect of D_2O and NaN_3 on the monomol emission generated by peroxynitrite/H_2O_2. Time course of the Ge-diode signal in: (A) H_2O, (B) 70% D_2O, and (C) 10 mM NaN_3 in 70% D_2O. A solution of acetic acid was injected in a 4.5 ml solution of 1.4 mM $ONOO^-$/14 mM H_2O_2 (final pH, 6), temperature was 37°C.

thermodissociation of $NDPO_2$ yielded 25 μM O_2 ($^1\Delta_g$) $min^{-1} \cdot mV^{-1}$ [14], so that we roughly estimate a flash of O_2 ($^1\Delta_g$) production of 50 μM O_2 ($^1\Delta_g$) for the reaction peroxynitrite/H_2O_2 shown in trace 3 in Fig. 1B. The generation of O_2 ($^1\Delta_g$) reaction of hypochlorite/H_2O_2 is also shown (Fig. 1B, trace 2). Neither $ONOO^-$ nor H_2O_2 nor hypochlorite elicited CL when present alone. The intensity of the CL was increasing with the $ONOO^-$ concentration tested up to 20 mM (not shown).

For further characterization, the effects of deuterated water and of azide were examined. In these experiments, the reaction was initiated by the addition of acetic acid. Upon replacement of H_2O by 70% D_2O, the CL intensity increased 8-fold in the dimol emission and 5-fold in the monomol emission at 1270 nm (Fig. 2B). This is consistent with the fact that the lifetime of O_2 ($^1\Delta_g$) increases in D_2O by about this factor [15]. As expected for O_2 ($^1\Delta_g$) as the emitter in the peroxynitrite/H_2O_2 reaction, sodium azide effectively quenched the signal in Fig. 2C compare with Fig. 2B.

To assess whether the CL (dimol and monomol emission) was dependent on hydroxyl radical formation, the scavengers dimethyl sulfoxide (10% v:v) and mannitol (100 mM) were used: in both cases, CL was not affected. Addition of a metal chelator, diethylenetriamine pentaacetic acid (DETAPAC, 20 mM), also did not affect the germanium diode signal.

The evolution of oxygen was followed in further experiments in 0.1 M phosphate buffer solutions, pH 7.4, previously purged with nitrogen, which contained 1 mM H_2O_2 and 0.5 mM $ONOO^-$ at room temperature (data not shown). The release of oxygen in the reaction was previously demonstrated by Mahoney [16].

Using the two CL methods described here, we also investigated the reaction of $NO^\bullet$ with H_2O_2 to produce O_2 ($^1\Delta_g$) as described by Noronha-Dutra et al. [8]. When deoxygenated solutions of $NO^\bullet$ or SIN-1 as a source of $NO^\bullet$ plus $O_2^{-\bullet}$ [17] were

injected into a solution of H_2O_2, no CL was recorded within the limits of detection.

Taken together, these observations serve as qualitative evidence for O_2 ($^1\Delta_g$) production by the reaction of $ONOO^-$ with H_2O_2. Further work is required to determine the yield of O_2 ($^1\Delta_g$) production in this reaction. Inspired by common chemical features shared by the peroxybenzoate/H_2O_2 system [9] and the reaction studied here, we envisage a concerted mechanism for O_2 ($^1\Delta_g$) formation via the *cis*-configuration of $ONOO^-$. In fact, the *cis* form of $ONOO^-$ was recently described to predominate at the more alkaline pH [18].

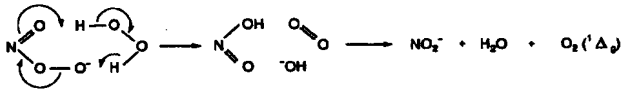

(Scheme I).

This reaction may be involved in the cytotoxicity of macrophages [19] and provides further insight into the cytotoxic potential of O_2 ($^1\Delta_g$).

Acknowledgements: The authors are indebted to the Conselho Nacional para o Desenvolvimento Cientifico e Tecnologico, CNPq e PADCT (Brazil), the Fundação de Amparo à Pesquisa do Estado de São Paulo, FAPESP (Brazil), the National Foundation for Cancer Research, Bethesda, MD (USA), and the Global Network for Molecular and Cell Biology (MCBN) of UNESCO for support.

References

[1] Beckman, J.S., Beckman, T.W., Chen, J., Marshall, P.M. and Freeman, B.A. (1990) Proc. Natl. Acad. Sci. USA 87, 1621–1624.
[2] Saran, M., Michel, C. and Bors, W. (1990) Free Rad. Res. Commun. 10, 221–226.
[3] Moro, M.A., Darley-Usmar, V.M., Goodwin, D.A., Read, N.G., Zamora-Pinto, R., Feelisch, M., Radomski, M.W. and Moncada, S. (1994) Proc. Natl. Acad. Sci. USA 91, 6702–6706.
[4] Palmer, R.M.J., Ferrige, A.G. and Moncada, S. (1987) Nature 327, 524–526.
[5] Ischiropoulos, H., Zhu, L. and Beckman, J.S. (1992) Arch. Biochem. Biophys. 298, 446–451.
[6] Radi, R., Beckman, J.S., Bush, K.M. and Freeman, B.A. (1991) J. Biol. Chem. 266, 4244–4250.
[7] Denicola, A., Rubbo, H., Rodriguez, D. and Radi, R. (1993) Arch. Biochem. Biophys. 304, 279–287.
[8] Noronha-Dutra, A.A., Epperlein, M.M. and Woolf, N. (1993) FEBS Lett. 321, 59–62.
[9] Akiba, K. and Simamura, O. (1964) Chem. Ind. 705–706.
[10] Radi, R., Rodriguez, M., Castro, L. and Telleri, R. (1994) Arch. Biochem. Biophys. 308, 89–95.
[11] Hughes, M.N. and Nicklin, H.G.J. (1968) Chem. Soc. A, 2450–2456.
[12] Murphy, M.E. and Sies, H. (1990) Methods Enzymol. 186, 595–610.
[13] Di Mascio, P., Devasagayam, T.P.A., Kaiser, S. and Sies, H. (1992) Methods Enzymol. 213, 429–438.
[14] Di Mascio, P. and Sies, H. (1989) J. Am. Chem. Soc. 111, 2909–2914.
[15] Merkel, P.B. and Kearns, D.R. (1972) J. Am. Chem. Soc. 94, 7244–7253.
[16] Mahoney, L.R. (1970) J. Am. Chem. Soc. 92, 5262–5263.
[17] Feelisch, M. (1991) J. Cardiovasc. Pharmacol. 17, 525–533.
[18] Crow, J.P., Spruell, C., Chen, J., Gunn, C., Ischiropoulos, H., Tsai, M., Smith, C.D., Radi, R., Koppenol, W.H. and Beckman, J.S. (1994) Free Rad. Biol. Med. 16, 331–338.
[19] Steinbeck, M.J., Khan, A.U. and Karnovsky, M. (1993) J. Biol. Chem. 268, 15649–15654.

Communication

THE JOURNAL OF BIOLOGICAL CHEMISTRY
Vol. 258, No. 10, Issue of May 25, pp. 5991-5993, 1983
Printed in U.S.A.

Singlet Oxygen Production by Lactoperoxidase

EVIDENCE FROM 1270 nm CHEMILUMINESCENCE*

(Received for publication, January 17, 1983)

Jeffrey R. Kanofsky

From the Medical Service, Hines Veterans Administration Hospital, Hines, Illinois 60141

Infrared chemiluminescence with maximum intensity near 1270 nm was detected in the lactoperoxidase, H_2O_2, Br^- system. No emission was observed when heat-inactivated enzyme was used or when Br^- or H_2O_2 was deleted from the system. The chemiluminescence was increased by a factor of 42 ± 5 (mean ± S.E.) in 98% ^2H_2O. These results are strong evidence for the production of $^1O_2$ in this system.

The enzyme system consisting of a peroxidase, H_2O_2, and a halide ion has been a useful model of killing by polymorphonuclear leukocytes (1). Allen and co-workers first reported chemiluminescence in this system leading them to postulate the production of singlet molecular oxygen ($^1O_2$) by the mechanism (2-4):

$$H_2O_2 + Cl^- \xrightarrow{\text{myeloperoxidase}} OCl^- + H_2O$$

$$OCl^- + H_2O_2 \rightarrow O_2(^1\Delta_g) + H_2O + Cl^-$$

Singlet oxygen could account for the microbicidal and cytotoxic activity of this system as well as the chemiluminescence (5, 6). In spite of several subsequent studies, however, the question of $^1O_2$ production remains unresolved. Evidence for the production of $^1O_2$ has included the conversion of $^1O_2$ traps to their expected $^1O_2$ oxidation products, the evolution of O_2, the reaction stoichiometry, and an analysis of the perturbations caused by $^1O_2$ traps, $^1O_2$ quenchers, and ^2H_2O (7-9). Under similar conditions, however, $^1O_2$ traps and quenchers have been shown to react with HOCl or Cl_2, so that all of the observed effects could be explained by the reactions of HOCl or Cl_2 (10, 11). The basic difficulty is the lack of an assay for $^1O_2$ with sufficient sensitivity and specificity to detect the low concentrations of $^1O_2$ that may be present in biological systems.

Singlet oxygen ($^1\Delta_g$) has strong emission bands at 634, 703, and 1268 nm and weak bands at 580, 1070, and 1580 nm (12, 13). The dimole emission bands at 580, 634, and 703 nm require the interaction of two molecules of $^1O_2$, and consequently their intensity is proportional to the square of the $^1O_2$ concentration (14). In contrast, the 1070, 1268, and 1580 nm bands result from a single molecule of $^1O_2$ and are directly proportional to the $^1O_2$ concentration (14). Thus, the 1268 nm band, which is both strong and directly proportional to the $^1O_2$ concentration, will be the most intense at low $^1O_2$ concentrations. Khan and Kasha (15) have proposed that 1268-nm emission be used to search for $^1O_2$ in biologic systems and have described a sensitive infrared spectrometer. Since all past studies of chemiluminescence in peroxidase, H_2O_2, halide systems have used photomultiplier tubes which were sensitive only to the dimole bands, we undertook a study of infrared chemiluminescence in the lactoperoxidase, H_2O_2, Br^- system.

EXPERIMENTAL PROCEDURES

Chemiluminescent Spectrometer—Infrared emission from 1050 to 1400 nm was measured with a liquid nitrogen-cooled, North Coast Optical Systems and Sensors EO-817L germanium detector. This detector had a specific detectivity 2000 times that of the lead sulfide detector used by Khan and Kasha (15).[1] Light to the detector passed through a chopping wheel (100 Hz) and a filter holder which selected one of four interference filters (50 nm band widths; center frequencies 1070, 1170, 1270, and 1370 nm). In experiments with ^2H_2O, a 2-mm pinhole reduced the detector aperture to prevent overload. The detector signal was processed by an Evans Associates model 4110 lock-in amplifier and displayed on a Houston Instruments model 35116-6 chart recorder. The integral of the light intensity was measured with an Evans Associates model 4130 long term integrator and an Intersil ICM7226A counter. Light from 400 to 850 nm was measured with an RCA 8852 photomultiplier using single photon counting. The tube was cooled to −20 °C by an EMI Gencom FACT 50 MK III thermoelectric cooler. Photomultiplier output pulses were processed by an EMI Gencom APED-1 amplifier/discriminator. A Packard Instruments model 280A ratemeter converted the pulse frequency to an analog signal which was displayed on the chart recorder. The sample enclosure was similar to the one described by Andersen and co-workers (16). Samples in glass tubes (12 mm diameter × 75 mm long) were contained in a light-tight box with an injection port to permit the measurement of chemiluminescence immediately after the addition of a reactant to the system.

Reagents—Lactoperoxidase ($A_{412\,nm}/A_{280\,nm}$ = 0.63; specific activity = 60 units/mg of protein) was obtained from Sigma. Heat-inactivated lactoperoxidase was heated to 90 °C for 15 min. Deuterium oxide (J. T. Baker Chemical Co.) had an isotopic purity of 99.75%. Hydrogen peroxide (30%), NaBr, sodium acetate, and acetic acid were all reagent grade. Sodium hypochlorite was a 5.25% commercial grade (Clorox). Water was glass-distilled.

Reaction Conditions—All experiments were done at 25 °C. The lactoperoxidase, H_2O_2, Br^- system was studied in 100 mM sodium acetate buffer, pH 4.5. For experiments in 98% ^2H_2O, the apparent pH, measured with a glass electrode, was adjusted to 4.8 to give a p^2H of 4.5 (17). Lactoperoxidase in 1.5 ml of buffer was placed in dark-adapted test tubes in the spectrometer. The reaction was initiated by the rapid injection of 1.5 ml of buffer containing NaBr and H_2O_2. The H_2O_2 + NaOCl reaction was studied in unbuffered H_2O and 98% ^2H_2O. Here the reaction was initiated by the injection of 1.5 ml of H_2O_2 solution into an equal volume of NaOCl solution already in the spectrometer.

Error Analysis—Experiments in H_2O were repeated four times; those in ^2H_2O were done in triplicate. The mean ± S.E. is reported in all cases.

RESULTS

Fig. 1 shows the chemiluminescence in the lactoperoxidase, H_2O_2, Br^- system detected with the RCA 8852 photomultiplier. This will subsequently be called short wavelength chemiluminescence. In agreement with the results of Harrison and

* This research was supported by the Veterans Administration Research Service, a Loyola University intramural research support grant, and Grant 5S07-RR05368 from the National Institutes of Health. The costs of publication of this article were defrayed in part by the payment of page charges. This article must therefore be hereby marked "*advertisement*" in accordance with 18 U.S.C. Section 1734 solely to indicate this fact.

[1] Calculated from manufacturers' specifications. Lead sulfide detector used by Khan and Kasha was obtained from Santa Barbara Research Center.

EXHIBIT G

co-workers (10), the decay of the chemiluminescence had two phases with a short burst of light followed by prolonged lower intensity emission. Deletion of Br^- markedly decreased the light, but there was still a short intense burst followed by persistent low level emission. Heat-inactivated lactoperoxidase produced low level prolonged chemiluminescence without an initial burst.

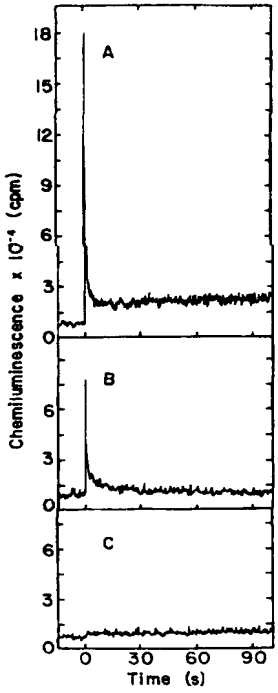

FIG. 1. **Chemiluminescence in the lactoperoxidase, H_2O_2, Br^- system detected with the RCA 8852 photomultiplier.** *A*, full system; *B*, Br^- deleted; *C*, heat-inactivated lactoperoxidase. Concentrations were 0.1 mg/ml of lactoperoxidase, 20 mM H_2O_2, and 20 mM NaBr in 100 mM sodium acetate, pH 4.5.

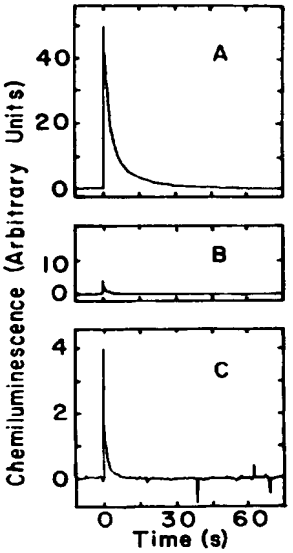

FIG. 2. **Infrared chemiluminescence at 1270 nm in the lactoperoxidase, H_2O_2, Br^- system.** Concentrations were 0.1 mg/ml of lactoperoxidase, 20 mM H_2O_2, and 20 mM NaBr. *A*, in 98% ^2H_2O with p^{2}H of 4.5; *B*, in H_2O, pH 4.5; *C*, in H_2O, sensitivity increased by a factor of 10. Note that the signal was relatively noisy, since it was obtained through a 2-mm pinhole to reduce the detector aperture.

TABLE I

Spectral analysis of infrared chemiluminescence

Values were compared to emission detected with a 1270-nm filter and corrected for the variation in detector sensitivity with wavelength and for filter transmission curves (data from manufacturers' specifications).

Filter[a]	Lactoperoxidase system[b]	H_2O_2 + NaOCl[c]
nm		
1070	0.00 ± 0.01[d]	0.00 ± 0.02
1170	0.00 ± 0.02	0.00 ± 0.02
1270	1.00 ± 0.02	1.00 ± 0.02
1370	0.23 ± 0.03	0.36 ± 0.04

[a] Center wavelength, band width 50 nm.
[b] Lactoperoxidase, 0.1 mg/ml, H_2O_2, 20 mM, and NaBr, 20 mM, in 100 mM sodium acetate, pH 4.5.
[c] Hydrogen peroxide, 5 mM; NaOCl, 5 mM.
[d] Mean ± S.E. for four experiments.

Fig. 2 shows the infrared chemiluminescence detected with the 1270-nm filter. It had a short half-life which corresponded roughly to the first phase of the decay of the short wavelength chemiluminescence. No 1270-nm chemiluminescence was detected when heat-inactivated lactoperoxidase was used or when Br^- or H_2O_2 were deleted from the system. Table I shows that the infrared emission had a maximum around 1270 nm, similar to the emission in the H_2O_2 + NaOCl reaction.

As seen in Fig. 2, the integral of 1270-nm emission in 98% ^2H_2O was 42 ± 5 times the emission in H_2O. This increase was due to a prolongation of the half-life of the chemiluminescence in addition to the increase in peak intensity. For the H_2O_2 + NaOCl reaction (5 mM, each), the integral of light intensity in 98% ^2H_2O was 27 ± 4 times that produced in H_2O. Here no lengthening of the half-life was noted and the enhancement was due only to an increase in peak intensity.

The intensity of the 1270 nm chemiluminescence in the lactoperoxidase, H_2O_2, Br^- system was estimated using the H_2O_2 + NaOCl reaction as a standard. The integral of light intensity for 0.7 mg/ml of lactoperoxidase, 10 mM H_2O_2, and 10 mM NaBr was 40 ± 2% of the integral for the reaction of 5 mM H_2O_2 with 5 mM NaOCl.

DISCUSSION

The detection of 1270-nm chemiluminescence in the lactoperoxidase, H_2O_2, Br^- system is strong evidence for the production of $^1O_2$. Light from both the enzyme system and the H_2O_2 + NaOCl reaction, a well studied source of $^1O_2$, had maximum intensity around 1270 nm. No 1070-nm emission was observed in either system, so that the intensity of this weak $^1O_2$ band must be below the detection limit of the current apparatus.

Much evidence suggests that short wavelength chemiluminescence is due to a variety of processes and is not simply related to $^1O_2$ production. It has a two-phase decay curve with a short half-life followed by a long half-life. The chemiluminescence in the second phase of the decay is the result of secondary reactions and is not dependent on enzymatic activity (10). Also, as confirmed by the current study, a small amount of chemiluminescence is produced with heat-inactivated enzyme and without the presence of halide ion (9). Experiments in ^2H_2O are often used as supporting evidence for the production of $^1O_2$, since the half-life of $^1O_2$ is 20 μs

compared to 2 μs in H_2O (18) and there is consequently an increase in $^1O_2$ concentration and emission. While dimole emission from the $^1O_2$ produced by the H_2O_2 + NaOCl reaction increases by a factor of 15 to 31 in ^2H_2O, the short wavelength chemiluminescence of the peroxidase, H_2O_2, halide system increases only a factor of 2 (8, 9, 19).

In contrast, 1270-nm chemiluminescence has a decay curve with a single half-life and is limited to the first or enzymatic-activity-dependent portion of the short wavelength emission. No 1270-nm emission is produced with heat-inactivated enzyme or in the absence of halide ion. Further, 1270-nm emission was multiplied 42 ± 5 times in ^2H_2O, similar to the 27 ± 4-fold enhancement seen with the H_2O_2 + NaOCl reaction. The perturbation of the system caused by ^2H_2O is not simple, however, since the half-life of the chemiluminescence was prolonged in addition to the 13-fold increase in peak intensity. There must be some alteration in reaction kinetics in addition to the increase in $^1O_2$ concentration.

The H_2O_2 + NaOCl reaction, which quantitatively produces $^1O_2$, was used as a standard to estimate the $^1O_2$ yield (20). For the concentrations used, the 1270-nm emission was 40% of that predicted by the mechanism of Allen and co-workers (2). This demonstrates that under appropriate conditions, $^1O_2$ is a major reaction product.

While only one system has been studied to date, the measurement of 1270-nm chemiluminescence appears to be a useful experimental method for the detection of $^1O_2$ in biological systems.

Acknowledgment—I wish to thank Larry Kynast for technical assistance in construction of the spectrometer.

REFERENCES

1. Klebanoff, S. J. (1968) *J. Bacteriol.* **95,** 2131–2138
2. Allen, R. C., Stjernholm, R. L., and Steele, R. H. (1972) *Biochem. Biophys. Res. Commun.* **47,** 679–684
3. Allen, R. C. (1975) *Biochem. Biophys. Res. Commun.* **63,** 675–683
4. Allen, R. C. (1975) *Biochem. Biophys. Res. Commun.* **63,** 684–691
5. Klebanoff, S. J. (1975) *The Phagocytic Cell in Host Resistance,* pp. 45–49, Raven Press, New York
6. Weishaupt, K. R., Gomer, C. J., and Dougherty, T. J. (1976) *Cancer Res.* **36,** 2326–2329
7. Rosen, H., and Klebanoff, S. J. (1977) *J. Biol. Chem.* **252,** 4803–4810
8. Piatt, J. F., Cheema, A. S., and O'Brien, P. J. (1977) *FEBS Lett.* **74,** 251–254
9. Piatt, J., and O'Brien, P. J. (1979) *Eur. J. Biochem.* **93,** 323–332
10. Harrison, J. E., Watson, B. D., and Schultz, J. (1978) *FEBS Lett.* **92,** 327–332
11. Held, A. M., and Hurst, J. K. (1978) *Biochem. Biophys. Res. Commun.* **81,** 878–885
12. Browne, R. J., and Ogryzlo, E. A. (1964) *Proc. Chem. Soc. London,* 117
13. Khan, A. U. (1980) *Chem. Phys. Lett.* **72,** 112–114
14. Bader, L. W., and Ogryzlo, E. A. (1964) *Discuss. Faraday Soc.* **37,** 46–56
15. Khan, A. U., and Kasha, M. (1979) *Proc. Natl. Acad. Sci. U. S. A.* **76,** 6047–6049
16. Andersen, B. R., and Brendzel, A. M. (1978) *J. Immunol. Methods* **19,** 279–287
17. Salomaa, P., Schaleger, L. L., and Long, F. A. (1964) *J. Am. Chem. Soc.* **86,** 1–7
18. Merkel, P. B., and Kearns, D. R. (1972) *J. Am. Chem. Soc.* **94,** 7244–7253
19. Kajiwara, T., and Kearns, D. R. (1973) *J. Am. Chem. Soc.* **95,** 5886–5890
20. Held, A. M., Halko, D. J., and Hurst, J. K. (1978) *J. Am. Chem. Soc.* **100,** 5732–5740

[1] Naphthalene Endoperoxides as Generators of Singlet Oxygen in Biological Media

By CHRISTEL PIERLOT, JEAN-MARIE AUBRY, KARLIS BRIVIBA, HELMUT SIES, and PAOLO DI MASCIO

Introduction

Molecular oxygen exhibits a remarkable electronic structure, as its higher occupied electronic level is constituted of two π^* orbitals of the same energy, so-called degenerated, filled with only two electrons. In the ground state, each of these electrons lies in one π^* orbital and their spins are parallel, hence it is a triplet state denoted $^3O_2(^3\Sigma_g^-)$. It behaves chemically as a poorly reactive oxidizing diradical despite its high oxidation potential. The first excited state has both electrons in the same orbital with opposite spins. It is a singlet state, denoted $^1O_2(^1\Delta_g)$, with a relatively long lifetime (45 min *in vacuo* and 4 μsec in water) and a substantial reactivity toward electron-rich organic molecules such as olefins, dienes, polycyclic aromatic compounds, sulfides, or phenols.[1]

Singlet oxygen has been shown to be generated in biological systems and can be implicated in defense mechanisms against viruses and bacteria by phagocytic cells.[2] Dark reactions (chemiexcitation), such as reactions catalyzed by peroxidases (myeloperoxidase) or oxygenases (lipoxygenase or cyclooxygenase), or the reaction of hydrogen peroxide with hypochlorite or peroxynitrite[3] or thermodecomposition of dioxetanes[4,5] can be responsible for $^1O_2$ generation in biological systems. Singlet oxygen is one of the major species mediating cytotoxic effects of photodynamic treatment. In addition to these cytotoxic effects, $^1O_2$ can be responsible for ultraviolet A-induced activation of gene expression (for review, see Ref. 6).

Biological targets for $^1O_2$ include unsaturated fatty acids, proteins, and

[1] A. A. Frimer, ed., "Singlet Oxygen," Vols. 1–3. CRC Press, Boca Raton, FL, 1985.
[2] M. J. Steinbeck, A. U. Khan, and M. J. Karnovsky, *J. Biol. Chem.* **268,** 15649 (1993).
[3] P. Di Mascio, E. J. H. Bechara, M. H. G. Medeiros, K. Briviba, and H. Sies, *FEBS Lett.* **355,** 287 (1994).
[4] K. Briviba, C. R. Saha-Möller, W. Adam, and H. Sies, *Biochem. Mol. Biol. Int.* **38,** 647 (1996).
[5] G. Cilento, *in* "Chemical and Biological Generation of Excited States" (W. Adam and G. Cilento, eds.), p. 279. Academic Press, New York, 1982.
[6] K. Briviba, L. O. Klotz, and H. Sies, *Biol. Chem.* **378,** 1259 (1997).

METHODS IN ENZYMOLOGY, VOL. 319
0076-6879/00 $30.00

EXHIBIT H

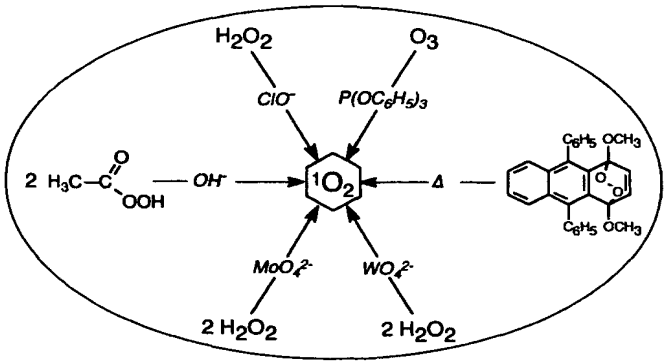

FIG. 1. Most efficient chemical sources of singlet oxygen $^1O_2$.

DNA.[7–10] Considering the complexity of biological systems and the great variety of reactive species generated by photochemistry, it is difficult to assess unambiguously the role of $^1O_2$ in the resulting biological effects. Therefore, alternative methods to generate $^1O_2$ without concomitant oxidants or toxic compounds have been sought. Several chemical sources of $^1O_2$ are able to convert in the dark an oxygen precursor into $^1O_2$ with almost quantitative yields[11] (Fig. 1). The conversion to $^1O_2$ by these compounds involves the oxidation (ClO^-), the disproportionation of hydrogen peroxide catalyzed by MoO_4^{2-}, WO_4^{2-}, or the reduction of ozone by triphenylphosphite, the base-catalyzed disproportionation of peracids, or the thermolysis of polycyclic aromatic endoperoxides. Unfortunately, conditions required by biological systems (aqueous environment, neutral pH, moderate temperature) are not compatible with these chemical sources of $^1O_2$. Further, these compounds are also toxic and are strong oxidants. Therefore, efforts have been devoted to develop suitable $^1O_2$ generators based on the thermolysis of endoperoxides. These compounds are chemically inert and have been employed as versatile sources of $^1O_2$.

The reversible binding of oxygen to polycyclic aromatic compounds was

[7] H. Sies and C. F. M. Menck, *Mutat. Res.* **275,** 367 (1992).
[8] H. Sies, *Mutat. Res.* **299,** 183 (1993).
[9] C. Menck, P. Di Mascio, L. F. Agnez, D. T. Ribeiro, and R. C. de Oliveira, *Quím. Nova* **16,** 328 (1993).
[10] P. Di Mascio, M. H. G. Medeiros, E. J. H. Bechara, and L. H. Catalani, *Ciência Cultura* **47,** 297 (1995).
[11] J. M. Aubry, in "Membrane Lipid Oxidation" (C. Vigo-Pelfrey, ed.), Vol. 2, p. 65. CRC Press, Boca Raton, FL, 1991.

discovered in 1926 by Dufraisse.[12,13] He also demonstrated that the oxygen released was in an "activated" state, but the precise nature of the species involved, i.e., $^1O_2(^1\Delta_g)$, was established in 1972 by Wasserman and Larsen[14] using the endoperoxide of 9,10-diphenylanthracene. When this endoperoxide is warmed to 80°, it decomposes into the parent compound and oxygen, 32% of which is in the singlet state.[11] The endoperoxide of 1,4-dimethylnaphthalene (DMN) evolves $^1O_2$ at lower temperatures and with a higher yield (76%).

Thus, water-soluble and nontoxic derivatives of DMN may act as carriers of $^1O_2$, as they trap this species at low temperature (0–5°). These endoperoxides, which may be stored for months at −80°, release a definite amount of $^1O_2$ on warming at 37° [reaction (1)], once dissolved in biological systems.

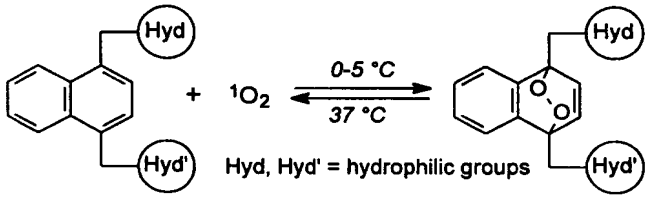

REACTION 1

The first water-soluble $^1O_2$ carriers reported by Nieuwint *et al.*[15] and Saito *et al.*[16] compounds **4** and **7** in Fig. 3, were designed to possess the properties described previously. These compounds bear one or two sodium propanoate substituents, respectively, grafted onto the 1,4 positions of the naphthalene core.[15,16] The corresponding endoperoxides have been used as chemical sources of $^1O_2$ to assess the activity of $^1O_2$ toward chemical, biochemical, or biological targets. However, these anionic compounds release $^1O_2$ in the aqueous phase, potentially far from the target. Subsequently, a second generation of carriers has been synthesized. They bear specific groups such as acridine moiety,[17] quaternary ammonium group **5**,[17]

[12] C. Moureu, C. Dufraisse, and P. M. Dean, *C.R. Acad. Sci.* **182,** 1140 (1926).
[13] C. Dufraisse and L. Velluz, *C.R. Acad. Sci.* **208,** 1822 (1939).
[14] B. H. Wasserman and D. L. Larsen, *J. C. S. Chem. Comm.* **253** (1972).
[15] A. W. M. Nieuwint, J. M. Aubry, F. Arwert, H. Kortbeek, S. Herzberg, and H. Joenje, *Free Radic. Res. Commun.* **1,** 1 (1985).
[16] I. Saito, T. Matsuura, and K. Inoue, *J. Am. Chem. Soc.* **103,** 188 (1981).
[17] T. Matsuura and K. Inoue, *Free Radic. Res. Commun.* **2,** 327 (1987).

TABLE I
HYDROPHILIC FUNCTIONS INSENSITIVE TO SINGLET OXYGEN

Function	Formula
Carboxylate	$-COO^-, Na^+$
Amide	$-CONHR_1R_2$
Phosphate	$-PO_4^{2-}, 2\ Na^+$
Sulfonate	$-SO_3^-, Na^+$
Sulfate	$-SO_4^-, Na^+$
Sulfonamide	$-SO_2NH_2$
Quaternary ammonium	$-N(CH_3)_3^+, Cl^-$
Alcohol	-OH

or nonionic hydrophilic groups (**6** and **8**) (Fig. 3)[18,19] in order to confer a particular affinity for polynucleotides, negatively charged sites, or intracellular targets to these molecules.

Strategy for Synthesis of Water-Soluble Carriers

Hydrophilic substituents grafted onto the naphthalene backbone must be insensitive to $^1O_2$ and to the photosensitizer or the chemical sources of $^1O_2$ that are required to prepare the endoperoxide. Moreover, the hydrophilic function must not act as a $^1O_2$ quencher as amino or phenol groups do. Table I presents the main functions meeting these requirements.

The naphthalene itself does not react with $^1O_2$; the direct binding of one of these electron-attractive groups to the aromatic core decreases its reactivity further. Therefore, at least one, and preferably two, electron-donating groups must be present on the positions 1,4 to allow the [4 + 2] cycloaddition of $^1O_2$ and to stabilize the endoperoxide. Thus, the relevant starting structure is DMN to which water-solubilizing groups must be added.

Figure 2 explains why the best position for anchoring lies on the 1,4-methyl group of DMN, provided that a sufficiently long alkyl spacer separates the hydrophilic group from the 1,4 carbons of the naphthalene moiety.

All the naphthalenic carriers of $^1O_2$ used in biological media can be prepared from the (inexpensive) 1-methylnaphthalene (compound **1**) using

[18] C. Pierlot, S. Hajjam, C. Barthélémy, and J. M. Aubry, *J. Photochem. Photobiol. B* **36,** 31 (1996).
[19] C. Pellieux, A. Dewilde, C. Pierlot, and J. M. Aubry, *Methods Enzymol.* **319,** [18] (2000) (this volume).

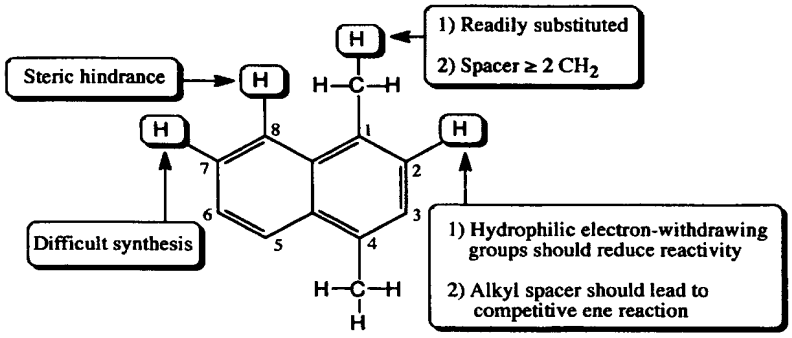

FIG. 2. Advantages and disadvantages of positions on DMN regarding the grafting of hydrophilic groups.

the general scheme presented in Fig. 3.[20–23] In the first step, compound **1** is chloromethylated, giving 4-methyl-1-chloromethylnaphthalene **2**, which leads to sodium 4-methyl-1-naphthalenepropanoate (MNP, **4**)[16] and 4-methyl-*N,N,N*-trimethyl-1-naphthaleneethanaminium chloride (MNEA, **5**),[18] anionic or cationic compounds, respectively, which bear only one water-solubilizing group. The conventional route to bifunctional naphthalene derivatives **6–8** was started by a double bromination of the (costly) DMN,[20,21] which, however, is no longer available commercially. An alternative access to 1,4-dihalogenomethylnaphthalene **3** is by monobromination of **2**, which then is converted into nonionic 1,4-naphthalenedimethanol (NDMOL, **6**) or anionic disodium 1,4-naphthalenedipropanoate (NDP, **7**) according to reported methods.[18,24] Synthesis of the new nonionic carrier *N,N'*-di(2,3-dihydroxypropyl)-1,4-naphthalenedipropanamide (DHPN, **8**), involving amidation of the diethyl ester of compound **7**, is described in detail later.

All five $^1O_2$ carriers **4–8** mentioned previously exhibit sufficient water solubility (10^{-2} *M*) for most biological applications (Table II). However, the solubility of MNP, **4**, and NDMOL, **6**, is sometimes insufficient and they may be advantageously replaced by NDP, **7**, and DHPN, **8**.

[20] C. S. Marvel and B. D. Wilson, *J. Org. Chem.* **23,** 1483 (1958).
[21] G. Lock and E. Walter, *Chem. Ber.* **75B,** 1158 (1942).
[22] G. Lock and R. Schneider, *Chem. Ber.* **91,** 1770 (1958).
[23] Kessar, P. Jit, K. Mundra, and A. Lumb, *J. Chem. Soc.* **2,** 266 (1971).
[24] P. Di Mascio and H. Sies, *J. Am. Chem. Soc.* **111,** 2909 (1989).

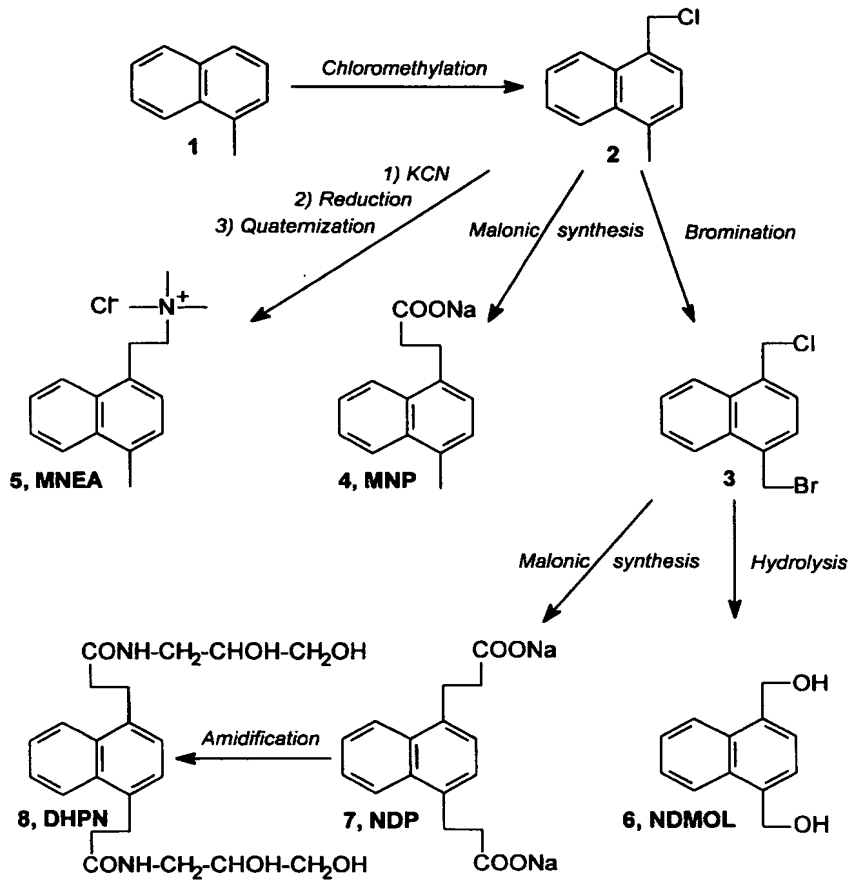

FIG. 3. Synthesis of water-soluble naphthalenic carriers of $^1O_2$.

TABLE II
MAIN PHYSICOCHEMICAL PROPERTIES OF $^1O_2$ CARRIERS

	MNP (4)	MNEA (5)	NDMOL (6)	NDP (7)	DHPN (8)
Water solubility (M)[a]	10^{-2}	>1	0.95×10^{-2}	>1	3.9×10^{-2}
10^{-5} k_t (M^{-1} sec^{-1})[b]	70	14	4	28	10

[a] In H_2O at 20°.
[b] Overall quenching rate constants of $^1O_2$ measured by flash photolysis in D_2O.[18,65]

Peroxidation of Naphthalenic Carriers

Two primary sources of $^1O_2$ can be used to prepare endoperoxides on a preparative scale: the regular photochemical method[25] [reaction (2)] and the molybdate-catalyzed disproportionation of hydrogen peroxide[26] [reaction (3)]. In both cases, the oxidation proceeds more rapidly in deuterated

$$^3O_2 + h\nu \xrightarrow{\text{Photosensitizer}} {}^1O_2$$

REACTION 2

$$2\,H_2O_2 \xrightarrow[\text{Water}]{MoO_4^{2-}} 2\,H_2O + {}^1O_2 \quad (100\%)$$

REACTION 3

solvents (D_2O and CD_3OD), as the lifetime of $^1O_2$ is much longer in these solvents than in protonated ones.

The choice of the oxidizing method depends on the physicochemical properties of the naphthalenic compound (water solubility, nature of the hydrophilic functions, and reactivity toward $^1O_2$). For instance, this chemical process is ideal for peroxidizing salts of carboxylated naphthalene derivatives (MNP **4** and NDP **7**) because the endoperoxides can be recovered readily by precipitating the acidic forms. For other $^1O_2$ carriers, photooxidation should be used on the condition that the photosensitizer can be eliminated at the end of the reaction.

The interaction of $^1O_2$ with naphthalenic compound **N** can be described by reactions (4) and (5). Singlet oxygen produced by a chemical or a

$$^1O_2 + N \xrightarrow{k_q} {}^3O_2 + N$$

REACTION 4

$$^1O_2 + N \xrightarrow{k_r} NO_2$$

REACTION 5

photochemical source is either quenched by N with rate constant k_q [reaction (4)] or reacted with N with rate constant k_r [reaction (5)]. Thus, the

[25] B. H. Wasserman and R. W. Murray, eds., "Singlet Oxygen." Academic Press, New York, 1979.

[26] J. Aubry, B. Cazin, and F. Duprat, *J. Org. Chem.* **54**, 726 (1989).

TABLE III
THERMOLYSIS OF NAPHTHALENE ENDOPEROXIDES IN WATER AT 37°

	$MNPO_2$	$NDPO_2$	$MNEAO_2$	$NDMOLO_2$	$DHPNO_2$
$t_{50\%}$ (min)[a]	23	23	22	70	23
$t_{95\%}$ (min)[b]	99	99	95	300	99
$^1O_2$ yield (%)[c]	45	50	65	51	59

[a] Half-time of decomposition.
[b] Time necessary to decompose 95% of naphthalenic endoperoxides.
[c] Cumulative yields of $^1O_2$ produced on thermolysis.

overall reactivity of N toward $^1O_2$ can be expressed by the sum $k_t = k_r + k_q$ (Table II).

To explain the difference in reactivity of 1,4-substituted carriers **4–8** toward $^1O_2$, two phenomena have to be considered: the electron density of the naphthalene core and the steric hindrance induced by the 1,4 substituents themselves or by additional groups located on the 2,3,5,8 positions. Electronic effects are of primary importance when a short spacer separates the hydrophilic groups from the naphthalene core. Thus, the electron-attractive effect caused by the quaternary ammonium group of MNEA **5** or by the OH functions of NDMOL **6** leads to molecules 5 and 17 times less reactive than MNP **4**, respectively. Longer alkyl spacers increase the electron density of the naphthalene core, but their steric hindrance lowers the rate of reaction with $^1O_2$ significantly. Thus, the weak overall rate constants ($k_r + k_q$) of NDP **7** ($2.8 \times 10^6\ M^{-1}\ sec^{-1}$) and of the more crowded DHPN **8** ($1.0 \times 10^6\ M^{-1}\ sec^{-1}$) are much lower than the value obtained with MNP **4** ($7.0 \times 10^6\ M^{-1}\ sec^{-1}$).

Thermolysis of the endoperoxide NO_2 [reaction (6)] follows a first-order

$$NO_2 \xrightarrow{k} N + \alpha\,{}^1O_2 + (1-\alpha)\,{}^3O_2$$

REACTION 6

kinetics with a rate constant k. More telling data, such as the half-time of decomposition ($t_{50\%} = \ln 2/k$) or the time necessary to decompose 95% of the starting endoperoxide ($t_{95\%} = \ln 20/k$), can be calculated. Table III indicates that most of the endoperoxides release 95% of their oxygen within 2 hr at 37°. This value is convenient for carrying out biological tests.[19]

A part of oxygen formed during the thermolysis is in the singlet excited state [reaction (6)]. It was measured by complete trapping with tetrapotassium rubrene-2,3,8,9-tetracarboxylate (RTC).[18,27] Finally, it can be consid-

[27] J. Aubry, J. Rigaudy, and K. C. Nguyen, *Photochem. Photobiol.* **33**, 149 (1981).

ered roughly that all the known naphthalenic carriers release $^1O_2$ in water with an approximate 50% yield (Table III).

Procedures for Synthesis and Oxidation of $^1O_2$ Carriers

Synthesis of naphthalenic carriers **4–7** and their corresponding endoperoxides has been reported previously,[18] and more detailed procedures for the preparation of endoperoxides of disodium 1,4-naphthalenedipropanoate ($NDPO_2$) and of sodium 4-methyl-1-naphthalenepropanoate ($MNPO_2$) are presented in Refs. 15 and 24 and 15 and 26, respectively. This article describes the synthesis of both reduced and oxidized forms of the new nonionic compound DHPN, **8**. It is noteworthy that both photochemical and chemical methods yield the wanted endoperoxide, but only photooxygenation leads to a pure sample suitable for biological assay.[19] We also describe the synthesis of 1-bromomethyl-4-chloromethylnaphthalene, **3**, which opens a new access to 1,4-disubstituted compounds **6–8**.

1-Bromomethyl-4-chloromethylnaphthalene 3

A mixture of 1-chloromethylnaphthalene **2** (292 g, 0.48 mol) and *N*-bromosuccinimide (86.6 g, 0.48 mol) in 1 liter of CCl_4 is stirred for 15 min. Then 1.5 g of benzoyl peroxide and 1.5 g of azobisisobutyronitrile are added to the solution, which is refluxed for 4 hr under magnetic stirring. The hot solution is filtered, and the cake is extracted with boiling CCl_4. The combined filtrates are evaporated, and the white solid is recrystallized from MeOH, affording 65 g (50%) of **3**. TLC: cyclohexane (R_f = 0.3); ^1H NMR ($CDCl_3$): d (ppm) = 8.1–8.3 (m; 2H, Ar), 7.5–7.9 (m; 2H, Ar), 5.05 (s; 2H, CH_2-Br), 4.95 (s; 2H, CH_2-Cl).

N,N'-Di(2,3-dihydroxypropyl)-1,4-naphthalenedipropanamide DHPN 8

A solution of diethyl 1,4-naphthalenedipropanoate (1 g, 2.6 mmol) and 3-amino-1,2-propanediol (3.78 g, 42 mmol) in 10 ml MeOH is stirred for 24 hr under reflux. After evaporation of the solvent, the residue is triturated with 50 ml of acetone. The colorless precipitate is filtered by suction and rinsed with acetone. Recrystallization from MeOH affords 685 mg (63%) of 8. mp: (165°); ^1H NMR (300 MHz, DMSO, TMS): d = 8.10–8.15 (m, 2H, H_5), 7.93 (m, 2H, CONH), 7.55–7.60 (m, 2H, H_6), 7.28 (s, 2H, H_2), 4.75 (d, 2H, CHOH), 4.55 (t, 2H, CH_2OH), 3.45 (m, 2H, CHOH), 3.2 (m, 8H, $NHCH_2$-CH_2OH), 3.0 (m, 4H, Ar-CH_2), 2.5 (m, 2H, CH_2CO); ^{13}C NMR (300 MHz, DMSO, TMS): d = 172.0 (s, CO), 135.9 and 131.6 (s, C1, C9), 125.7, 125.5 and 124.4 (s, C2, C5, C6), 70.6 (CH(OH)), 63.7 (CH_2(OH)),

42.2 (CH_2-N), 36.5 (s, Ar-CH_2), 28.4 (CHCO); MS: *m/z* 441 (MNa^+), 419 (MH^+).

Endoperoxide of N,N'-Di(2,3-dihydroxypropyl)-1,4-naphthalenedipropanamide DHPNO$_2$

DHPN, **8** (1 g, 2.3 mmol), 160 μl of an aqueous (D_2O) solution of 10^{-3} *M* methylene blue and 10 ml of deuterated water are introduced into a cylindrical glass cell (F = 4 cm; thickness = 1 cm). After gentle warming to dissolve **8**, the limpid solution is cooled at 5° and irradiated with a sodium lamp (150 W) under continuous bubbling of oxygen. Some methylene blue is added periodically during photooxygenation to compensate for its fading. After 4 hr, HPLC analysis shows 80% transformation. One hundred milligrams of cationic resin (Touzart-Matignon) is then added to the mixture, and the blue solution is stirred for 15 min at 0° until complete fixation of the sensitizer onto the insoluble polymer. The solution is filtered onto a polymeric membrane (porosity, 0.45 μm) and stored at −80°.

Analysis

The rate of formation and purity of the endoperoxide may be determined either by UV spectroscopy or by HPLC. Ultraviolet spectra of diluted aqueous solutions (2×10^{-4} *M*) are recorded between 250 and 350 nm. The naphthalenic compound shows a strong maximum at 288 nm (ε = 7780 M^{-1} cm^{-1}), whereas the absorbance of the endoperoxide is negligible at this wavelength. Hence, the purity of the sample may be calculated by comparing the absorbance at 288 nm of fresh and preheated (3 hr at 37°) solutions. HPLC analysis of aqueous solutions (2×10^{-4} *M*) is carried out with a Waters system and a reversed-phase column (Nova-Pack C-18, 25 cm) using a mixture of H_2O 59.9/MeOH 40/H_3PO_4 0.1 as eluent and UV detection at 210 nm. The purity of the endoperoxides is determined by comparison of the chromatograms of the fresh aqueous solution before and after warming at 37° for 3 hr.

Detection and Identification of $^1O_2$

An important method for the detection and characterization of $^1O_2$ is to measure chemiluminescence arising from the radioactive transition of $^1O_2$ to the ground state. There are two types of chemiluminescence derived from $^1O_2$.[28]

[28] M. Kasha and A. U. Khan, *Ann. N.Y. Acad. Sci.* **171,** 5 (1970).

Dimol Emission

The bimolecular transition [$^1O_2 + {}^1O_2 \rightarrow 2\,{}^3O_2 + h\nu$ (λ = 634 and 703 nm)] can be monitored by means of a red-sensitive, thermoelectrically cooled photomultiplier tube connected to a discriminator, amplifier, and recording system as developed by Boveris *et al.*[29] Dimol emission has often been used in complex systems such as enzymatic model reactions, suspensions of subcellular fractions and cells, perfused organ, or *in situ* for an exposed organ.[30]

Monomol Emission

In 1979, Khan and Kasha[31] developed spectroscopic instrumentation capable of direct solution spectral studies of $^1O_2$ emission [$^1O_2 \rightarrow {}^3O_2 + h\nu$ (λ = 1270 nm)] using a thermoelectrically cooled lead sulfite detector. The further development of a more sensitive spectrometer by Khan,[32] based on a germanium diode photodetector, augmented the capability for the examination of many reactions generating $^1O_2$. The intensity of this emission is directly proportional to the concentration of $^1O_2$, e.g., using the endoperoxide $NDPO_2$ [reaction (1)] as a source of $^1O_2$,[24] and provides a direct measure of the amount produced.

Chemical Traps

Trapping techniques are based on detection of the chemical product resulting from $^1O_2$ added to an appropriate substrate. The reactions of various types of substrates with $^1O_2$ are quite well established. They include the Diels–Alder reaction of dienes to form endoperoxides ([2 + 4] cycloaddition)[33] and the "*ene*" reaction of alkenes to give allylic hydroperoxides.[34] In the $^1O_2$ "*ene*" reaction, olefins containing allylic hydrogens are oxidized to the corresponding allylic hydroperoxides in which the double bond is shifted to the adjacent position. In addition, $^1O_2$ reacts with electron-rich alkenes without allylic hydrogens or sterically hindered to form 1,2-dioxetanes ([2 + 2] cycloaddition).[35]

[29] A. Boveris, E. Cadenas, and B. Chance, *Fed. Proc.* **40,** 195 (1981).
[30] E. Cadenas and H. Sies, *Methods Enzymol.* **105,** 221 (1984).
[31] A. U. Khan and M. Kasha, *Proc. Natl. Acad. Sci. U.S.A.* **76,** 6046 (1979).
[32] A. U. Khan, *J. Am. Chem. Soc.* **103,** 6516 (1981).
[33] A. J. Bloodworth and H. J. Eggelte, *in* "Singlet O_2" (A. A. Frimer, ed.), Vol. II. CRC Press, Boca Raton, FL, 1985.
[34] K. Alder, F. Pascher, and A. Schmitz, *Ber. Dtch. Chem. Ges.* **76,** 27 (1943).
[35] A. L. Baumstark, *in* "Singlet O_2" (A. A. Frimer, ed.), Vol. II. CRC Press, Boca Raton, FL, 1985.

Use of Deuterated Solvent

The use of deuterated solvent as a tool to characterize the presence of $^1O_2$ has become universal. It is based on the fact that the lifetime of $^1O_2$ in D_2O is approximately 15–18 times longer than in water and in deuterated organic solvents.[36] In cases where either $^1O_2$ and $O_2^{-\cdot}$ might be involved and the reaction is accompanied by product formation, the technique based on deuterated solvents cannot be used because both $^1O_2$ and $O_2^{-\cdot}$ lifetimes are longer in those solvents.[37]

Exposure of Nucleic Acids or Cells to Naphthalene Endoperoxides

In order to characterize the molecular nature of $^1O_2$-induced DNA damage and mutations in mammalian cells, plasmid DNA or a SV40-based shuttle vector were reacted with $^1O_2$ arising from the thermal decomposition of $NDPO_2$.[24] The reactivity of $^1O_2$ toward nucleic acids has been reported[6–8,38,39] and is discussed elsewhere in this volume.[40] Strand breaks and alkali-labile sites were identified on DNA molecules exposed to different sources of $^1O_2$, including $NDPO_2$.[24,41] Guanine oxidation sites were found to be adjacent phosphodiester breaks.[39] Using *in vitro* models treated with $NDPO_2$, it has been shown that DNA polymerases may be blocked when replicating single-stranded DNA templates containing lesions induced by $^1O_2$.[42,43] These base lesions in DNA are premutagenic candidates *in vivo,* and $^1O_2$ mutagenicity was reported in bacteria[44] or in mammalian cells.[45] Similar to $NDPO_2$, $^1O_2$ can be generated by thermodecomposition of $DHPNO_2$. As with $NDPO_2$, $DHPNO_2$ releases $^1O_2$ on incubation at 37° with a similar time course.[46]

[36] T. Kajiwara and D. R. Kearns, *J. Am. Chem. Soc.* **95,** 5886 (1973).
[37] B. H. J. Bielski and E. Saito, *J. Phys. Chem.* **75,** 2263 (1971).
[38] P. Di Mascio, H. Wefers, H.-P. Do-Thi, M. V. M. Lafleur, and H. Sies, *Biochem. Biophys. Acta* **1007,** 151 (1989).
[39] J. Cadet, M. Berger, T. Douki, B. Morin, S. Raoul, J.-L. Ravanat, and S. Spinelli, *Biol. Chem.* **378,** 1275 (1997).
[40] J. Cadet, T. Douki, J.-P. Pouget, and J.-L. Ravanat, *Methods Enzymol.* **319,** [14] (2000) (this volume).
[41] E. R. Blazek, J. G. Peak, and M. J. Peak, *Photochem. Photobiol.* **49,** 607 (1989).
[42] J. Piette, C. M. Calberg-Bacq, M. Lopez, and A. Van de Vorst, *Biochem. Biophys. Acta* **781,** 257 (1984).
[43] D. T. Ribeiro, F. Bourre, A. Sarasin, P. Di Mascio, and C. F. M. Menck, *Nucleic Acids Res.* **20,** 2465 (1992).
[44] P. Di Mascio, C. F. M. Menck, R. G. Nigro, A. Sarasin, and H. Sies, *Photochem. Photobiol.* **51,** 293 (1990).
[45] D. T. Ribeiro, C. Madzak, A. Sarasin, P. Di Mascio, and H. Sies, *Photochem. Photobiol.* **55,** 39 (1992).
[46] L. O. Klotz, C. Pellieux, K. Briviba, C. Pierlot, J. M. Aubry, and H. Sies, *Eur. J. Biochem.* **260,** 917 (1999).

Reaction of Deoxyguanosine with $^1O_2$

In DNA, $^1O_2$ reacts preferentially with deoxyguanosine residues, leading to the formation of at least four different reaction products: two 4*R** and 4*S** diastereomers of 4-hydroxy-8-oxo-7,8-dihydro-2′-deoxyguanosine, the main product, and 8-oxo-7,8-dihydro-2′-deoxyguanosine (8-oxodGuo).[39,40] The amount of 8-oxodGuo present in the solution is analyzed by HPLC using a Shimadzu (Kyoto, Japan) system, connected to a UV detector, and set at 285 nm and an electrochemical detector at a potential of 650 mV. A reversed-phase column C_{18} (Spherex, 250 × 4.6 mm, 5 μm) is used, and the mobile phase is KH_2PO_4, 50 m*M*, pH 5.5, with 10% methanol and 2.5 m*M* EDTA.[39] The 4-OH-8-oxodGuo is measured by HPLC with the UV detector using a normal phase amino-substituted silica gel Hypersil NH_2 column (250 × 4.6 mm, 5 μm) and a mobile phase of 25 m*M* ammonium formate and acetonitrile (40:60). Electrospray ionization mass spectrometry is also used to identify the oxidation products of dGuo after reaction with $^1O_2$. Samples are analyzed with a Quattro II (Micromass, Manchester, UK) mass spectrometer with an electrospray ion source. A 10-μl sample of the mixture of dGuo and **1** optical density of methylene blue or Rose Bengal in H_2O, pH 7.0, irradiated for 30 min or treated with $NDPO_2$ is injected. Positive-ion electrospray spectra are recorded at a capillary voltage of 3.5 kV, a cone voltage of 50 V, and a source temperature of 80°. Data are processed with MassLynx software. The mass spectrum obtained exhibits peaks at m/z = 268.11, 284.12, and 300.14 attributed to $[M + H]^+$ of dGuo, 8-oxodGuo,[47] and 4-OH-8-oxodGuo, respectively. The peak at m/z = 274.09 is attributed to 2′-deoxyguanidinohydantoin.[48] The loss of the sugar ring produces peaks at m/z = 151.90, 157.94, and 183.93, corresponding to guanine, guanidinohydantoin, and 4-OH-8-oxoGuo, respectively.

Exposure of Plasmid DNA to $^1O_2$ Generated by $NDPO_2$

DNA samples (1–2 μg/200 ml) are incubated at 37° for 90 min in 50 m*M* sodium phosphate buffer in H_2O or D_2O, pH/pD 7.4 in the presence of 10 m*M* $NDPO_2$. During the first 30 min of incubation, the samples are vortexed every 2 min in order to distribute evenly the $^1O_2$ produced in the solution. After treatment, the DNA samples may be used directly for analysis or sterilized and purified with chloroform before transfection into mammalian cells and/or shutting into *Escherichia coli.*

Separation of the different pBR322 DNA conformations is performed

[47] J.-L. Ravanat, A. Duretz, T. Guiller, T. Douki, and J. Cadet, *J. Chromatogr. B* **715,** 349 (1998).

[48] C. J. Burrows and J. G. Muller, *Chem. Rev.* **98,** 1109 (1998).

by gel electrophoresis using 0.7% agarose gels in a horizontal gel electrophoresis chamber at 30 mA for 120 min in 89 m*M* Tris borate/2 m*M* EDTA buffer. DNA (10 μl, 100 ng) is mixed with 2 μl of gel-loading buffer (15% Ficoll type 400/0.25% bromphenol blue) and applied to the gel. After gel electrophoresis, the DNA bands are stained with ethidium bromide and visualized by fluorescence in a UV DNA transilluminator. The DNA bands are quantified by scanning the negatives of the gel pictures using a densitometer. The number of single-stranded breaks is calculated based on the Poisson distribution. For supercoiled double-stranded DNA (FI), a correction factor of 1.4 is applied to account for its relatively lower fluorescence compared to the open circular form (FII)[49]: $e^{-x} = 1.4 \times FI/(1.4 \times FI + FII)$. For single-stranded DNA, the number of breaks is calculated, taking the ratio of molecules with zero or one break from treated DNA (T-DNA) to untreated DNA (C-DNA): $e^{-x}(1 + x) = T\text{-}DNA/C\text{-}DNA$. A role of $^1O_2$ in DNA damage, such as breaking the DNA backbone, was studied by replacing H_2O by D_2O in the buffer, leading to an increased percentage of breaks generated in keeping with the longer lifetime of $^1O_2$. To study the effect of inhibitors, some of the solutions contained sodium azide (1 m*M*) or freshly dissolved spermine or spermine hydrochloride,[50] in addition to 10 m*M* $NDPO_2$.

Virucidal Activity of Singlet Oxygen Generated by $NDPO_2$

A broad range of enveloped viruses (e.g., human herpes simplex virus type 1 or human immunodeficiency virus type 1) are inactivated rapidly when irradiated in the presence of photoactive dyes.[51–53] Singlet oxygen is suggested to have antiviral activity in these photodynamic procedures; however, apart from the direct generation of $^1O_2$ by the type II reaction, the excited sensitizer may also react in type I (free radical) reactions, interacting directly with the substrate to yield reactive-free radicals. A direct antiviral effect of $^1O_2$ was demonstrated using $NDPO_2$ to exclude the participation of type I reactions, which may occur using photoactive dyes. Singlet oxygen generated by $NDPO_2$ is capable of killing enveloped viruses, herpes simplex virus type 1 or suid herpes virus type 1,[54] human

[49] R. S. Lloyd, C. W. Haidle, and D. L. Robberson, *Biochemistry* **17,** 1830 (1978).
[50] A. U. Khan, P. Di Mascio, M. H. G. Medeiros, and T. Wilson, *Proc. Natl. Sci. U.S.A.* **89,** 11428 (1992).
[51] J. R. Perdrau and C. Todd, *Proc. Roy. Soc. Ser. B* **112,** 288 (1993).
[52] J. Lenard, A. Rabson, and R. Vanderoef, *Proc. Natl. Acad. Sci. U.S.A.* **90,** 158 (1993).
[53] H. Margolis-Nunno, E. Ben-Hur, P. Gottlieb, R. Robinson, J. Oetjen, and B. Horowitz, *Transfusion* **36,** 743 (1996).
[54] K. Müller-Breitkreutz, H. Mohr, K. Briviba, and H. Sies, *J. Photochem. Photobiol. B Biol.* **30,** 63 (1995).

immunodeficiency virus type 1, and cytomegalovirus,[55,56] but has little effect on nonenveloped virus such as adenovirus and poliovirus 1. In the study using herpes simplex virus type 1, 90% inactivation was observed after treatment with 3 m*M* $NDPO_2$, which generates a steady-state concentration of $^1O_2$ of about 10^{-12} *M* in H_2O-based phosphate-buffered saline (PBS). In the presence of human blood plasma (80%, v/v), which quenches $^1O_2$, virus killing was diminished substantially, e.g., 10 m*M* $NDPO_2$ was necessary to induce a loss of viral infectivity by 90%. In contrast to viruses, mammalian cells in culture are not as sensitive to $NDPO_2$; concentrations up to 20 m*M* were not toxic in various cell culture systems.

Regarding the mechanism of virus inactivation, it appears that $^1O_2$ causes inactivation by damaging viral envelopes, as can be deduced from the enhanced susceptibility of enveloped viruses in comparison to nonenveloped viruses to $^1O_2$.[55] However, $^1O_2$ may also modify DNA, particularly guanine residues, leading to the formation of 8-oxodG and other products. The exact mechanism by which $^1O_2$ inactivates viruses remains to be established.

Exposure of Cultured Cells to Singlet Oxygen Generated by Endoperoxides

Cells are grown to approximately 80% confluence in petri dishes, washed with PBS, and covered with PBS containing Ca^{2+} and Mg^{2+} or with serum-free medium at a temperature of 37°. Chemical generation of $^1O_2$ is achieved by adding $NDPO_2$ or $DHPNO_2$ over a concentration range of 0.3–10 m*M* to cells. The cells are incubated with $NDPO_2$ or $DHPNO_2$ for up to 1 hr at 37°. Control experiments are performed with solutions of preheated $NDPO_2$ and $DHPNO_2$ for 24 hr at 37°. These solutions contain the decomposition products NDP and DHPN, respectively. After treatment, the cells are covered with medium and are incubated at 37° for a desired time, washed with PBS at room temperature, and used for analysis as described in Refs. 57–61.

[55] A. Dewilde, C. Pellieux, S. Hajjam, P. Wattre, C. Pierlot, D. Hober, and J. M. Aubry, *J. Photochem. Photobiol. B. Biol.* **36,** 23 (1996).

[56] A. Dewilde, C. Pellieux, C. Pierlot, P. Wattre, and J. M. Aubry, *Biol. Chem.* **379,** 1377 (1998).

[57] K. Scharffetter-Kochanek, M. Wlaschek, K. Briviba, and H. Sies, *FEBS Lett.* **331,** 304 (1993).

[58] M. Wlaschek, K. Briviba, G. P. Stricklin, H. Sies, and K. Scharffetter-Kochanek, *J. Invest. Dermatol.* **104,** 194 (1995).

[59] M. Wlaschek, J. Wenk, P. Brenneisen, K. Briviba, A. Schwarz, H. Sies, and K. Scharffetter-Kochanek, *FEBS Lett.* **413,** 239 (1997).

[60] S. Grether-Beck, S. Olaizola-Horn, H. Schmitt, M. Grewe, A. Jahnke, J. P. Johnson, K. Briviba, H. Sies, and J. Krutmann, *Proc. Natl. Acad. Sci. U.S.A.* **93,** 14586 (1996).

The treatments of $NDPO_2$ or $DHPNO_2$ are nontoxic to human skin fibroblasts or keratinocytes tested up to 10 m*M*, as determined by means of the reduction of [3-(4,5-dimethylthiazol-2-yl)-2,5-diphenyl-2*H*-tetrazolium bromide (MTT)]. The cellular accumulation of $^1O_2$ sources ($NDPO_2$ or $DHPNO_2$) is discussed elsewhere in this volume.[62]

Singlet oxygen can also be produced by irradiating PBS containing 0.3 μM of Rose Bengal (RB; Sigma) or RB-agarose (Molecular Probes, Eugene, OR) for 10 min with a commercially available 500-W halogen lamp from a fixed distance of 66 cm. Approximately 130 μM (cumulative concentration) of $^1O_2$ is generated during 10 min of irradiation of 0.3 μM RB as determined by the bleaching of *p*-nitrosodimethylaniline.[62]

Activation of Gene Expression by $NDPO_2$

Singlet oxygen generated by thermodecomposition of $NDPO_2$ has been shown to induce the gene expression of interstitial collagenase (matrix metalloproteinase-1, MMP-1) in skin fibroblasts,[57,58] IL-1α/β, IL-6,[59] intercellular adhesion molecule-1 (ICAM-1) in keratinocytes,[60] and FAS ligand in skin-infiltrating T-helper cells Fas-ligand.[61] For example, using 3 m*M* $NDPO_2$ in H_2O-based PBS at 37°, an increase in mRNA of interstitial collagenase (MMP-1) in cultured human fibroblasts was observed.[57] Further, the expression of heme oxygenase-1 is enhanced by $^1O_2$ generated photochemically.[63]

Collagenase (MMP-1) induction by $^1O_2$ and UVA seems to be an indirect effect mediated by interleukins IL-1α/β and IL-6. Singlet oxygen generated by the thermodecomposition of $NDPO_2$ induced expression of IL-1α/β and IL-6. Singlet oxygen is made responsible for a leakage of preformed cytosolic IL-1, which then binds to its receptor, thereby stimulating the gene transcription of collagenase, its own gene, and IL-6.[59] IL-6, in turn, once synthesized and secreted, binds to the IL-6 receptor and stimulates collagenase synthesis.[64]

Transcription factor AP-2 but neither AP-1 nor NF-κB has been proven

---

[61] A. Morita, T. Werfel, H. Stege, C. Ahrens, K. Karmann, M. Grewe, S. Grether-Beck, T. Ruzicka, A. Kapp, L. O. Klotz, H. Sies, and J. Krutmann, *J. Exp. Med.* **186,** 1763 (1997).

[62] L. O. Klotz, K. Briviba, and H. Sies, *Methods Enzymol.* **319,** [13] (2000) (this volume).

[63] S. Basu-Modak and R. M. Tyrrell, *Cancer Res.* **53,** 4505 (1993).

[64] M. Wlaschek, G. Heinen, A. Poswig, A. Schwarz, T. Krieg, and K. Scharffetter-Kochanek, *Photochem. Photobiol.* **59,** 550 (1994).

[65] J. M. Aubry, B. Mandard-Cazin, M. Rougee, and R. V. Bensasson, *J. Am. Chem. Soc.* **117,** 9159 (1995).

to be responsible for the induction of ICAM-1 by singlet oxygen generated by $NDPO_2$.[60]

Some of the intermediate steps in the signaling network, such as the activation of mitogen-activated protein kinases, which can be involved in induction processes leading from $^1O_2$ generated by $NDPO_2$, $DMNO_2$, Rose Bengal plus light (RB/hν), methylene blue plus light (MB/hν), or UVA (320–400 nm) to induced gene expression, are shown in Fig. 4 and are also reviewed in Klotz *et al.*[62]

Conclusion

Due to the difficulties involved in obtaining $^1O_2$ free from other reactive contaminants, there is a paucity of detailed studies on the aspects of $^1O_2$ biochemistry mentioned earlier. The aim of this article is to present a useful tool to generate $^1O_2$ using endoperoxides of water-soluble naphthalene

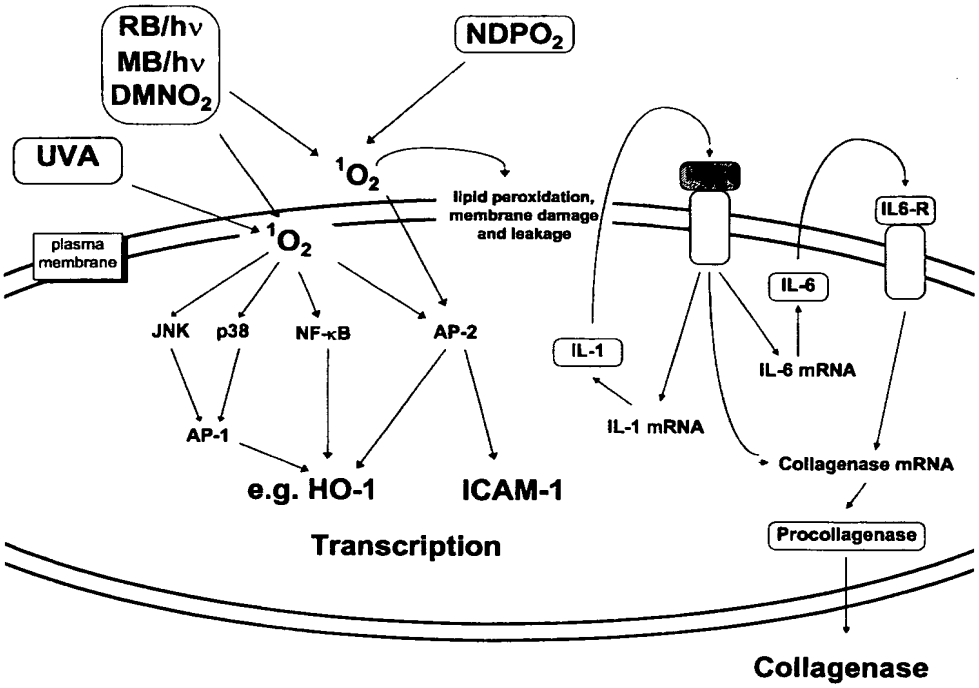

FIG. 4. Scheme outlining effects on gene expression of singlet oxygen generated by $NDPO_2$, $DMNO_2$, Rose Bengal plus light (RB/hν), methylene blue plus light (MB/hν), or UVA (320–400 nm). Modified from Briviba *et al.*[6]

derivatives. The physicochemical properties are suitable as chemical sources of $^1O_2$ in biological media.

Acknowledgments

Supported by the Fundação de Amparo à Pesquisa do Estado de São Paulo, FAPESP (Brazil), the Conselho Nacional para o Desenvolvimento Cientifico e Tecnológico, CNPq (Brazil), and the Programa de Apoio aos Núcleos de Excelência, PRONEX/FINEP (Brazil), Universidade de São Paulo/Comité Français d'Evaluation de la Coopération Universitaire avec le Brésil (USPCOFECUB), by the Deutsche Forschungsgemeinschaft, SFB 503, Project B1. Flash photolysis experiments were performed at the Paterson Institute for Cancer Research Free Radical Research Facility (Manchester, UK) with the support of the European Commission through access to large-scale facilities activity of the TMR program.

[2] Photosensitized Production of Singlet Oxygen

By IRENE E. KOCHEVAR and ROBERT W. REDMOND

Introduction

Photosensitization provides a simple, clean, and controllable method for producing singlet oxygen in solution or in cultured cells. In this process, the photosensitizer molecule, PS, absorbs the energy of a photon ($h\nu$) of ultraviolet or visible radiation to become an excited singlet state, $^1PS^*$, which rapidly converts into an excited triplet state, $^3PS^*$. The lifetime of $^3PS^*$ is longer (typically microseconds) than that of $^1PS^*$ (typically nanoseconds), so that energy transfer from ^3PS to dissolved oxygen molecule to form singlet oxygen, $O_2(^1\Delta_g)$, is possible [Eq. (1)]. In this

$$PS \xrightarrow{h\nu} {}^1PS^* \rightarrow {}^3PS^* \xrightarrow{O_2} PS + O_2(^1\Delta_g) \quad (1)$$

process, $^3PS^*$ is converted back to PS, the initial (ground) state, which can subsequently absorb another photon to begin the cycle again. Thus, each PS molecule can generate many (typically 10^3–10^5) singlet oxygen molecules before being bleached by reacting itself with singlet oxygen or by another reaction.

The amount of singlet oxygen generated by a PS is determined by the rate of absorption of photons, the triplet quantum yield, and the efficiency of the energy transfer process. The rate of absorption of photons is dependent on the concentration and molar absorption coefficient of the PS, the overlap between the emission spectrum of the light source and the absorption spectrum of the PS, and the intensity of the light. The efficiency for

0076-6879/00 $30.00